Exchange coupling of magnetic molecules to magnetic and non-magnetic substrates

Inauguraldissertation

zur

Erlangung der Würde eines Doktors der Philosophie

vorgelegt der

Philosophisch-Naturwissenschaftlichen Fakultät

der Universität Basel

von

Ján Girovský

aus Vranov nad Topľou (Slowakei)

Basel, Switzerland, 2016

Genehmigt von der Philosophisch-Naturwissenschaftlichen Fakultät auf Antrag von:

Prof. Dr. Thomas Jung

Prof. Dr. Ernst Meyer

Basel, den 14th October 2014

Prof. Dr. Jörg Schibler
Dekan

Abstract

This thesis summarizes an experimental investigation of magnetic behaviour of square-planar paramagnetic molecules (e.g. metallo-phthalocyanines and metallo-porphyrins) adsorbed on magnetic and non-magnetic substrates. Magnetic and electronic properties of the molecules are studied by means of X-ray Photoelectron Spectroscopy, Scanning Tunnelling Microscopy, Low-Energy Electron Diffraction and synchrotron based X-ray Absorption Spectroscopy and X-ray Magnetic Circular Dichroism. The experimental results are complemented by Density Functional Theory calculations conducted by Kartick Tarafder, Mohammed Ali Ehesan and Peter Oppeneer from Uppsala University, Sweden. Main results of the thesis include studies on:

Exchange coupling of chromium-tetraphenylporphyrin chloride (CrTPPCl) molecules to bare ferromagnetic Co(001) thin films. Adsorption of CrTPPCl species on the bare Co substrate leads to an induced magnetic moment on Cr ion. The magnetic moment is shown to couple antiferromagnetically with the substrate magnetization. Furthermore, CrTPPCl molecules adsorbed on the bare cobalt thin film change their oxidation state from 3+ to 2+ upon release of chlorine ligand from the Cr ion. Microscopic origin of the observed AFM coupling is described by a 90° indirect cation-anion-cation exchange coupling between less than half-filled 3d shell of the Cr(II) ion, 2p orbitals of molecular nitrogen and out-of-plane 3d orbitals of cobalt atoms.

Exchange interaction of manganese- and iron-tetraphenylporphyrin chloride (Mn- & FeTPPCl) molecules to nitrogen and chlorine terminated Co(001) thin films. Insulating spacer inserted between the paramagnetic molecules and the cobalt substrates is formed by an atomically thin layer of cobalt nitride or cobalt chloride, respectively. The layers are shown to alter molecule-substrate exchange coupling resulting in reduced electronic interaction of the ad-molecules with both substrates as evidenced by formation of self-assembled molecular 2D arrays. Magnetic moments resolved on Mn and Fe ions of the molecules are observed to couple antiferromagnetically with N/Co substrates. Microscopic origin of the interaction is explained by an indirect 180° cation-anion-cation exchange coupling between 3d orbitals of Mn(Fe) ions, $2p_z$ orbital of substrates' nitrogen atoms and out-of-plane orbitals of cobalt atoms. The pre-adsorbed nitrogens possess sizeable magnetic moment on the $2p_z$ orbital which is induced due to the exchange interaction with the cobalt atoms. The magnetic moment of pre-adsorbed nitrogens is shown to couple ferromagnetically with that of cobalt. Adsorption of MnTPPCl molecules at chlorine

terminated Co film has revealed an antiferromagnetic coupling between a relatively small magnetic moment induced on Mn ion and the substrate magnetization. Surprisingly, the XMCD signal measured at Fe $L_{3,2}$ edges of FeTPPCl species adsorbed on Cl/Co substrate, resolves a subtle molecule-substrate coupling. Our magnetic measurements reveal ferromagnetic coupling between magnetic moment of Fe and that of the cobalt thin film. Analysis of XAS/XMCD spectra acquired at $L_{3,2}$ and K edges of chlorine suggest that the exchange interaction between adsorbed molecules and the underlying substrate is mediated by 3d-orbitals of the chlorine atoms pre-adsorbed at the surface, i.e. 180 degree indirect exchange coupling.

Exchange coupling of manganese-tetraphenylporphyrin chloride (MnTPPCl) molecules to Co(001) substrates through a chromium spacer. Chromium spacer in the form of a wedge is shown to alter magnetic exchange coupling between MnTPPCl molecules and ferromagnetic cobalt substrates as a function of increasing thicknesses of chromium spacer. Magneto-chemical origin of the exchange coupling at the organic-inorganic interface is investigated by X-ray Photoelectron Emission Microscopy, i.e. spectro-microscopy correlation approach. At higher thicknesses of the chromium layer, the magnetic coupling between the molecules and the substrate is reduced due to the fact that induced spin waves decay exponentially with increasing distance.

Long-range ferrimagnetic order in supramolecular 2D Kondo lattice consisting of paramagnetic manganese-phthalocyanine (MnPc) and hexadeca-flourinated iron-phthalocyanine (FeFPc) molecules self-assembled into checkerboard array on Au(111) substrate. Magnetic moments of the molecules show magnetic remanence in absence of magnetic substrate or external magnetic field. Exchange coupling between the molecules, leading to a long-range ferrimagnetic order, is attributed to RKKY coupling mediated by the conduction electrons of the underlying gold substrate. Remanent molecular magnetic moments align in out-of-plane direction and reveal a notable contribution from orbital magnetic moment. Interestingly, the magnetic measurements performed for two different geometries (i.e. normal and grazing) suggest easy-plane anisotropy. Furthermore, the interaction of molecular magnetic moments with the substrate electronic states leads to a profound many body Kondo effect.

Presented results demonstrate the ability to control magnetic properties of paramagnetic molecules by means of exchange coupling to magnetic or via non-magnetic surfaces.

Table of Contents

List of Abbreviations

The following table lists the abbreviations used throughout the thesis:

2D	two-dimensional
3D	three-dimensional
AFM	antiferromagnetic
CF	Crystal Field
CrP	Chromium Porphine
DFT+U	Density Functional Theory + U
DOS	Density of States
e-beam	electron beam
fcc	face centered cubic
FeP(Cl)	Iron Porphine (Chloride)
FM	ferromagnetic
Gbit	gigabit
GKA	Goodenough-Kanamori-Anderson
GMR	Giant MagnetoResistance
HS	High-Spin
IS	Intermediate-Spin
LEED	Low Energy Electron Diffraction
LS	Low-Spin
ML	monolayer
M-Pc	metallo-phthalocyanine
M-TPP	metallo-tetraphenylporphyrin
MO	molecular orbitals
M-OeP	metallo-octaethylporphyrin
PEEM	Photo-Emission Electron Microscopy
PEY	Partial Electron Yield
QCMB	Quartz Crystal Microbalance
RKKY	Ruderman-Kittel-Kasuya-Yosida
SMM	single molecule magnet
STM	Scanning Tunneling Microscopy

STS	Scanning Tunneling Spectroscopy
TEY	Total Electron Yield
TFY	Total Flourescence Yield
XAS	X-ray Absorption Spectroscopy
XLD	X-ray Linear Dichroism
XMCD	X-ray Magnetic Circular Dichroism
XMLD	X-ray Magnetic Linear Dichroism
XNCD	X-ray Natural Circular Dichroism
XNLD	X-ray Natural Linear Dichroism
XPS	X-ray Photoelectron Spectroscopy

1

Introduction

Since ancient times an attractive/repulsive interaction between magnetic minerals provided a fascinating phenomenon. Magnetism was recognized as a "*magic power*" and has been used for a benefit of the human kind already 2 centuries B.C. People of past knew about the lodestone (magnetite – Fe_3O_4) magic stone that attracts or repels another piece of lodestone, but definitely attracts iron. The first time the term magnet has been coined in the literature is attributed to Thales of Miletus [pre-Socratic Greek philosopher (624 – c. 546 BC)], who stated that lodestone has a soul and therefore attracts iron. The first 'scientific' discussion dealing with magnetism is attributed to Lucretius [Roman poet and philosopher (c. 99 BC – c. 55 BC)], who discussed the magnetism in his work *De rerum natura* (On the Nature of Things). Magnets, in his view, consist of the small objects (atoms) which are emitted from the lodestone and remove the air in the vicinity of the magnet. This causes that a piece of iron is 'sucked' towards the lodestone due to the missing air atoms. Chinese recognized that a tiny piece of magnetic materials which was suspended on a thin thread always points towards north and south cardinal directions. This early discovery of the compass was helpful to travellers and explorers alike.

It took a long time until magnetism started to bother the minds of scientists in the 18th century. First pioneers of renaissance period focused mainly on the effects caused by electric charge rather than those caused by magnetism. In following years the investigations of phenomena caused by electric charge have been studied by pioneers such as B. Franklin, L. Galvani (a doctor and professor of anatomy at University of Bologna) and A. Volta. They had a tremendous impact on the field of electro-magnetism. Few years later, H. Ch. Oersted, A. M. Ampere, J. B. Biot, F. Savart, M. Faraday and C. F. Gauss have performed experiments that helped to connect the electricity with magnetism. Later, electricity and magnetism were unified and recognized as one of the four fundamental forces. It was Faraday and later Maxwell who conjunct the electricity, magnetism and optics into one unified theory of electro-magnetism described by four simple equations, that *"every physicists shall remember, even awaken in the mid of deep sleep"*.

$$\boldsymbol{\nabla}.\boldsymbol{E} = \frac{\rho}{\varepsilon_0} \tag{1.1}$$

$$\boldsymbol{\nabla}.\boldsymbol{B} = 0 \tag{1.2}$$

$$\boldsymbol{\nabla} \times \boldsymbol{E} = -\frac{\partial \boldsymbol{B}}{\partial t} \tag{1.3}$$

$$\boldsymbol{\nabla} \times \boldsymbol{B} = \mu_0 \left(\boldsymbol{J} + \varepsilon_0 \frac{\partial \boldsymbol{E}}{\partial t} \right) \tag{1.4}$$

, where $\boldsymbol{\nabla}$ is lambda operator, $\boldsymbol{E}$ – vector of electric field, ρ – charge density, ε_0 – permittivity of free space, $\boldsymbol{B}$ – vector of magnetic field, μ_0 – permeability of free space and $\boldsymbol{J}$ – vector of current density.

As such, this has led towards a development of many devices, such as the telegraph in the early days, television, radio, personal computers and smartphones, nowadays. Living in the era where the information is stored and processed by computers rather than people, who are only operating them, we experience the increasing demand for the fast and reliable storage devices with extremely high storage density. The recent most advanced hard drives are capable of storing about 1.4Gbit of information per square millimetre. At the thickness of d = 20 nm, the magnetic layer in a hard drive stores one bit of information in approximately 10^6 atoms. This is a pretty large number, so the question is whether we can possibly reduce the amount of the atoms needed for storing a bit of information, into single one. This is theoretically possible and there are many feasible ways how to do it. It remains however also many decades away from what is currently predicted as a fundamental limit. Therefore, magnetism at nanoscale provides an important challenge to increase the density of data storage while maintaining the reliability of the current technology.

The physics of magnetic materials at macro- and mesoscopic dimensions differs to that observed at nanoscale. The main difference is caused by emergence of quantum effects governing the behaviour of nano-objects. In the recent years, studies on magnetism in single atoms[1,2,3] or single magnetic molecules[4,5,6,7] has provided new challenges and opportunities to investigate quantum magnetism. Furthermore, manipulation of spins in atoms/molecules is foreseen in "*spintronics*" devices. In general, the possibility to store a bit of information onto atomic spin has been driving force towards such devices. However, adsorption of atoms and molecules at substrates leads to a hybridization of atomic orbitals with those of the surface. In case of strong exchange interaction between magnetic moments and non-magnetic conducting substrates, the properties of ad-atom, especially lifetime of spin excited states is altered. In order to reduce exchange coupling and increase spin lifetime a thin insulating layer separating ad-atoms and the substrate has to be used[1,2].

Optionally, molecules comprising magnetic atom(s) can also behave as a permanent magnet with hysteresis loop opening under critical temperature.

Examples of such molecular magnets are Mn_{12}, Fe_8 or Fe_4 molecules containing a few magnetic atoms in the molecular framework[7,8]. Magnetic atoms within these molecules interact via exchange coupling and the crystal field of molecular framework helps to stabilize their magnetic moment[9]. Molecular magnets have therefore attracted a wide scientific interest due to the possibility of application of the molecules in the storage devices[10]. However, adsorption of such big molecules on surface leads to their collapse. In 2009, it was reported[7] that it is actually possible to deposit the molecular magnets on the surface while the molecules still behave as molecular magnets. However, there are still many problems which need to be solved. In particular, molecules tend to adsorb randomly at the surface and they require very low temperatures in order to stabilize their magnetic moments.

Alternatively, magnetic atoms (molecules) can be adsorbed on magnetic substrates leading to an induced magnetic moment due to the magnetic exchange interaction with the substrate. Such a stabilized magnetic moment is shown to remain aligned at room temperature and beyond[4,5,11]. Magnetic molecules became especially interesting due to their versatility. In the pioneering work by Scheybal, et al. MnTPPCl molecules adsorbed flat on ferromagnetic cobalt thin films show induced magnetic moments stable at room temperatures[4]. Magnetic moments of MnTPPCl species have been shown to couple ferromagnetically to substrate magnetization. The authors proposed three possible mechanisms for the ferromagnetic exchange coupling between the Mn ion and substrate's cobalt atoms: i) super-exchange through chlorine atom positioned between Mn and top most layer of the substrate, ii) indirect exchange via delocalized electrons of porphyrin ligand and iii) direct exchange. In the follow up study by Wende et al., FeOePCl molecules were deposited on nickel and cobalt thin films revealing a 90 degree indirect ferromagnetic exchange coupling via delocalized porphyrin states as resolved by density functional theory[5]. They also demonstrated that the molecular magnetic moment aligns along the easy-axis of the substrate magnetization, i.e. out-of-plane for nickel and in-plane for cobalt. Chylarecka et al. experimentally confirmed theoretical proposition of the 90° indirect exchange in the MnTPP(Cl) molecules adsorbed on the ferromagnetic cobalt substrates[12]. Additionally, the possibility of the exchange coupling mediated by the chlorine atom has been excluded based on an observation of chlorine desorption during the process of adsorption at the ferromagnetic substrate[13]. Javaid et al. in their study on MnPc/Co/Cu(001) system proposed direct exchange as a mechanism inducing a ferromagnetic coupling on the magnetic moment of the Mn ion[14,15] based on the theoretical calculations, without detailed experimental confirmation. In all cases, energy of the exchange coupling would correspond to magnetic fields of several tens of tesla, thus undesirable for experiments and real applications.

In order to tune magnetic coupling of the molecules to magnetic substrate, two strategies can be employed. First, exchange interaction between molecules and substrate can be altered introducing a spacing layer. Bernien et al.[16] and Chylarecka et al.[13] demonstrated tailoring a molecule-substrate exchange coupling by terminating the surface of the FM cobalt substrate with oxygen. The magnetic

moments of the molecules in both studies were shown to couple AFM due to the 180° indirect exchange coupling (Mn-O-Co). In addition to their study, Chylarecka et al.[13] provided an evidence of self-assembled molecules on these substrates. The self-assembly of the molecules is directed by the molecule-molecule interaction, which is neglected for molecules on bare cobalt substrate where much stronger molecule-substrate interaction plays a dominant role[12-16].

Instead of using an insulating spacer layer, Hermanns et al. [17] placed a thin sheet of graphene in between CoOeP molecules and ferromagnetic nickel substrate in order to alter their exchange interaction. In this case an AFM exchange coupling was observed due to the exchange coupling of delocalized porphyrins electrons with the extended π-electrons of the graphene. The π-states of graphene are subtly spin-polarized due to exchange coupling with the underlying nickel substrate. Such indirect exchange coupling is relatively weak compare to magnetic interaction of paramagnetic molecules adsorbed on oxygen reconstructed ferromagnetic substrates, because the exchanged electrons make longer path between the central metal ion and the ferromagnetic substrate.

Insertion of conducting non-magnetic spacer layer between molecules and magnetic substrate has been proposed and experimentally investigated by Fu et al.[18]. Using lead (Pb) as the spacer layer between MnPc molecules and ferromagnetic iron film the authors revealed an AFM alignment of the Mn spin with the magnetization of underlying iron substrate. Origin of AFM coupling has been attributed to RKKY-type coupling mediated by the conducting electrons of lead spacer layer.

Molecular magnetic moments can also be tuned on the "vacuum" side of the molecules. This side is easily accessible for external chemical ligands, such as NH_3, NO or CO. The magneto-chemistry well known in the solution chemistry can be exploited at surfaces, i.e. *on-surface magneto-chemistry*. Beautiful example of the coordination chemistry of porphyrins is found in the human body where O_2 molecules bind at the centre of haemoglobin (contain Fe-porphine molecule)[19]. Wäckerlin et al.[20] have demonstrated that CoTPP molecules adsorbed on the ferromagnetic nickel substrate change their magnetic moment from S=1/2 to S=0 upon coordination with nitric oxide (S=1/2) molecules. Demonstration of spin tuning by means of external stimuli has triggered broad interest in the scientific community and was later demonstrated for many other porphyrins and phthalocyanines molecules[21,22].

An ultimate goal in quantum magnetism and alternatively in spintronic applications is to construct a low dimensional magnetic materials where individual magnetic moments are assembled in a periodic manner, easily accessible by experimental technique and with possibility to control their properties by external stimuli. Several studies, theoretical and experimental, have focused to achieve such two-dimensional structures. Gambardella et al.[23] presented two dimensional supramolecular array consisting of Fe atoms coordinated by 1,4-

benzenedicarboxylic acid molecules assembled on Cu(001) substrate. In this array the authors were able to manipulate magnetic anisotropy of Fe ions, from in-plane to out-of-plane orientation, by means of chemical stimuli with oxygen coordinated at the Fe atoms. In other study, Tsukahara et al. investigated an array of FePc molecules assembled on Au(111) by means of Scanning Tunnelling Spectroscopy[24]. Adsorption of individual FePc molecules on Au(111) substrate leads to an emergence of Kondo effect at the centre of the molecules. In the array of FePc a splitting of Kondo signature has been observed and attributed to an emergence of antiferromagnetic RKKY-coupling between nearest neighbours with the proposal of antiferromagnetic ground state.

This thesis presents the study of molecule-substrate exchange coupling in several systems. From the list of publications presented above it appears that the topic is still very appealing. Detailed study on metallo-porphyrins comprising early 3d-transition metal ions with less-than half-filled 3d-shell, e.g. Cr, V has not been presented so far. One of the reasons to investigate these systems is to address a role of electron occupancy on molecule-substrate magnetic exchange coupling. The exchange coupling depends on the occupation of the orbitals involved in the interaction and on the angle between magnetic ions. Chromium compare to manganese lacks an electron which results in empty Cr-$d_{x^2-y^2}$ orbital. It was demonstrated that this orbital is responsible for FM indirect exchange coupling between MnTPP and cobalt substrate[25]. Therefore, deficit of one electron may change the sign and strength of the exchange coupling. The results discussing exchange coupling of CrTPPCl species to bare cobalt substrates are presented in Chapter 4.

Chapter 5 presents a study on exchange coupling of MnTPPCl and FeTPPCl with nitrogen and chlorine terminated cobalt thin films. Presence of the spacer layer (e.g. oxide or graphene) at the molecule-substrate interface was shown to alter the sign and strength of the exchange coupling. Especially interesting, is the case of chlorine reconstruction, where a role of chlorine 3d orbitals is discussed in regards to the molecule-substrate exchange coupling.

Chapter 6 comprises a study of the exchange coupling between MnTPPCl and the cobalt substrate through the non-magnetic chromium spacer layer of increasing thickness, i.e. wedge. In the results part we discuss a dependence of the molecule-substrate exchange coupling on the thickness of the spacer layer.

Exchange coupling between MnPc and FeFPc molecules adsorbed in the checkerboard pattern on Au(111) substrates is studied. The interaction of molecular magnetic centres with conduction electrons of Au(111) substrate has been proposed to lead to a coexistence of two competing mechanisms; the Kondo effect and RKKY coupling.

2

Exchange Coupling

Magnetism is described as a collective behaviour of multiple magnetic moments, e.g. atomic spins. In very simple picture magnetic moment can be represented as an arrow pointing from a negative "magnetic charge" ("south pole") to a positive "magnetic charge" ("north pole"). The magnetic field created by this moment is directed in the opposite direction from the positive to the negative end. The magnetic moment is always connected with the matter while magnetic field can exists independently of the matter in the form of electromagnetic radiation. Magnetic moment is an intrinsic property of the object, i.e. an electron possessing a spin magnetic moment. Spin angular momentum of an electron can be oriented either "up" ($\boldsymbol{s}$=½) or "down" ($\boldsymbol{s}$=-½). The spin magnetic moment of the electron is proportional to the spin angular momentum $|\boldsymbol{m_s}| = g\boldsymbol{\mu_B}\sqrt{s(s+1)}$, where g is gyromagnetic factor, g ~ 2 for electron and $\boldsymbol{\mu_B}$ is Bohr magneton. Magnetic moment is also created when charged particle flows on circular path. Magnetic moment "created" this way is proportional to a current and an area enclosed by the loop. Electron circulating around nuclei in atomic orbital creates an orbital magnetic moment $\boldsymbol{m_o}$ as well. The orbital magnetic moment is than proportional to the angular orbital momentum $\boldsymbol{l}$ of the electron $|\boldsymbol{m_o}| = \boldsymbol{\mu_B}\sqrt{l(l+1)}$[26].

Depending on the interaction of magnetic moments (spin or orbital) with each other and/or their interaction with external magnetic field we can divide materials into three main groups: diamagnetic, paramagnetic and magnetically ordered materials.

FIGURE **2.1** | Pyrolytic graphite levitating above permanent magnets due to the repulsion of magnetic field by the graphite.

Diamagnetic materials repel magnetic field from their bulk. These materials are described by their relative permeability being less than or equal to 1, $0 \leq \boldsymbol{\mu_r} \leq 1$. As a consequence of the repulsion, diamagnetic materials can be applicable in levitating transport vehicles. A piece of highly orientated pyrolytic graphite levitates above strong permanent magnets (see Figure 2.1). Gold, bismuth and superconductors, which are ideal diamagnetic materials with $\boldsymbol{\mu_r} = 0$.

Paramagnetic materials exhibits an opposite behaviour to that of diamagnetic materials, i.e. paramagnets, are attracted by external magnetic field. The attraction of the paramagnets by external magnetic field is caused by alignment of the magnetic moments of the materials along magnetic field, thus creating magnetic field of opposite sign inside the paramagnet. Paramagnets in comparison with diamagnetic materials have much larger applications, for example as cooling medium using the adiabatic demagnetization[27]. The energy of the aligned magnetic moments of paramagnetic material is consumed and transformed to thermal excitations of the material.

In both diamagnetic and paramagnetic materials magnetic moments, are considered free without interaction with each other. However, magnetic moments can interact between themselves, thus leading to magnetically ordered materials, e.g. ferrite.

When energy of the interaction between magnetic moments is higher than the thermal energy, the magnetic moments align along certain direction below critical temperature even in the absence of external magnetic field. In very simple picture, neighbouring magnetic moments can align parallel along one direction i.e. ferromagnetic coupling or anti-parallel, i.e. antiferromagnetic interaction. Materials comprising two sub-lattices of unequal magnetic moments with an anti-parallel alignment form a ferrimagnetic state. The interaction between the magnetic moments can be of different kind and in the following section some of them will be introduced.

The typical interaction occurring between magnetic moments is the ***dipole-dipole interaction***. Kids know this type of interaction very well when playing with magnets and tricking parents that iron ball can be moved by a thought. It may appear that this kind of magnetic interaction is very strong; however, it is relatively weak. The strength of the dipole-dipole interaction is proportional to the size of the magnetic dipoles (m_1, m_2) and inversely proportional to the cubic of the distance (r) separating them (c.f. Eq. 2.1). Term μ_0 stands for permeability of vacuum.

$$E = -\frac{\mu_0}{4\pi r^3}(3(m_1 r)(m_2 r) - m_1 m_2) \qquad (2.1)$$

Energy of magnetic moments of two electrons interacting with each other via the dipole-dipole interaction would be in order of 1K, which suggests that for many materials that exhibit magnetic behaviour at room temperature, the dipole-dipole interaction is not strong enough to achieve that. Much stronger type of interaction is

a so-called ***exchange coupling*** between magnetic moments of the atoms. As the name suggests there is an exchange of electrons between two atoms dictating thus the type of alignment. Electrons are localized within certain orbitals of atoms. Two atoms brought close together start to overlap their orbitals and electrons can "hop" from one to another. As a consequence the bond between atoms is created with new molecular orbital (MO) formed. Electrons forming the bond are governed by the Pauli Exclusion Principle and by the Coulomb interaction. Pauli Exclusion Principle states that two electrons cannot occupy same quantum state which is described by 4 quantum numbers. Therefore we cannot find two electrons with same quantum numbers. Two bond forming electrons with same energy differ in spin quantum number, i.e. have opposite orientation of their spin moments. The Coulomb repulsion is an energy needed to bring two electrons close together to occupy same site.

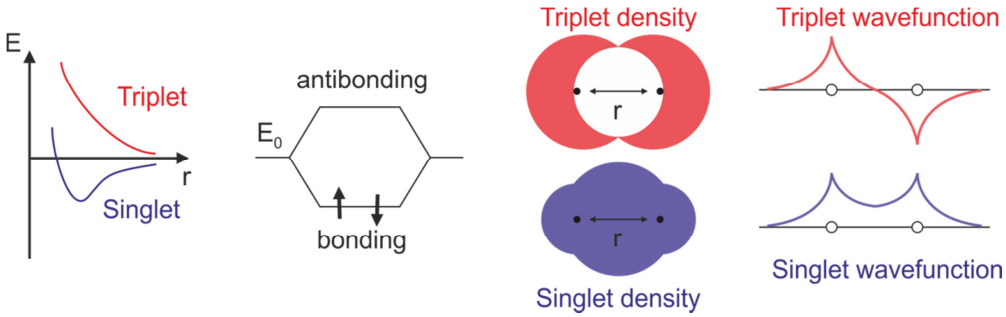

FIGURE **2.2** | Singlet (bonding) and triplet (antibonding) state of H_2 molecule given by Heiter-London valence band theory[27].

The situation can be described by Hubbard Hamiltonian written in second quantization notation:

$$H = -t\left(c_{1,s}^{+}c_{2,s'} + c_{2,s'}^{+}c_{1,s}\right) + U\sum_{i=1}^{2} n_i \qquad (2.2)$$

, where t is hopping term (kinetic energy) of electrons between sites *1* and *2*, $c_{i,s}^{+}$, $c_{i,s}$ are creation and annihilation operators, respectively, which "create/destroy" an electron at the site i with the spin *s.* Term U represents a Coulomb interaction between two electrons with opposite spins (cf. Pauli Exclusion Principle) occupying the same site. Occupancy is given by operator n_i, where $n_i = 0$ for empty or singly occupied site, $n_i = 1$ for doubly occupied site. Depending on the strength of the terms t and U, we discriminate several situations.

Simplest type of exchange interaction is ***direct exchange coupling*** where orbitals of two atoms are directly overlapping. In this case, the Hubbard Hamiltonian is dominated by t term. The mechanism of direct exchange is schematically described on the simplest model, a hydrogen molecule H_2 shown in Fig. 2.2. Hydrogen 1s orbital contains an unpaired electron. Two hydrogen atoms brought close together will overlap their 1s orbitals forming bonding or antibonding molecular orbital. Bonding orbital is created when electrons spend most of their time in the space

between two nuclei. On the other hand, if electrons spend most of the time outside the centre of mass, an antibonding orbital is defined. The newly formed MOs contain two electrons. Spins of both electrons in these cases can be aligned either parallel forming triplet state (S=1) or antiparallel, i.e. singlet (S=0). In hydrogen molecule, the energy of singlet state is lower compared to that of triplet state and at certain distance of hydrogen's nuclei, the energy of singlet state is lower than the energy of two separated hydrogen atoms (E_0) and H_2 molecule is stable and diamagnetic (S=0) (Fig. 2.2). In some cases the triplet state can be energetically favourable e.g. diatomic molecule of oxygen O_2, which is paramagnetic (S=1)[27].

In many materials magnetic ordering is observed even if they are not entirely metallic, for example oxides or halides of magnetic elements (e.g. Co, Fe, Mn, Ni), which are mostly insulators. Direct overlap between the orbitals of magnetic atoms is negligible and cannot lead to a magnetic ordering. In those materials the magnetic exchange is mediated via non-magnetic atoms (e.g. oxygen, chlorine, fluorine) and is called ***indirect exchange coupling*** or ***super-exchange***. The sign of interaction between two magnetic atoms (i.e. FM or AFM) depends on the angle between orbitals, the occupancy [empty ($0e^-$), half-filled ($1e^-$), fully-filled ($2e^-$)] and their symmetry (orthogonal vs. non-orthogonal). Three simple examples of indirect exchange coupling are shown in Figure 2.3. For the indirect exchange coupling the Coulomb interaction dominates over the kinetic term.

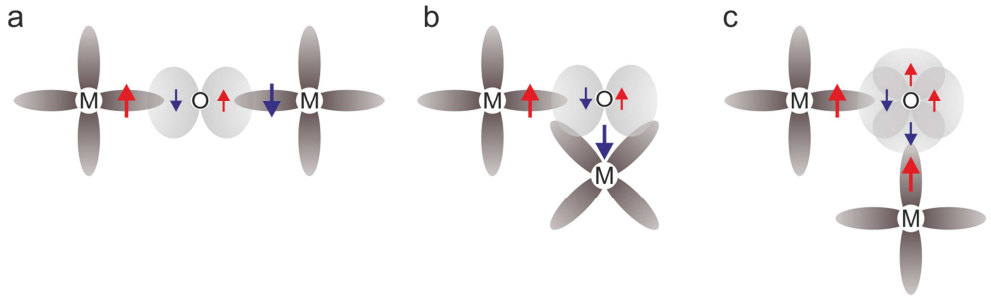

FIGURE **2.3** | Scheme of indirect exchange coupling between two half-filled metal 3d-orbitals for (a) an antiferromagnetic 180° indirect exchange interaction between two orbitals of same symmetry mediated by oxygen 2p-orbital. (b) antiferromagnetic 90° indirect exchange coupling between two orthogonal 3d-orbitals interaction through one 2p-orbital and (c) ferromagnetic 90° indirect exchange coupling between two non-orthogonal 3d-orbitals interacting via two orthogonal 2p-orbitals.

Assume we have two half-filled 3d-orbitals (one electron on each - Fig. 2.3a) connected through a 2p-orbital of oxygen enclosing an angle of 180 degrees. Oxygen orbital is fully filled, with one spin-up and one spin-down electron. Let us assume that left 3d orbital possesses an electron with spin-up orientation. The left 3d orbital overlaps with 2p orbital of oxygen forming a sigma bond. Due to the overlapping wavefunctions, the electron from left 3d orbital spends some time at the O 2p orbital which causes that the 2p orbital aligns its spin antiparallel to that of the left orbital. Spin of the second 2p electron therefore orients with spin up. The second 2p electron is exchange with the right 3d orbital again via sigma bond. An electron on

the right 3d-orbital thus aligns with spin down due to the Pauli Exclusion Principle. As a result we observe an antiparallel, i.e. antiferromagnetic alignment between these two half-filled 3d-orbitals (Fig. 2.3a). Ferromagnetic arrangement in this case is also possible, but it would cost an extra energy as one electron from a metal ion would need to be in the excited state. The above mentioned example stands for 180° indirect exchange coupling. Another example is antiferromagnetic 90° indirect exchange coupling between two orthogonal (non-overlapping) 3d-orbitals coupled through an intermediate oxygen 2p-orbital via a sigma and a pi bond (Fig. 2.3b). Fig. 2.3c presents a ferromagnetic 90° indirect exchange coupling between two orbitals of same symmetry sigma bonded to two orthogonal oxygen 2p-orbitals. In this particular case the Coulomb interaction between the orthogonal 2p-orbitals of oxygen atom causes a ferromagnetic alignment. The sign and strength of the indirect exchange coupling can be qualitatively predicted to high extend using Goodenough-Kanamori-Anderson (GKA) rules for a priori known angle, orbital occupancy and the nature of the non-magnetic elements bridging the magnetic ions[28]. Indirect exchange coupling mediated via anions (e.g. oxygen, chlorine or fluorine) exploits the localized electrons. Localized electrons have higher potential energy (Coulomb energy) and smaller kinetic energy and cannot travel long distances in the sample.

Exchange coupling can also be mediated by the delocalized electrons, i.e. free-like conduction electrons in metals. When magnetic impurity is surrounded by the sea of the conduction electrons, spin moment of those electrons feel weak magnetic field produced by magnetic impurity. In the vicinity of the magnetic impurity the magnetic field is strongest and electrons align their spins antiparallel to that of the impurity in order to minimize their energy (Fig 2.4a).

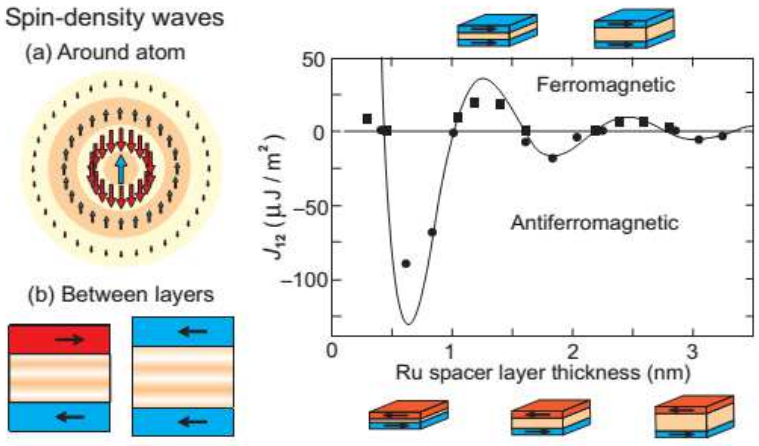

FIGURE **2.4** | Scheme of the RKKY-like coupling. The electrons close to magnetic impurity are spin polarized, with the increasing distance the sign and amount of the spin polarization is varies. Adapted from[26].

The first layer of spin-polarized electrons also produces the magnetic field and electrons' spins in the next layer align antiparallel with respect to the magnetic field created by first layer. The spin-polarization of the electrons then oscillates from

AFM to FM alignment with the increasing distance, but the amplitude of the spin-polarization decays exponentially. For simplicity, let us consider two magnetic impurities embedded into the sea of conduction electrons separated by distance R that is not very large. Clouds of spin-polarized electrons around impurities start to interfere below certain temperature and magnetic impurities begin to feel each other. This type of magnetic exchange interaction is called ***Ruderman-Kittel-Kasida-Yosida (RKKY) coupling*** after researchers who contributed to discovery and description of this phenomenon[26]. Energy of RKKY coupling can be estimated using the following formula (3D case):

$$E \sim \frac{m_1 m_2}{R^4}[2k_F R\cos(2k_F R) - \sin(2k_F R)] \tag{2.3}$$

The strength and sign of the RKKY coupling depends on the size of interacting magnetic moments (m_1, m_2), electronic density of states ($\sim k_F$) and on the distance R. The RKKY coupling can be also observed for two magnetic thin films separated by the conducting non-magnetic spacer layer (c.f. Figure 2.4b). One of the films induces spin waves in the spacer layer whose propagate through the spacer towards the second film. Depending on the thickness of the spacer layer, the sign of magnetic interaction oscillates between FM or AFM and the strength of coupling decreases exponentially with increasing thickness. The RKKY phenomenon has been used to demonstrate the Giant Magnetoresistance (GMR). The conductance between two magnetic thin films separated by non-magnetic metallic spacer depends on the alignment of their magnetic moments. If both magnetic moments are aligned parallel the resistance is low, if they align antiparallel the resistance is very high[29]. This effect is recently used in manufacturing the reading heads of hard drives and it allowed decreasing the size of the storage units.

Along the RKKY-type coupling, a complementary phenomenon known as the ***Kondo effect***[30] is observed. Magnetic impurity (e.g. single magnetic atom) embedded in the metallic material is surrounded by the conduction electrons, similar to those in RKKY coupling (Fig. 2.5a). However, the spins of the conduction electrons are spin-flipped due to scattering at the impurity resulting in a screening of the magnetic moment, i.e. the moment is quenched. The Kondo effect causes the renormalization of the density of states at the Fermi level leading to a formation of narrow band resolved by differential conductance spectroscopy as a zero-energy feature (Fig. 2.5b,c,d). Kondo phenomenon was first observed for metallic alloys with very small concentration of magnetic impurities, causing an ohmic resistance to increase below critical temperature. The Kondo effect thus favours the spin-singlet ground state according to following equation:

$$E \sim J\boldsymbol{S}.\boldsymbol{s} \tag{2.4}$$

, where J < 0 is AFM coupling between magnetic impurity $\boldsymbol{S}$ and conduction electrons with spins $\boldsymbol{s}$.

In contrast to RKKY coupling, which couples spins over long-distances (long-range ordering); the Kondo effect destabilizes the magnetic ordering by screening the magnetic moment of the magnetic impurity (short-range interaction).

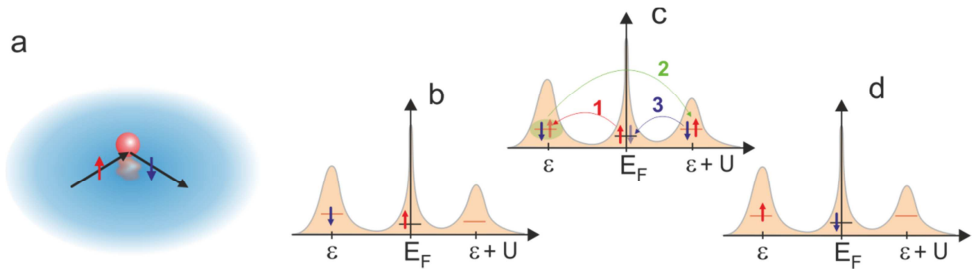

FIGURE **2.5** | In the Kondo effect a spin of conduction electron is flipped after scattering at the magnetic impurity (a). (b) Energy ε of half-filled orbital of the magnetic impurity is found below Fermi level E_F. (c) Due to the strong interaction of magnetic impurity with conduction electrons of host material, the spin-up electron from host hops on the impurity orbital (process 1). Two electrons at one orbital have higher energy due to the Coulomb repulsion (U) and total energy is then ε+U, found above Fermi level (process 2). (d).These configuration is not stable leading to another hop of spin-down electron back to sea of conduction electrons leaving spin-up electron on the magnetic impurity orbital (process 3)

Last two types of exchange coupling to mention briefly are ***Zener double exchange***[26] and anisotropic ***Dzyaloshinsky-Moriya exchange interaction***[31]. Zener double exchange explains the interaction in the materials, which have magnetic atoms of the different valence, e.g. M^{2+} and M^{3+}. According to theory of superexchange those systems should be rather insulating and antiferromagnets, while they have metallic behaviour and often ferromagnetic ground state. ***Dzyaloshinsky-Moriya exchange interaction (DMI)*** was used first time to explain the weak ferromagnetic signal in certain antiferromagnetic materials. The magnetic moments of the atoms are not perfectly aligned and spins are canted due to the spin-orbit coupling in the magnetic atoms[32].

3

Experimental Setup

All experiments were carried out in the ultra-high vacuum conditions to avoid contamination of the samples. Typical pressure in the chambers where the samples have been prepared and analysed was below $p < 10^{-9}$ mbar (1 mbar = 100Pa). For comparison, at the ambient pressure ($p=10^5$ Pa) sample surface would be covered with a full monolayer of the residual gas within 1ns, assuming all impacting molecules staying at the surface. If the pressure is lowered to $p=10^{-9}$ mbar, the time required to form a full monolayer is increased to 1 hour. Furthermore, at the UHV conditions all reactive substances, e.g. oxygen, water, are removed by a turbo pump or ion getter pump that further increases the absorption time to form a monolayer at the surface.

Sample preparation, XPS, STM and LEED experiments have been performed in the Surface Science Laboratory at Paul Scherrer Institut, Villigen, Switzerland. Sample preparation consists of several steps described in the following paragraphs. For studies on paramagnetic molecules adsorbed at magnetic substrates, i.e. Co, Cr/Co, N/Co and Cl/Co thin films, Cu (001) single crystals have been used to grow thin magnetic films. Additionally, Au (111) single crystals were used in the experiments without magnetic substrates. All samples were cleaned by Argon sputtering with ions accelerated to E=2keV. Ions have been directed towards the sample under the angle 20 degree with respect to the crystal's surface normal, i.e. 70 degree from the surface plane.

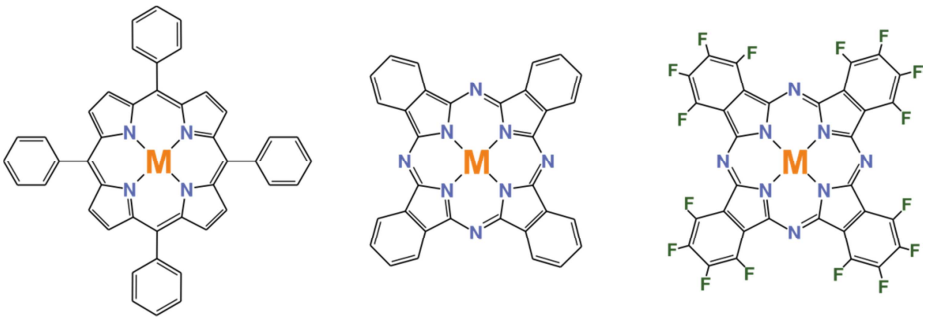

FIGURE **3.1 |** Sketch of the metallo-porphyrin, metallo-phthalocyanine and fluorinated metallo-phthalocyanine (M=Cr, Mn or Fe) molecules studied within this thesis.

Samples have been sputtered for 20 minutes, followed by 20 minutes of sputtering and annealing cycle with sample temperature T=900K for Cu(001) crystals and T=800K for Au(111) substrates. After that, samples have been post-annealed for another 20 minutes at the same temperatures. After the cleaning procedure, samples were cooled down to room temperature and cleanness was checked by the XPS technique, looking for the most common contaminants, i.e. carbon, oxygen, nitrogen and traces of metals such as cobalt, iron, nickel and manganese.

Growth of magnetic Co thin films:

Thin films of cobalt are prepared by E-beam evaporation. In the first step, 10 atomic layers of cobalt are deposited on the clean Cu(001) substrate. Deposition rate is controlled by Quartz Crystal Microbalance (QCMB) prior the cobalt deposition and adjusted to rate ~0.5ML per minute. Low evaporation rate allows for the formation of large terraces over wide range. During the first round of deposition, the samples are kept at room temperature[33]. In the next step, sample is moved from the evaporation chamber and annealed to 500K for 15 minutes, whilst the deposition rate is adjusted. Additional 10 layers are deposited on the sample kept at ~ 450K. Total thickness of cobalt film is 20 atomic layers. Such thin cobalt films are shown to exhibit very low coercivity, an in-plane orientated easy axis of magnetization along [110] axis and Curie Temperature $T_C \sim 1300$ K[34]. Low coercivity is required in order to manipulate the direction of the magnetization with magnetic field of about ~ 100mT. Substrates are consequently cooled down to room temperature and cleanness is checked with XPS looking at signatures of carbon, nitrogen and oxygen.

Preparation of nitrogen reconstructed Co thin films:

Diatomic nitrogen molecule N_2 is one of the most stable molecules known. It requires high amount of energy to break the triple bond between two nitrogen atoms. Thus N_2 molecules would not easily react with the copper surface. Nitrogen reconstructed copper surface is prepared by sputtering of clean Cu(001) crystals with nitrogen ions possessing a kinetic energy E=500 eV. Prior the nitrogen sputtering, the samples are annealed to ~ 500K for 15 minutes. Samples are sputtered for 10 minutes, while the angle between the beam of nitrogen ions and the surface normal is set to zero, allowing nitrogen ions to be embedded into the surface, without significant material being removed from the surface. During the sputtering process the substrates are kept at T~500K to assure uniform distribution of the nitrogen atoms at the surface. After nitrogen sputtering, the samples were post-annealed for additional 10 minutes and consequently cooled down to room temperature. Sputtering results in formation of c(2x2)-like reconstruction of Cu(001)[35](cf. Fig. 5.1). Amount of nitrogen atoms is controlled by XPS measurements. On top of the nitrogen reconstructed Cu(001) surfaces, a cobalt thin film with thickness of 20 atomic layers is deposited according to procedure described in the previous paragraph. Surfactant-like growth of nitrogen atoms causes diffusion of nitrogen atoms on the top of the cobalt films resulting in the c(2x2) nitrogen reconstructed cobalt substrates.

Preparation of chlorine reconstructed Co thin films:

Chlorine reconstructed Cu(001) surfaces are prepared by deposition of an anhydride of Copper(II) Chloride salt (purity ~ 99.99%, Sigma-Aldrich). Copper(II) chloride is filled into the crucible (Figure 3.2a) that is heated to temperature T~550K, at which $CuCl_2$ starts to sublime. Cu(001) crystals are preheated to ~450K for 10minutes and subsequently positioned above the crucible while temperature of the samples is kept at 450K. Deposition rate is adjusted within the range of 0.1ML to 0.25ML per minute. After deposition of a monolayer, samples are post-annealed for additional 5 minutes to ensure homogenous distribution of copper chloride at the surface. Chlorine similarly to nitrogen forms a c(2x2)-like reconstruction of Cu(001) (cf. Fig. 5.4). The cleanness and quality of the Cl-terminated Cu(001) substrates is checked by XPS. In the last step, 20 ML of cobalt are deposited on the prepared substrate as described above. Chlorine atoms, similarly to nitrogens diffuse on the top of the cobalt films, i.e. surfactant-like growth, resulting in c(2x2) chlorine reconstructed cobalt surfaces.

Preparation of Chromium wedge layer on top of Cobalt thin films:

Chromium spacer layer was deposited by means of e-beam evaporation on prepared cobalt film (20 ML). Chromium layer of increasing thickness (from 0 to nominally 8 atomic monolayer) is prepared in steps of equal width and one nominal monolayer height over the total wedge extension of about 3 mm. Half of the sample surfaces is uncovered, such that this area allows for a direct comparison between the bare Co and the Cr covered part of the sample.

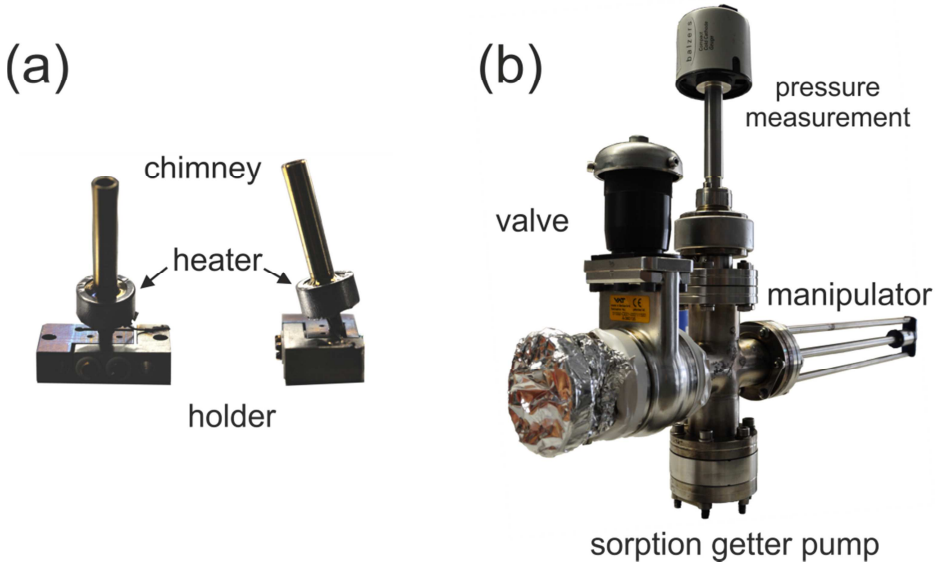

FIGURE **3.2** | (a) Crucible used for thermal sublimation of the molecules and/or copper(II) chloride. Portable vacuum "suitcase" used for the sample transport.

Deposition of molecules:

Molecules are deposited onto prepared surfaces by means of thermal sublimation. Samples are kept at room temperature during the deposition of the molecules. Crucible (Figure 3.2a) with paramagnetic molecules is heated to T ~ 500K for CrTPPCl, MnTPPCl and FeTPPCl molecules. Deposition of MnPc and FeFPc molecules is trickier and temperatures of crucibles were adjusted; such the ratio between the molecules is approximately 1:1 as measured with a Quartz Crystal Microbalance. The 1:1 stoichiometry between the molecules has been verified with the XPS technique by looking at the characteristic fluorine and carbon 1s signals typical for fluorinated metallo-phthalocyanines[36]. For deposition of the molecules, the sample is placed above the crucible. The amount of the molecules is controlled by means of QCMB during deposition and by XPS technique after the deposition.

XAS/XMCD measurement setup:

Magnetic measurements exploiting XAS/XMCD were performed at the Surface/Interface Microscopy (SIM) and X-Treme beamlines of the Swiss Light Source (SLS) located at Paul Scherrer Institut (PSI). Experiments involving Photo-Emission Electron Microscopy (PEEM) presented in chapter 6 were conducted at SIM beamline. SIM beamline operates two Apple II type undulators with permanent magnets delivering 10^{12} photons/s with linear(horizontal/vertical) and circular (left/right) polarization in the energy range 90-2000 eV [for more details see U. Flechsig, et al., AIP Conference Proceedings **1234**, 319 (2010)]. SIM beamline hosts XAS/XMCD endstation equipped with helium flow cryostat (T=50-300K) positioned in the centre of solenoid producing magnetic fields up to 125mT along direction of incoming x-rays. Cryostat is mounted on rotary feedthrough enabling measurements at various angles. XAS/XMCD spectra were acquired in TEY mode and normalized to the flux intensity of the incoming beam. PEEM microscope (Model: LEEM III, Elmitec GmbH) is a permanent endstation of SIM beamline allowing imaging with spatial resolution down to 50nm and energy resolution of 0.2 eV within temperature range T=150-1800 K.

X-Treme beamline is equipped with one Apple II type undulator producing linearly and circularly polarized photons with maximal flux of 4.7×10^{12} photons/s. X-Treme optics allows working in wide energy range from 150eV up to 8000eV (31^{st} harmonics). Experimental chamber at the X-Treme beamline allows measurements at temperature as low as T = 2K and in magnetic fields up to B = 7T. [see C. Piamonteze, et al., J. Synchrotron Rad. **19**, 661 (2012)] Experimental chamber is equipped with a vector magnet, which can produce magnetic field of strength 7 T along the beam direction or field of 2T in the direction perpendicular to the beam in the plane of the synchrotron ring. Spectra measured at X-Treme beamline were acquired in TEY mode and normalized to the flux intensity of the incoming beam.

Sample preparation as described above was carried at the Surface Science Lab located at the east side of the PSI campus, while SLS is located on the west side. For the synchrotron measurements the samples were transported to the beamlines in the portable "vacuum suitcases" (c.f. Figure 3.2b), under the UHV conditions. Suitcase was equipped with a holder for 4 samples and sorption getter pump (SAES), which maintains vacuum inside the suitcase. During the transport, pressure inside the vacuum suitcase did not exceed 10^{-9} mbar.

STM/STS experiments at low temperatures were realised with a LT STM microscope (Omicron Nanotechnology GmbH with Nanonis SPM control system) using mechanically cut $Pt_{90}Ir_{10}$ tips, which were treated *in situ* by Ar sputtering and controlled indentation in the bare Au(111) substrate. The bias voltage was applied to the tip and with these settings, the negative bias voltages result in tunnelling of electrons from the tip into the unoccupied states of the sample. STS spectra were recorded with open-feedback loop and with initial tip conditions 100 mV/500 pA (lock-in frequency 513 Hz; zero-to-peak amplitude: 1.5 mV). Room temperature STM measurements were acquired using Aarhus STM with the Bias voltage applied to the sample. Positive voltage at the sample leads to a tunnelling of tip electrons into unoccupied states of the sample. Aarhus STM uses etched tungsten tip that were treated by Ar sputtering. STM data were acquired in constant current mode and were processed using Gwyddion software.

3.1 Interaction of photons with matter

X-ray based techniques employ an interaction of photons with electrons in the matter. This interaction is described using simplified one-electron picture for the purpose of the thesis. Let's assume photon with energy $E = \hbar\omega$ (E falls within soft X-ray region, i.e. 100 eV < E < 2000 eV). Interaction of incoming photon with the electron is described with the Hamiltonian:

$$\boldsymbol{H} = \frac{e}{m_e}\boldsymbol{p}.\boldsymbol{A} \tag{3.1}$$

, with e being electron's charge, m_e electron's mass, $\boldsymbol{p}$ – momentum of electron and $\boldsymbol{A}$ – is the vector potential of electromagnetic field (photon): $\boldsymbol{B} = \boldsymbol{\nabla} \times \boldsymbol{A}$ and $\boldsymbol{E} = -\frac{\partial \boldsymbol{A}}{\partial t}$.

Incoming photon colliding with electron in the initial state $|i>$ transfers its energy to this electron. Excited electron *"searches"* for new state with energy matching that of the photoelectron, i.e. the electron is transferred into final state $|f>$ with certain probability $w_{i->f}$ given by the Fermi golden rule,

$$w_{\boldsymbol{i}\to\boldsymbol{f}} = \frac{2\pi}{\hbar}| < f|\boldsymbol{H}|i > |^2\rho_f \tag{3.2}$$

, ρ_f denotes density of states of the final energy level and $\hbar$ is reduced Planck constant. Electrons in the periodic potential of crystal lattice are distributed into

energy levels forming a band structure. All energy levels are occupied below Fermi level, i.e. boundary between occupied and unoccupied electronic states at T=0K. Photo-excited electron can thus be transferred only to states above Fermi level. The excited electron can reach empty level only when the energy gained by absorption of the photon is higher than difference between the initial state and Fermi energy; otherwise electron will not find an unoccupied final state. This effect is known as a *photoelectric effect* and is described by following formula:

$$E_f = \hbar\omega - E_i - \varphi \tag{3.3}$$

, where E_f is a kinetic energy of photoelectron, E_i energy of the electron in the initial state, term φ stands for workfunction, the minimal energy needed to excite electron from Fermi level into continuum and the term $\hbar\omega$ is an energy of the photon. When energy adsorbed by electron is higher than the energy of the initial state, but lower than the sum of energies of initial state and the workfunction; electron is excited from the core levels into unoccupied states above the Fermi level, but does not have enough energy to leave the crystal. When kinetic energy of the photoelectron is higher than the sum of the energy of initial state and the workfunction, only then the photoelectron can leave the sample into the continuum with the kinetic energy given by the formula (3.3). Electrons in the atom occupy respective orbitals (i.e. 1s, 2s, 2p, …) and as the charge of nucleus varies from element to element the atomic orbitals have different potential (binding) energy for different elements. One can say that every element has its own fingerprint given by the binding energy of core level states. Using photons of constant energy (e.g. $\hbar\omega$=1000 eV) the photoelectron excited from 1s orbital of the pure carbon would have a kinetic energy of about ~ 715eV, but photoelectron from 1s shell of oxygen excited with photon of the same energy would possess kinetic energy of about ~ 470 eV.

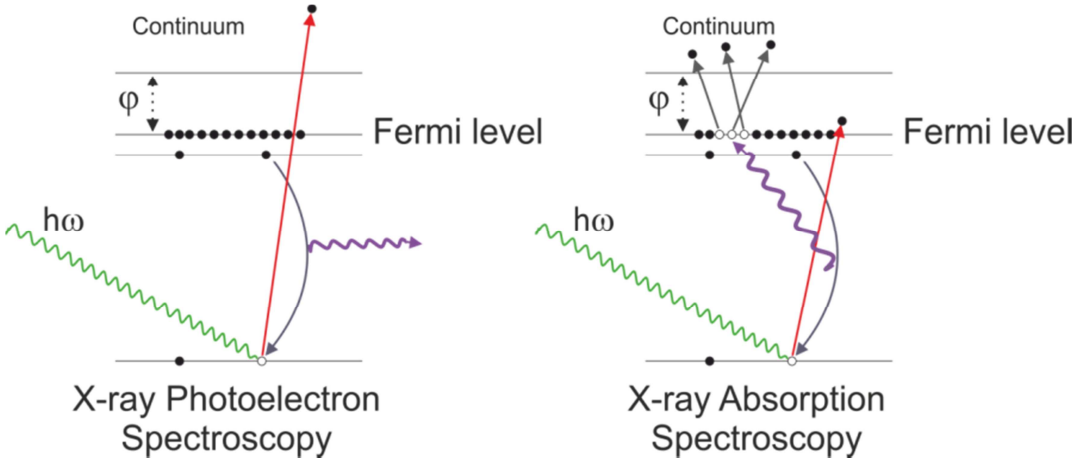

FIGURE **3.3** | Schematics describing the principles of X-ray Photoelectron Spectroscopy (XPS) and X-ray Absorption Spectroscopy (XAS). XPS uses photons of constant energy and measures a kinetic energy of outgoing photoelectrons. XAS method uses X-ray photons of various energies and a probability of transition from core states to Fermi level is probed.

Using x-rays of variable wavelength on the other hand, enables to measure probabilities for transition from core levels to Fermi level given by absorption of x-rays when energy of photon matches that of the given transition, i.e. X-ray Absorption Spectroscopy. Both, XPS and XAS methods provide information about chemical composition of the material and valence state of the probed element. Furthermore, XPS and XAS spectroscopies are capable of unravelling magnetic properties of probed systems when using circularly polarized light.

3.2 X-ray Photoelectron Spectroscopy

The XPS technique is surface sensitive method that enables the semi-quantitative analysis of examined samples. X-rays can penetrate quite deep into the sample due to relatively weak photon-electron interaction. However, the strong electron-electron interaction between photo-excited electrons and the matter limits the mean free path of photoelectrons to few monolayers.

The XPS technique uses x-rays of a constant energy in order to excite electrons from core levels into continuum thus probing occupied states of conducting materials. Photoelectron that is leaving the sample possesses a kinetic energy given by equation 3.3, which is being detected providing information about probed element/material. Photoelectrons are detected through systems of electrostatic lenses directing the photoelectrons towards energy analyser where photoelectrons are discriminated according to their kinetic energy. In the analyser an adjustable magnetic field bends trajectory of the photoelectrons due to Lorentz force and only electrons with the desired kinetic energy are directed towards the detector. Knowing the strength of the magnetic field, the kinetic energy can be determined. Knowing energy of x-rays and the kinetic energy of the photoelectrons binding energy can be readily extracted. The scheme of the principle is shown in Figure 3.3.

Atoms in crystals experience an interaction with the surrounding environment leading to a change in the local electric field, i.e. change of oxidation state, when electrons are transferred from one atom to another, e.g. atom can be either positively or negatively charged. Charging of the probed atom leads to tiny changes in the electrostatic potential resulting in the shift of energy levels due to the additional Coulomb interaction. Electrons in positively charged atom are attracted towards the nucleus stronger and binding energies (energy levels) are therefore increased. In that case, photoelectron requires more energy in order to leave the sample and the kinetic energy of the photoelectron is thus reduced. Similarly, negatively charged atom causes decrease in the binding energy of the electrons and photoelectron therefore gains on the kinetic energy. This effect is known as *chemical shift* and reveals the information about the oxidation state of the probed element.

Absorbing a photon by an electron creates a photoelectron-hole pair. The core hole is immediately filled with the electron from the upper orbitals. As the electron falls down from the higher levels, the photon with the energy given by the difference

between those two states is emitted. The photon interacts with the electrons in the material and excites electron(s) on higher orbitals. This higher order photoelectric process is known as Auger decay. Such a filling of the core holes can be repeated several times in the sample, until the entire energy of the initial photon is not consumed. Auger decay, similarly to first order photoelectric effect, produces photoelectrons having kinetic energy specific for every element and can be thus used from chemical analysis purposes. Sequence of Auger processes creates photo-electrons with small kinetic energies and those photoelectrons do not bear any meaningful information, but rather contribute to the background signal.

XPS spectrum on specific orbitals can consist of either one peak, i.e. singlet (XP spectra of s-orbitals) or of two peaks, i.e. doublet for all the other orbitals. Observation of doublets in the XP spectra is caused by spin-orbit coupling affecting the photoelectron in the final state. Electron in the atomic shell has orbital angular momentum $\boldsymbol{l}$ ($\boldsymbol{l}$=0, 1, 2, 3 for s, p, d and f orbitals, respectively) and spin angular momentum $\boldsymbol{s}$ = ½ or -½. Total angular momentum of the photoelectron is given by $\boldsymbol{j = l \pm s}$. The $\boldsymbol{j}$ value of the photoelectron from s-orbital is determined only by the spin of the electron and because there is no magnetic field breaking time-reversal symmetry. It is therefore not possible to discriminate between electron with $\boldsymbol{s}$ = ½ or $\boldsymbol{s}$= -½. However, higher orbitals with $\boldsymbol{l} \neq 0$ possess small magnetic field proportional to the orbital angular momentum. This field then *"sorts"* photoelectrons according to their total angular momentum $\boldsymbol{j = l \pm s}$.

3.3 X-ray Absorption Spectroscopy & X-ray Magnetic Circular Dichroism

X-ray Absorption Spectroscopy technique uses x-rays of variable energy and investigates the absorption coefficient of the sample. X-ray photons of various wavelengths are produced at the synchrotron. In the synchrotron, bunches of electrons circulate in ring at speed close to the speed of light. To produce photons of a specific wavelength, the electrons need to be accelerated or decelerated. Instead of decreasing their speed, a trajectory of the electrons is altered. The electrons are bended in the magnetic field and at the tangential point of bended trajectory the cone of light propagates further in the tangential direction – c.f. Figure 3.4. The simplest insertion device producing synchrotron radiation is a bending magnet. Instead of using just one magnet, it is possible to increase numbers of bending points inserting multiple magnets in the single row; an insertion device is called undulator. The undulator consists of several magnets placed close to each other and electron which passes through, wiggles and produces photons at each bend (Figure 3.4a). At the end of the undulator the cone of light have smaller angular distribution and much higher intensity compared to the light emitted from bending magnet – see Figure 3.4c. The position of the magnets in the undulator can be shifted in 2

directions producing linearly or circularly polarized light. The change of the gap between the upper and the lower part of the undulator leads to the change of a wavelength of emitted light. Using undulator we gain a full control of the parameters of the x-rays (i.e. wavelength and polarization).

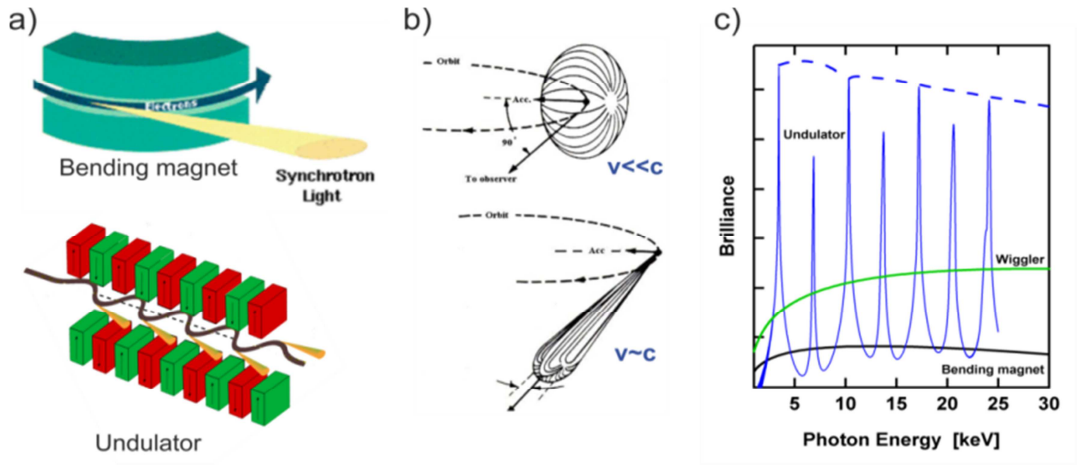

FIGURE **3.4** | Schematic on a production of synchrotron light (a) Light is emitted from a bunch of electrons after its trajectory is bent. (b) The angular distribution of the emitted light depends on the relativistic speed of the electrons. (c) Spectrum of the emitted light from bending magnet, wiggler and undulator. Adapted from[26]

As described above every element has a specific energy of the core levels; a fingerprint of the element. In the XAS, we tune the energy of the x-rays towards the resonance condition (Eq. 3.3). At the resonance, the electron from the core level is excited to the unoccupied states at the Fermi level. The resonance energy is given exactly by the binding energy of the electron in the atom. The excited electron follows the dipole selection rule ($\Delta \boldsymbol{l} = 1$) which means that an electron from s orbital can only be transferred to p orbital, electron from p orbital to d or s orbital and so on. It is also possible that an electron is transferred such that $\Delta l = 2$ (e.g. second order process); however the cross-section of these processes is very small (<1%). Specific transition has its own labelling, e.g. transition of an electron from 1s orbital to Fermi level is denoted as K-edge transition, transition from 2s as L_1-edge, excitations of electrons from 2p orbital as $L_{3,2}$-edge transition (note two subscripts at L, this is due to spin-orbit splitting of the final states), transition from 3s to Fermi level as M_1 edge, from 3p as $M_{3,2}$ edge, from 3d as $M_{5,4}$ edge and so on. The most relevant transitions within scope of the thesis will be K and $L_{3,2}$ edges.

Elements such as oxygen, carbon and nitrogen have the strongest transition from 1s orbital, i.e. K-edge transition. For 3d transition metals, energies of the K-edge transition fall into the hard X-ray region (E > 5keV) where the X-ray absorption coefficient is relatively low. For the investigation of the 3d transition metals we used soft x-rays with energy between 200 and 1000 eV. Compared to XPS which is used to probe the occupied states, X-ray Absorption Spectroscopy explores unoccupied states in the valence band region (these above the Fermi level). The valence band is

responsible for the chemical bonding of the elements and both XAS as well as XPS provide the information about the chemical environment of the probed element (i.e. oxidation state). Further information about the energy levels above the Fermi level can be extracted from XA spectra using the multiplet theory[37].

Absorption coefficient is also related to the polarization of incoming x-rays in relation to the spatial shape of atomic orbitals. Atomic s orbitals have spherical symmetry and the absorption of vertically/horizontally polarized light is exactly the same at any given angle. On the other hand, p orbitals have 3 components (p_x, p_y, p_z) with lobes orientated along Cartesian axis. The absorption coefficient thus depends on the angle of incident and on degree of X-ray polarization. Assume an atom with $p_{x,y,z}$ orbitals orientate along Cartesian axis and an X-ray photon coming in the x direction possessing vertical polarization, i.e. electric component of the photon oscillates along z direction. In this case electron on p_z orbital will interact with the incoming photon and the electrons on p_x, p_y remain unaffected. The p_x and p_y orbitals can be probed in similar fashion, for x-rays propagating in the z direction with electric component of the photon oscillating along the x and y direction, respectively. This phenomenon is called search light effect[26] and is widely used to determine orientation of atoms, molecules at the surfaces or in bulks exploring the difference in the absorption coefficient between horizontally and vertically polarized light, X-ray Linear Dichroism (XLD). The XLD technique is further divided to X-ray Natural Linear Dichroism (XNLD) and X-ray Magnetic Linear Dichroism (XMLD). Both uses linearly polarized light, however the XNLD signal is given by the difference in charge distribution along specific directions, while XMLD signal is related to the variation of the magnetic order along specific axis as magnetic ordering correlates with the charge distribution[26]. The XMLD is mainly used to investigate the magnetic ordering in the antiferromagnetic materials and/or multiferroics. Antiferromagnetic materials have zero net magnetization $\boldsymbol{M}=0$, however, there is an ordering along specific axis and magnetization square is non-zero $\boldsymbol{M}^2\neq 0$. Nice examples how XNLD and XMLD are used can be find elsewhere[26].

X-ray absorption spectroscopy exploiting circularly polarized light is used to study magnetic ordering in samples with non-zero magnetization or chiral distribution of the electric charges within chiral crystals. Magnetic properties are investigated by technique called X-ray Magnetic Circular Dichroism (XMCD). The Chiral distribution of the electric charge is recognized with X-ray Natural Circular Dichroism (XNCD). In general the XNCD signal is very often connected with XMCD effect and requires careful analysis. More on XNCD technique can be found in Ref.[22].

XMCD technique is very unique method which investigates magnetic properties of the materials. It is a very sensitive method able to resolve magnetic moments of the order of $0.01\mu_B$ (Bohr magnetron). It is element specific, surface sensitive and can reveal information about the chemical state. The principle of XMCD is explained in one-electron two-step model shown in the Figure 3.5a. Circularly polarized photon bears an angular momentum $L_z = +h$ or $-h$ (+ for left-handed/anti-clockwise and – for right-handed/clockwise rotation of photon). Photon absorbed by electron in the

core level transfers its angular momentum onto the electron due to conservation of total angular momentum.

Spin-orbit coupling within the core level causes that excited electrons are spin-polarized (number of photoelectrons with spin up and down is not equal) for given polarization of the x-rays (Figure 3.5a). In the next step, the electron is transferred into the unoccupied state at the Fermi level. In magnetic materials, the number of electrons with spin up and with spin down at the Fermi level is unbalanced. Therefore photo-electrons with spin-up polarization see different number of unoccupied states than is seen by spin-down electrons. The XMCD spectra are thus given by the difference between the XA spectra acquired with circularly right and left polarized light (Figure 3.5c).

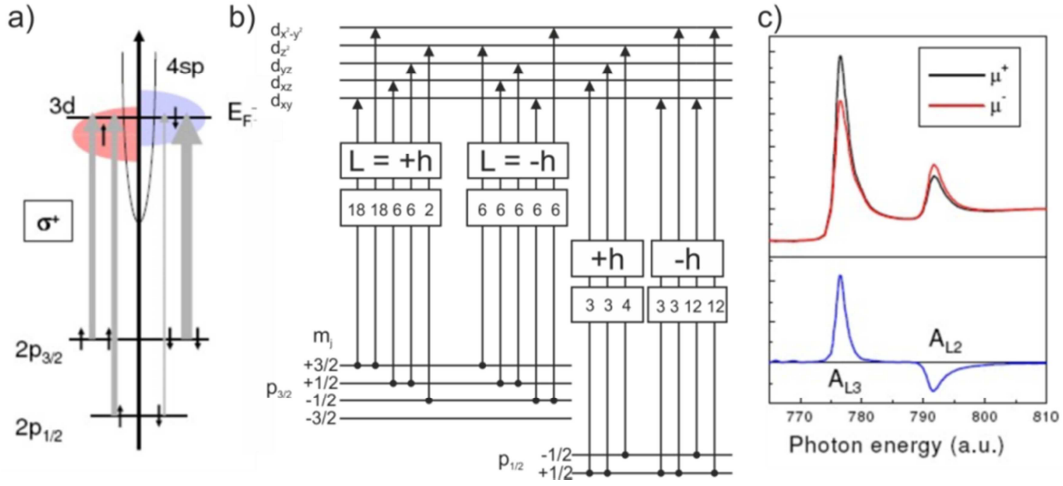

FIGURE **3.5** | One electron two-step model describing X-ray Magnetic Circular Dichroism technique. (a) Circularly right polarized x-rays excite majority of spin down electrons from 2p core level. (b) Relative transition probabilities for electron excited from 2p shell into the 3d orbitals with circularly left or right polarized light for 2p-electron with s=½. c) XA spectra acquired with circularly left and right polarized light and XMCD spectra given by their difference.

Presence of the spin-orbit coupling in the core level is necessary in order to acquire the spin-polarized photo-electrons. However, the XMCD effect was first observed at K-edge of Fe[38], where electrons on 1s orbital do not experience spin-orbit coupling. The XMCD effect can also be observed at the K-edge, but requires that the valence states are spin-split by external magnetic field or due to the internal exchange coupling with the surrounding. XMCD signal measured at the K-edge is very weak and therefore is used only in the specific type of experiments. The K-edge circular dichroism is of particular interest in the magnetism of light non-magnetic elements, i.e. oxygen, nitrogen or carbon.

Question is how the absorption coefficient of the x-rays is measured as the electron excited from the core level does not leave the sample and information is still enclosed within the atom. The principle is quite simple and makes use of the

Auger decay. Absorption of photon creates electron-hole pair. The core hole is immediately filled by an electron from higher orbitals via Auger process. This process produces slow secondary electrons leaving the sample, which is being ionized. Sample is grounded and flowing current is measured as a function of photon energy. This mode of data acquisition is called Total Electron Yield (TEY) as we receive information about total number of electrons that have left the sample. A big advantage of the TEY acquisition mode is an enhanced surface-sensitive due to the short mean-free path of the secondary electrons. Other acquisition modes are Partial Electron Yield (PEY) and Total Fluorescence Yield (TFY). In PEY mode, sample is on higher potential compared to the surrounding environment and only those photoelectrons whose kinetic energy is higher than the sample potential can be emitted. In the TFY mode the total amount of the x-rays emitted from the sample is measured. This mode is particularly interesting for studies on bulk properties as mean-free path of photons is much higher compared to that of photoelectrons. The XMCD signal can be additionally acquired in the transmission mode where the amount of the light transmitted through the thin sample is measured[26].

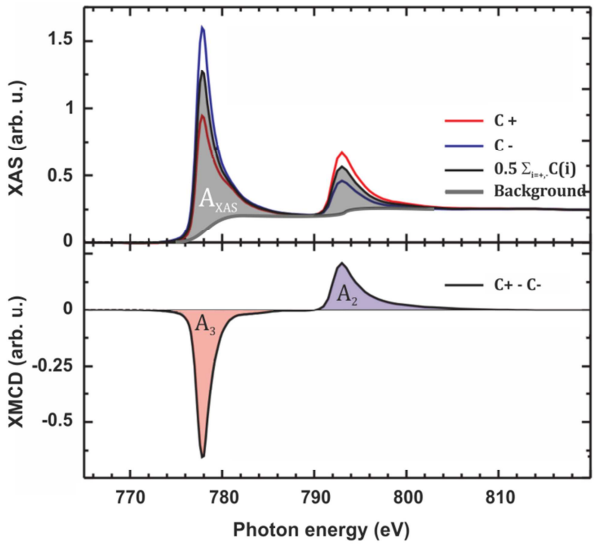

$$m_L[\mu_B] = -4\langle N_h\rangle(A_3+A_2)/3A_{XAS}$$

$$m_{SE}[\mu_B] = -2\langle N_h\rangle(A_3-2A_2)/A_{XAS}$$

FIGURE **3.6** | Principle of sum rule analysis explained on XAS/XMCD spectra of Cobalt (001) thin film.

The most important feature of XMCD technique is its ability to deliver information on absolute values of the spin and orbital magnetic moments. This information can be extracted from the spectra using the sum rules analysis (see Figure 3.6)[39,40]. The absolute value of the orbital and spin angular momentum can be calculated within 5% uncertainty. However, the early 3d transition metals (Ti, V, Cr, Mn) experience the core hole-valence electron correlation effect, which makes the sum rule analysis difficult to interpret for these elements[41].

3.4 Photo-Electron Emission Microscopy

Another technique used to investigate magneto-organic interfaces within the scope of this thesis is Photo-Electron Emission Microscopy (PEEM). PEEM is an imaging technique used to extract information on spatial distribution of various order parameters, e.g. element concentration, valence state, magnetization, etc. PEEM uses synchrotron x-rays that are being focused on the sample. Incoming x-rays excite photo-electrons from the sample as described before and these photoelectrons are consequently collected by high voltage optics, accelerated and collimated towards the fluorescence screen, where the image of the sample in real space is captured with a CCD camera. PEEM in combination with x-rays of different polarization and/or wavelength can be used to study various properties.

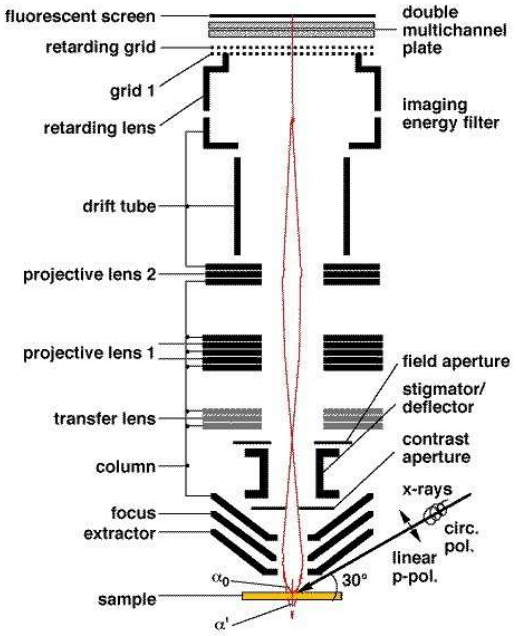

FIGURE **3.7** | Schematics of Photo-Electron Emission Microscope. Image taken from www.physik.fu-berlin.de/einrichtungen/ag/ag-kuch/research/techniques/peem/index.html

It is for example possible to investigate a spatial chemical composition of the sample tuning energy of x-rays towards absorption edge of desired element in a few consecutive measurements. Acquiring images at different x-ray energies corresponding to two valence states of probed element a map of oxidation state can be revealed. The biggest strength of PEEM technique is however, recognized in the investigation of the magnetic properties, when PEEM is complemented with the XMCD allowing to resolve magnetic properties spatially at the surface of magnetic materials. Using XMCD-PEEM approach researchers showed how an antiferromagnet is exchange coupled with the ferromagnetic substrate underneath, for example[42]. Besides the microscopy modes, PEEM can also be used for

spectroscopy measurements providing full approach on spectro-microscopy correlation.

3.5 Low Energy Electron Diffraction

Low Energy Electron Diffraction method provides information about a crystallographic structure at the surface of material. Heart of LEED apparatus is electron gun, which produces electrons that are accelerated towards the sample, where they are reflected back towards LEED optics and afterwards projected on the fluorescence screen. Information about the sample's surface topography is carried by low energy electrons and the image projected on fluorescence screen is the reciprocal representation of the surface lattice. Reciprocal lattice of the sample can be calculated using de Broglie formula on the wavelength of particles with kinetic energy E:

$$\lambda = \frac{h}{\sqrt{2mE}} \tag{3.4}$$

, where h is Planck constant and m – mass of an electron. In order to resolve sample's lattice in real space, application of Fourier transformation on the resolved LEED pattern is required. Details about the LEED technique can be found elsewhere[43]. In the scope of this thesis, the LEED technique is used to determine a type of surface reconstruction and molecular assembly at various surfaces.

3.6 Scanning Tunnelling Microscopy

LEED technique provides very useful information on the periodic arrangement of surfaces and adsorbents at the surfaces. Big disadvantage of LEED is that in order to acquire LEED pattern, relatively large area of the surface must possess periodic arrangement. In case a surface shows amorphous (short-range) ordering, LEED will resolve concentric circles on the fluorescence screen. Therefore there is always a demand for atomic scale imaging in real space. In 1981, researchers (Gerd Binning and Heinrich Rohrer) from IBM Zürich invented Scanning Tunnelling Microscopy (STM) technique that allows acquiring atomically resolved images of surface topography on conducting substrates in real space. STM exploits quantum tunnelling phenomenon. Quantum objects such as electrons and/or atoms are constrained by the Heisenberg principle of uncertainty, which says that parameters which do not commute cannot be observed simultaneously. We can only measure particle's position without knowing its exact speed or we know particle's speed, but do not know where the particle is located. Quantum objects are described by a wavefunction and square of the wavefunction provides information about probability that the particle with momentum p can be found in the volume V. Such definition of the particle properties may have quite interesting consequences on the behaviour of the quantum objects.

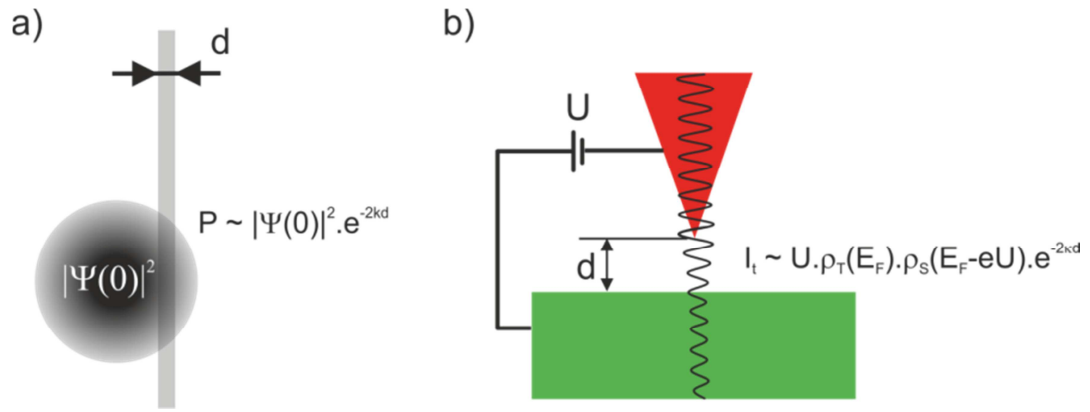

FIGURE **3.8** | Principle of quantum tunnelling. (a) Probability that electron is found on the other side of the wall is proportional to the square of the wavefunction and to the thickness of the barrier. The decay term κ is related to the "energy" of the wall, i.e. its thickness. (b) In the scanning tunnelling microscope the tunnelling current is measured. The tunnelling current is proportional to the distance between the sample and the tip and to the density of states of both the sample and the tip.

Let us consider a barrier in the form of very high thin wall. In the classical picture, if we want to get the particle on the other side of the barrier we have to increase the energy of the particle above the wall threshold. However, in the quantum world, if the particle is brought very close to the barrier, there is non-zero probability that particle can be found on the other side of the wall. Particle actually does not climb over the wall, but rather tunnel through the barrier (Fig 3.8a). To some extend, it is also possible to calculate the probability of a man "tunnelling" through a concrete wall. The probability of this event is non-zero, but it is so close to zero, that it would take nearly infinite number of trials until the tunnelling will really happen.

In the STM, electrons from one electrode (tip) tunnels through the barrier (vacuum) to other electrode (sample) if these two electrodes are close enough the wavefunctions of both electrodes start to overlap (see Figure 3.8b). The relatively sharp tip with the applied bias voltage is brought close towards the sample, until a tunnelling current is flowing between the tip and the sample. The tunnelling current is proportional to the density of states at the sample surface and the tip and correlates with the distance between them (Figure 3.8b). However, the tip and sample are not in the direct contact. The fact that there is no direct contact between these two electrodes suggests that position of one of them can be changed without surface being damaged. Distances at which tunnelling effect occurs are in order of nanometres, where precise positioning is controlled with piezo-electric elements. Piezoelectric effect transforms energy of the electric potential into mechanical deformations, i.e. piezo-electric material is elastically deformed upon application of an electric voltage. Topography images are acquired by measuring tunnelling current while position of the tip is changed in the XY plane. Topography images can be acquired in two modes. In first mode, STM keeps tunnelling current between the tip and the sample at constant value, which requires use of a feedback loop to adjust

distance (z-axis) between the tip and the sample, in case of defects at the surface, e.g. step edges, impurities. Second mode, which is used less frequently, keeps distance between the sample and the tip constant and measures variation of tunnelling current while scanning in XY plane. This mode requires very flat samples, as z-axis piezo component does not compensate for big steps at the sample surface and there is possibility of tip crashing into the surface of the sample. The STM is able to image the topography of surfaces of the conducting materials in the real-space and also to image non-periodic structures which cannot be easily resolved with diffraction methods.

One of the great pros of Scanning Tunnelling Microscope is capability of measuring local density of states (LDOS). Tunnelling current flowing between the tip and the sample at given bias voltage U is an integral of the density of states within the energy range from 0 to eU. Performing numerical or experimental derivation of the current over bias (dI/dV ~ LDOS) we can extract information on local density of states at the specific energy. Experimental method of acquiring dI/dV works as follow; alternating voltage of small amplitude with frequency f is added to an applied bias voltage, which then results in modulation of tunnelling current. In order to avoid variations in the LDOS caused by the changing distance, the tip is kept at fixed position above the sample whilst bias voltage is swept across the voltage range (0, U). Modulated bias signal and tunnelling current are fed into lock-in amplifier that compares amplitude of both of them at the specific frequency f and outputs the dI/dV signal. Scanning Tunnelling Spectroscopy can be performed at any position on the sample providing an opportunity to study spatial variation in LDOS at sample's surface[44].

4

Exchange Coupling of CrTPP Molecules to Co(001) Substrate

Spin-bearing molecules offer a wide range of tuneable chemical functionalities[13,16,36,45] that derive from the interaction of the metal centre with the planar ligands. Upon adsorption at the surfaces, novel properties may arise when the magnetic and electronic characteristics of the metal-organic species are subtly modified by the molecule-substrate interaction. The magnetic exchange coupling of the magnetic moment of metallo-porphyrins or metallo-phthalocyanines with that of ferromagnetic (FM) substrates (Co and Ni) was found to induce stable magnetic order in the paramagnetic molecules at and above the room temperature[4,5,14]. So far studied metallo-phthalocyanines and –porphyrins were found to align their magnetic moments parallel (i.e. ferromagnetic coupling) to those of the bare FM substrate. Origin of this alignment has been much discussed[4,5,14,45,46] and assigned either to direct or indirect magnetic exchange coupling via the chemical bonds across the interface. Particularly interesting is a case, when AFM coupling can be achieved between two magnetic materials. To date, an antiferromagnetic (AFM) indirect exchange interaction has been reported for magnetic molecules assembled on oxygen reconstructed Ni and Co substrates[13,16] or when a graphene interlayer[17] was introduced between the molecule and substrate. An indirect AFM coupling was also observed for the rare-earth double-decker Terbium bis-phthalocyanine adsorbed on a metallic FM substrate, with one of the phthalocyanine macrocycles acting as an interlayer[47]. However, for transition-metal porphyrins and phthalocyanines on bare FM substrates an AFM coupling has never been observed. In this chapter we present study of Cr(II)-tetraphenylporphyrin (CrTPP) molecules adsorbed on a FM bare Co substrate. The observed AFM coupling between the Cr ion, with less than half-filled 3d-shell and the Co substrate is explained by a 90° indirect exchange coupling mediated by nitrogen atoms within the porphyrin ligand.

*Parts of this chapter have been published in: J. Girovsky, et al. *Phys. Rev. B* **90**, 220404(R) (2014).

4.1 XPS & STM study of CrTPP/Co(001)

Upon deposition of CrTPPCl species on cobalt thin films, the actual species, as resolved by XPS and STM technique, are Cr(II)TPP molecules. Cr(III)TPPCl molecules transform upon contact with the substrate due to the release of the Cl ligand as described further below. The chemical state of the CrTPP(Cl) molecules adsorbed on the bare cobalt substrate is investigated by XPS (Figs. 4.1a,b). At first, a multilayer (~10 ML) of CrTPPCl molecules is deposited on clean Au(111). The XP spectrum acquired at Cr $2p_{3/2}$ region resolves the peak maxima at a binding energy of E_B~576.8 eV (Fig. 4.1a, blue dots) indicating a 3+ oxidation state of Chromium ion. This is expected due to the presence of the axial chloride ligand. In contrast, the position of the Cr $2p_{3/2}$ peak for the single layer of CrTPP(Cl) molecules on Co(001) is found at a lower binding energy E_B~575.0 eV revealing a change of the oxidation state of the Cr ion from 3+ to 2+.

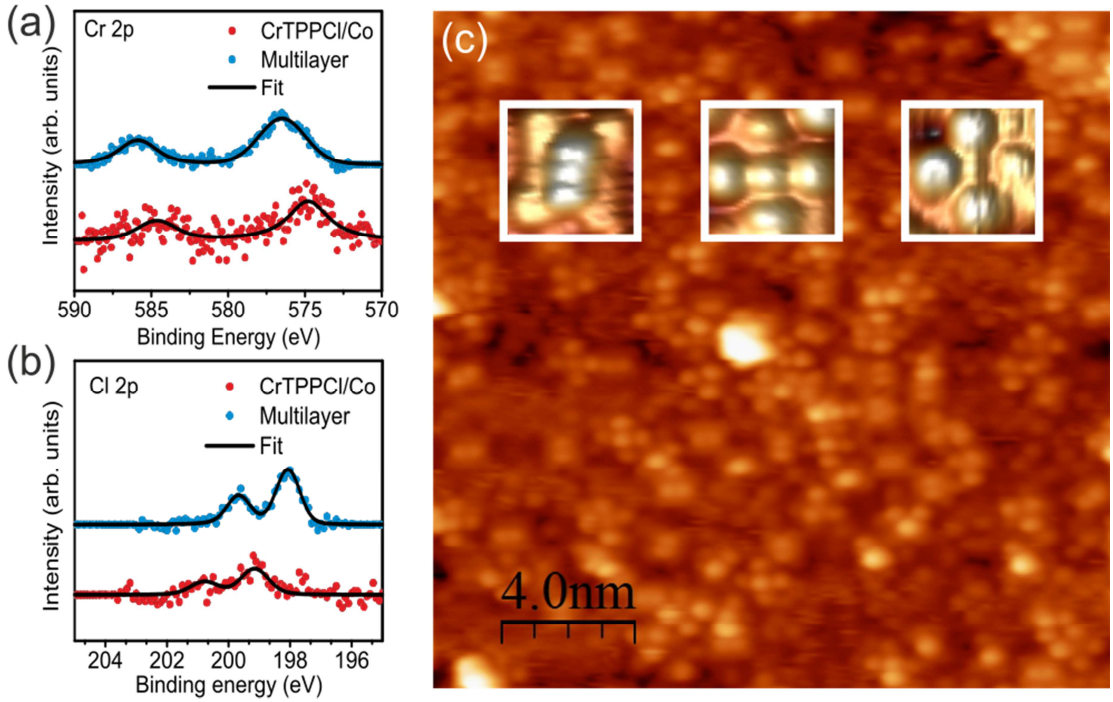

FIGURE **4.1** | XP spectra acquired at the 2p core levels of Cr (a) and Cl (b) for a single layer of CrTPP molecules adsorbed on Co(001) substrate (red dots) and a multilayer of CrTPP-Cl species deposited on Au(111) (blue dots). The solid lines give the results of a Gaussian-Lorentzian fit of the spectra. (c) Scanning tunnelling micrograph of CrTPP molecules on Co(001). Three characteristic patterns observed on the sample are shown in the insets and assigned to different conformations of the molecules (6-lobe, 5-lobe, 4-lobe, from left to right). STM Image acquired at U=−2.1 V, I_t=−10 pA and T=300 K.

In Fig. 4.1b, the XPS data measured at the Cl 2p level show peak maxima at higher binding energy for CrTPPCl multilayer in comparison to that found for CrTPP

monolayer on Co(001). The shift in the position of peak maxima suggests the chlorine loss upon adsorption of the molecules on the metallic Co substrate and evidences strong interaction of chlorine atoms with underlying Co substrate[12].

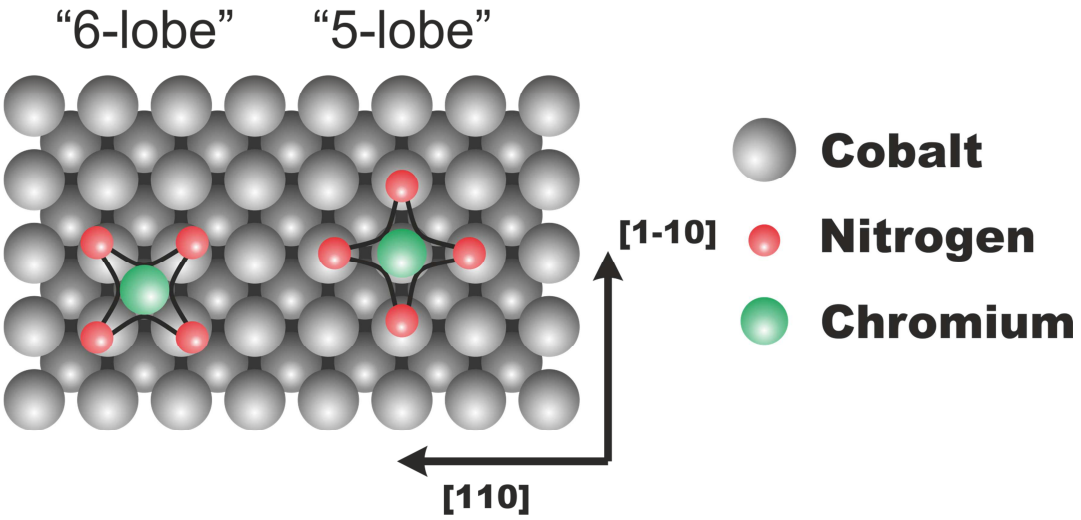

FIGURE **4.2** | Proposed adsorption schemes for “6-lobe” and “5-lobe” species as resolved by STM. In the “5-lobe” configuration CrTPP molecules are expected to adsorb with nitrogen (red) and chromium (green) atoms on-top of the underlying cobalt atoms (grey). The N-Cr-N linkage of CrTPP molecules in the 5-lobe configuration is parallel with <110> directions. The “6-lobe” adsorption configuration resolves nitrogen atoms sitting on top of the cobalt atoms with the chromium ion at the hollow site. The N-Cr-N linkage in this case aligns along the <100> direction.

Investigation of spatial distribution and shape conformations of the adsorbed CrTPP molecules on Co(001) substrate is explored by STM (Fig. 4.1c). CrTPP molecules are resolved to adsorb randomly at the surface. STM further resolves three different conformations of the molecules characterized by 6, 5 and 4-lobes species (cf. insets in Fig. 4.1c). The majority of the molecules (~ 90%) are found in the six- and/or five-lobe conformation (Fig. 4.1c, left and middle inset, respectively). As these conformations are in the majority, we attribute them to CrTPP molecules, those without an axial ligand and being in the oxidation state 2+ as resolved by XPS.

The four-lobe species (right inset of Fig. 4.1c) are assigned to molecules with an axial ligand. The axial ligand can be either Cl or any other common contaminant present in the residual gas in the chamber. The ratio between the 5- and 6-lobe species is determined to be very close to 1:1. The specific orientation of both conformations is analysed and further discussed. The 5-lobe species adsorb with the N-Cr-N linkages aligned along the substrate’s crystallographic <110> axis. For this conformation, nitrogen atoms and chromium ion of the molecule resides on top site of underlying cobalt atoms (Figure 4.2). The rectangular shape of the 6-lobe species preordains the molecules to adsorb in two different orientations with respect to the substrate’s crystallographic axis. In comparison to 5-lobes species, the

6-lobes molecules align the N-Cr-N linkage along the hard axis (<100> directions) of the magnetization of the substrate (Figure 4.2). Molecules in 6-lobe conformation are assumed to adsorb on the surface with the nitrogen atoms sitting on the top of the cobalt atoms and chromium ion residing at the hollow site (Figure 4.2). The two different orientations of the 6-lobe species are equally present on the surface. The bright spots at the sides of the four- and five-lobe species resolved by the STM are the phenyl rings of the TPP ligand. Note that the six-lobe conformation with rectangular shape is attributed to a saddle-shape conformation (Fig. 4.1c, left inset). Saddle-shape indicates a characteristic tetrahedral distortion in the porphyrin macrocycle upon adsorption[48].

4.2 XAS/XMCD study of CrTPP/Co(001)

Prior the magnetic measurements samples have been magnetized by an external magnetic field applied along the Co[110]-direction, an easy-axis of the substrate magnetization. The geometry during the XAS/XMCD experiments is determined by sample's [110]-axis, the surface normal $\boldsymbol{n}$ and $\boldsymbol{k}$-vector of the circularly polarized x-rays lying in one plane. The angle $\boldsymbol{\theta_k}$ between the x-rays $\boldsymbol{k}$-vector and the surface normal $\boldsymbol{n}$ is set to 70°. In this geometry we predominantly probe the in-plane components of the magnetic moments of the substrate (white arrows) and of the molecules (yellow arrows) (Fig. 4.3a).

The direction of the substrate magnetization is flipped by applying an external magnetic field $\boldsymbol{H}$ with a magnitude of $|\boldsymbol{H}| \sim 120$ mT. The XA/XMCD spectra are measured in remanence. XA spectra of the substrate recorded at the Co $L_{3,2}$ edges with circularly polarized x-rays of opposite helicities, denoted as C^+ and C^-, are shown in Fig. 4.3b. These spectra together with the XMCD signal, given by the difference of C^+ and C^-, indicate a magnetically saturated Co substrate. Cooling from 300 K down to 70 K reveals a subtly increased XMCD magnitude which reflects a temperature dependent saturation of the Co magnetization[12,16]. In the same configuration at room temperature the relatively weak XMCD signal at the Cr $L_{3,2}$ edges reveals that magnetic moment of the Chromium ion couples antiferromagnetically with respect to the substrate magnetization (Fig. 4.3c). Further, the magnitude of the Cr XMCD signal increases by about a factor of two at temperature T=70 K (Fig. 4.3d) when compared to room temperature data.

Such a notable increase in the magnitude of the XMCD signal suggests a relatively weak exchange coupling between the CrTPP molecules and bare ferromagnetic cobalt substrate. Detailed analysis of the XA spectra at the Cr $L_{3,2}$ edges reveals broad features with two well resolvable peaks at the photon energies of 576.0 eV and 577.5 eV, respectively. The shape and the position of the peaks in the XA spectra indicate Cr ion in a 2+ oxidation state[49]. The observation of the actual Cr(II)TPP species on bare cobalt substrate is in agreement with the previous study on MnTPPCl/Co(001)[12,50], where it was found that these molecules lose the axial chlorine ligand upon adsorption at the substrate changing thus oxidation state from

3+ to 2+. Based on the XPS and XAS data we conclude the Cr ion in the CrTPP molecules possesses four unpaired electrons in the 3*d*-shell with the corresponding electronic configuration $(d_{xy})^1$, $(d_{\pi})^2$ [$(d_{xz})^1$, $(d_{yz})^1$] and $(d_{z^2})^1$, i.e. the high spin state with spin moment S=2[49].

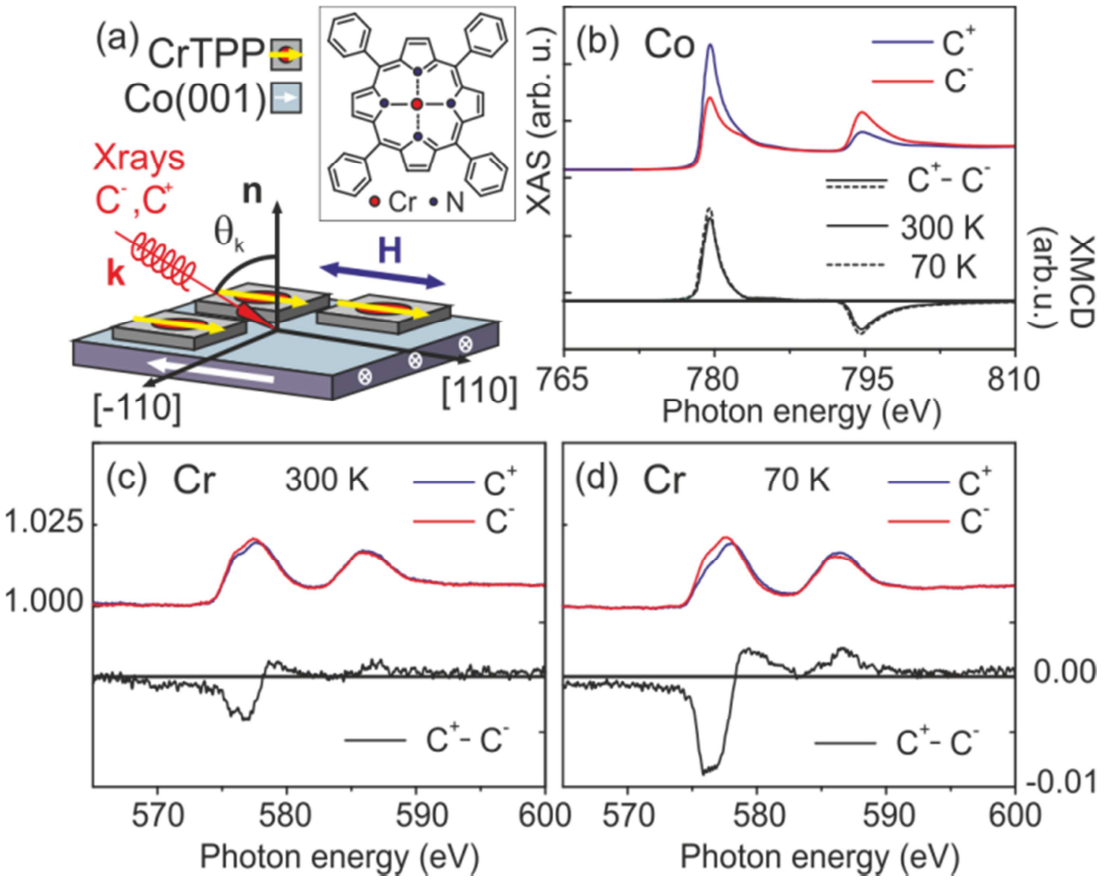

FIGURE **4.3** | Setup of the XAS/XMCD experiments and XAS/XMCD of CrTPP/Co(001) system. (a) CrTPP molecules adsorbs flat on the Co(001) substrate. The AFM coupling of the molecules with respect to the substrate is depicted by the yellow and white arrows. A scheme of CrTPP species is shown in the inset. (b) XA acquired with Circ$^+$ (blue) and Circ$^-$ (red) polarized x-rays and XMCD spectra (black and dashed lines) acquired at the Co $L_{3,2}$ edges of the substrate, at 300 K and 70 K. XA and XMCD spectra of the CrTPP molecules measured with circ$^+$ (blue) and circ$^-$ (red) at the Cr $L_{3,2}$ edges at 300 K (c) and 70 K (d), respectively.

The observed antiferromagnetic exchange coupling between the CrTPP and the Co surface can have several possible origins. One of the possible explanations suggests a case that CrTPPCl adsorbs in top-down orientation (i.e. with chlorine placed between Cr and Co); similarly CrTPP, after Cl loss, may re-adhere to the Cl present on the substrate. The XAS/XPS and STM data evidence that a predominant fraction of the Cr ions (~90%) is detached from Cl, some Cr ions may, however, still be coupled via Cl and thereby undergo a 180° AFM superexchange coupling via Cl to the Co substrate spins. To examine this possibility, we have prepared a chlorine

covered Co(001) substrate on which we have deposited CrTPPCl molecules. XAS spectra measured at the chromium $L_{3,2}$ edge for such system indicate the chromium ion to be in the 3+ oxidation state (Fig. 4.4b,c), hinting that chlorine atom is not present either below or above the chromium ion in CrTPP/Co(001) system.

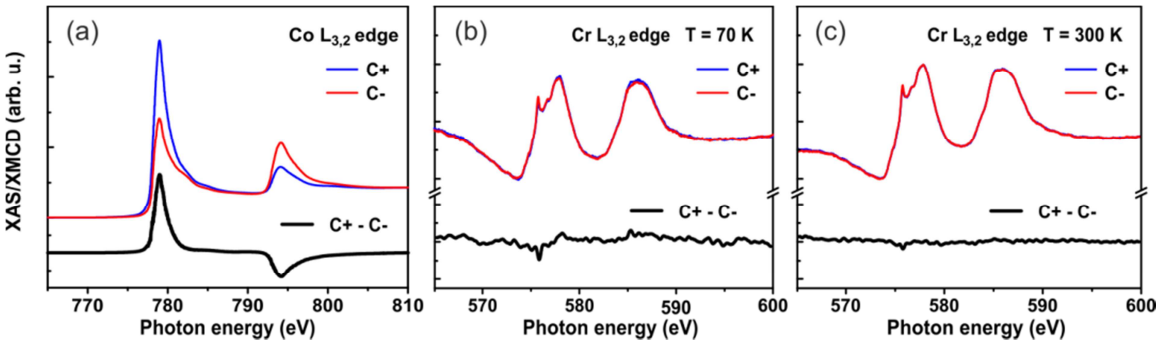

FIGURE **4.4 |** XAS and XMCD of CrTPP(Cl) molecules deposited on a chlorine-treated cobalt(001) substrate measured at the Co $L_{3,2}$ edge (a) and at Cr $L_{3,2}$ edge, at 70K (b) and 300K (c). The Cr XMCD spectra resolve a very weak, almost negligible AFM alignment of the chromium magnetic moments with respect to the substrate magnetization. Position of XAS maxima at Cr L_3 edge corresponds to Chromium oxidation state 3+. XMCD spectra resolve negligible exchange coupling between CrTPP(Cl) molecules and Cl-terminated cobalt substrate.

Subsequently we investigated the magnetic coupling with x-ray magnetic circular dichroism (XMCD). A comparison of the XMCD spectra of CrTPP(Cl) molecules on the bare cobalt substrate (Fig. 4.3c) and of CrTPP(Cl) species adsorbed on the chlorine covered cobalt substrate at room temperature (Fig. 4.4c) reveals a significant difference. There exists no measureable Cr – Co exchange coupling for the molecules on the chlorine terminated Cobalt substrate. Cooling the sample to 70K does not increase the XMCD signal observed for CrTPPCl molecules on the chlorine terminated cobalt substrate (Fig. 4.4b). Consequently, the XMCD spectra shown in Fig. 4.4 demonstrate that any magnetic exchange coupling between CrTPP(Cl) molecules and cobalt substrate via a chlorine bridge remains below the limit of detection, i.e. is extremely weak. This data and analysis provides considerable evidence that the observed AFM exchange coupling between the Cr ion in the molecule and the Co substrate for CrTPP(Cl) on Co is not mediated by a chlorine atom underneath the CrTPP.

4.3 DFT+U calculations

DFT+U calculations have been performed to study the magnetic exchange coupling between Cr-porphine (Cr-P) molecules and the Co(001) surface. Details of the employed computational method can be found elsewhere[25,45]. The Coulomb *U* and exchange *J* parameters were 4 and 1 eV, respectively[51], the generalized-gradient approximation[52] was used, and van der Waals dispersion corrections were taken into account[53]. The Cr-P molecule is computed to adsorb preferably in the hollow

site position, with a distance of 3.1 Å between the Cr ion and the topmost Co layer. This would correspond to 6-lobe species resolved by STM. The chromium ion is calculated to be in a high-spin state $S \approx 2$ and to couple antiferromagnetically to the Co substrate magnetization. In Fig. 4.5b the local magnetic density of states (DOS) of Cr-P adsorbed on the Co(001) substrate is presented. The d_{xy}, d_{xz}, d_{yz}, and d_{z^2} orbitals are singly occupied, i.e., the Cr ion has a less than half-filled 3*d*-shell. The d_{π} orbitals [note that only one of (d_{xz}, d_{yz}) is shown] are practically degenerated, as dictated by the symmetry for square-planar complexes. The $d_{x^2-y^2}$ orbital of Cr is split into bonding and antibonding molecular orbitals; the bonding molecular orbital at about −5.2 eV is partly occupied, due to σ-donation from the ligands to the metal centre (and back-bonding)[54].

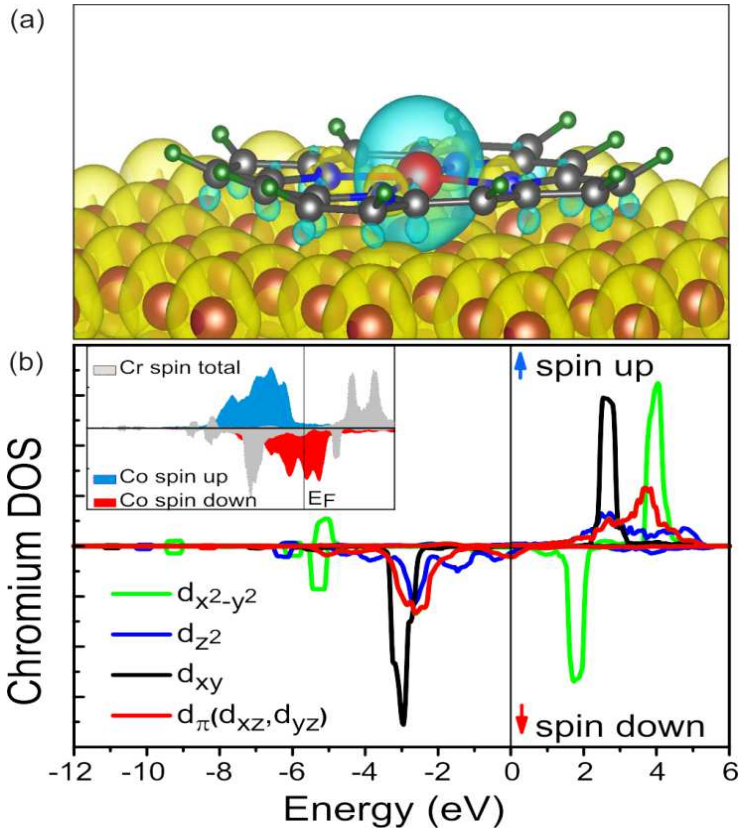

FIGURE **4.5 |** DFT+U calculations of Cr-P adsorbed on Co(001) substrate. (a) Plot of the magnetic spin-density isosurfaces of the Cr-P/Co system. Yellow (blue) coloured hypersurfaces depict spin-majority (spin-minority) magnetization. (b) Spin-resolved density of states calculations of Cr d-orbitals reveal AFM coupling of the spin moment of the Cr ion to that of Co. The inset shows the spin resolved density of states of the Co substrate with spin-up (blue) and spin-down (red) bands, and the spin-polarized total DOS of Cr in grey.

The magnetic isosurface around the Cr ion has an elongated shape along the normal direction (*z* axis) (Fig. 4.5a), which is also indicative of a predominantly unoccupied $d_{x^2-y^2}$ orbital. The inset of Fig. 4.5b shows the DOS for the minority (red) and

majority (blue) spin bands of the spin-polarized Co substrate; the AFM coupling of the Cr spin to the Co substrate spin is apparent from its occupied DOS being in the spin-down channel (grey shaded area). The hybridization between the molecule's and the substrate's electronic states is best seen from the charge density plot (see Fig. 4.6).

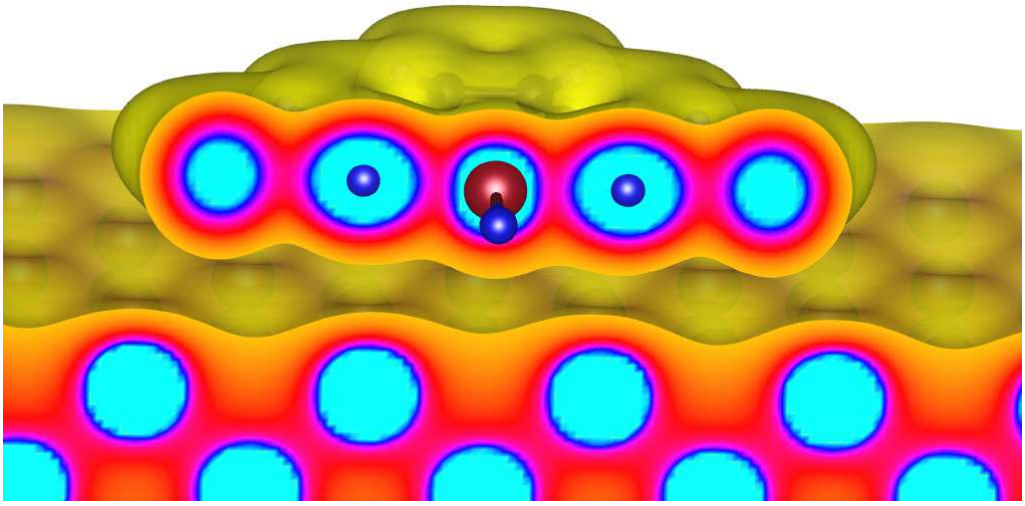

FIGURE **4.6 |** Isosurface of the charge density calculated for Cr-P on fcc Co(001) substrate. The lobe of charge density around the chromium towards the cobalt substrate may suggest subtle overlapping of the chromium 3*d*-orbitals with cobalt 3*d*-orbitals. Note however, that the chromium atom sits in the hollow site of the cobalt substrate which indicates low interaction here.

4.4 Discussion

The so-far observed coupling mechanisms between the metal-organic species and magnetic substrates can be classified into four schemes: i) direct FM exchange coupling between the central ion of the molecule and the substrate[14], and three types of indirect magnetic exchange coupling: ii) indirect 180° AFM coupling via oxygen or graphene[13,16,17], iii) indirect 90° FM coupling[4,5,12,25] and iv) oscillatory RKKY exchange coupling through an interlayer with a substrate[18]. The 180° indirect exchange coupling via chlorine has been excluded based on the experiments with the CrTPP(Cl) molecules deposited on the chlorine c(2x2) reconstructed cobalt(001) surface where the negligible the XMCD signal at the Cr $L_{3,2}$ edge was resolved (see Figure 4.4).

None of the above listed exchange coupling schemes can appropriately describe the here observed AFM coupling of CrTPP to Co(001). Employing the Goodenough-Kanamori-Anderson (GKA) theory[28] as a guidance, we can model the AFM coupling of CrTPP to Co(001) as an AFM indirect 90° exchange coupling. The Cr ion in the CrTPP, not the CrTPPCl molecule, is found in the oxidation state 2+ on the Co surface, implying a $(d_{xy})^1$, $(d_{\pi})^2[(d_{xz})^1, (d_{yz})^1]$, $(d_{z^2})^1$ electronic configuration (left part

of Fig. 4.7) and high-spin state S=2, as evidenced by the DFT+U calculations (Fig. 4.5). The magnetic coupling of the Cr d-shell electrons with the substrate can occur either by direct exchange interaction with the out-of-plane orbitals of the Co atoms [14,55] or via indirect exchange interaction through the nitrogen orbitals[5,12,25]. Since a strong direct exchange interaction (overlap between d_{z^2} orbital of Cr and out-of-planes orbitals of Co) would be accompanied by FM coupling[14] and smaller temperature difference in the Cr XMCD signal, the AFM coupling is assigned to an indirect coupling via the nitrogen electrons. We note, however, that a broadening of the Cr d_{z^2} in DOS occurs in Fig. 4.5b that indicates a competing, but weaker direct interaction.

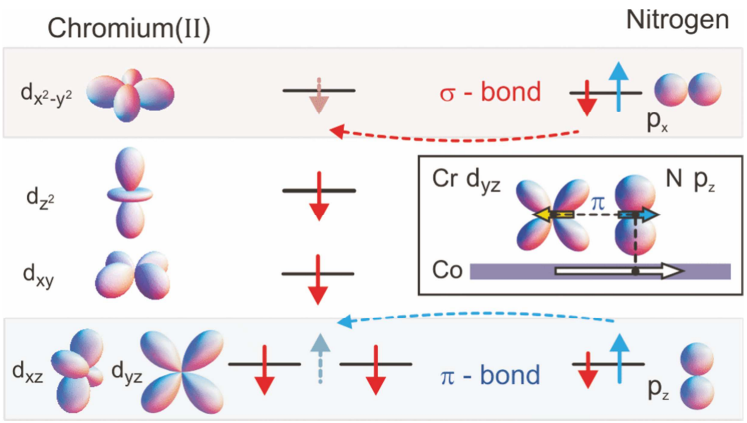

FIGURE **4.7** | Left: 3d-orbitals of the Cr ion and their electron occupations in CrTPP/Co(001) according to Hund's rules. Due to indirect coupling (via nitrogen) to the spin-up polarized Co substrate, the Cr electrons exhibit a spin-down orientation (red arrows). Right: The nitrogen $2p_x$ and $2p_z$ orbitals. The N-p electrons show an imbalance of spin-down (red arrows) and spin-up (blue arrows) polarized electrons due to interaction with the Co substrate. The effective electron exchange through the σ- and π-bonds is indicated by the dashed arrows. Box: Schematic side view of the indirect 90◦ exchange coupling of the spins in CrTPP/Co(001).

Upon contact with the FM substrate the nitrogen atoms in the porphyrin macrocycle obtain a small net magnetic moment which is aligned parallel to the substrate magnetization (see the nitrogen spin density in Fig. 4.4a). The bonding to the Co out-of-plane orbitals occurs via interaction of the spin-down electron from the N-p_z orbitals. The N-p_z orbitals also form a π-bond with the Cr d_{xz}, d_{yz} orbitals (lower row of Fig. 4.7). This configuration is equivalent to a 90° cation-anion-cation interaction scheme (cf. box in Fig. 4.7) and is intuitively treated within the GKA model[28]. Here, the cations involved in the interaction are comprised by the Cr ion on one side and the Co substrate on the other side, while the nitrogen atoms within the porphyrin ring provide the anion. The formation of the π-bond between the Cr d_{xz}, d_{yz} orbitals and the N-p_z orbitals leads to an exchange interaction between the spin-up electron from nitrogen and the Cr ion (lower row of Fig. 4.7). The substrate induced spin-up polarization of the nitrogen p electrons together with Pauli's exclusion principle force the Cr d_π electrons to align their spins antiparallel to the electrons of the N-p_z orbitals. The intra-atomic FM interactions induce a parallel spin

alignment of all Cr 3*d*-shell electrons. As a result the total electron spin of Cr is AFM coupled to the Co substrate as observed experimentally and in our DFT+U calculations. The observed effect is assigned to the less than half-filled 3*d*-shell in the Cr(II)TPP molecules.

To prove the principle of the proposed model we now discuss the role of an extra electron in the 3*d*-shell of the magnetic ion in a similar environment, e.g., in MnTPP on Co(001). Starting with the d^4 configuration, the fifth d electron of such a system will occupy the $d_{x^2-y^2}$ orbital, which forms an σ-type bond with the N-p_x orbital. The overlap of the Cr-$d_{x^2-y^2}$ and the N-p_x orbitals leads to a sharing of the spin-down electron from nitrogen by both orbitals. Note that the electrons in the N-p_x orbitals do not contribute to the bonding with the Co substrate. Due to the intra-atomic FM interaction between nitrogen orbitals, the N-p_x orbital possesses a spin-up polarization. Thus, the additional 3*d* electron in the $d_{x^2-y^2}$ orbital will experience a strong exchange interaction with the polarized N-p_x electrons resulting in a parallel alignment of magnetic moments of N and Mn atoms. The σ-bond is much stronger than the π-bond and hence the spin polarization of $d_{x^2-y^2}$ orbital is intra-atomically transferred to the remaining 3*d*-shell electrons of Mn. Consequently, a FM coupling for the magnetic ion with one more electron is observed compared to the here studied CrTPP species. This is observed experimentally as well as theoretically in DFT+U calculations for MnTPP on Co(001)[4,45,55]. These considerations show that the 3*d*-shell occupation, which differs by one electron between Cr and Mn, plays a crucial role for the magnetic coupling of porphyrins (and possibly for phthalocyanines as well) to magnetic substrates.

In summary, the AFM exchange coupling observed between a magnetic Cr-porphyrin molecule and bare FM Co substrate is discussed. The AFM coupling is assigned to the less than half-filled 3*d*-shell of the high spin Cr ion in the Cr(II)TPP molecules. In agreement with the Goodenough-Kanamori-Anderson (GKA) theory the indirect exchange coupling between the Cr ion and Co substrate occurs dominantly via the N atoms in the porphyrin. Our findings demonstrate that magnetic coupling of molecules on surfaces can be controlled by external stimuli, e.g., using donation (withdraw) of an electron from(to) an external ligand to(from) the metal centre transforming an initial d^4(d^5) configuration to a final d^5(d^4) configuration to induce a FM to AFM transition or vice versa. A transition from FM to AFM coupling was recently demonstrated when MnTPP molecules on Co substrate are ligated with a strong electron acceptor, nitric oxide, transforming the Mn ion from a $3d^5$ to a $3d^4$ configuration[45]. Such control of the interface exchange coupling could be used to engineer suitable organic-inorganic spin-interfaces for applications in molecular spintronic and/or logic devices.

5

Mn- and FeTPPCl Molecules on N- and Cl- terminated Co(001) Substrates

Magnetic moments of spin-bearing molecules can be stabilized by cooling to low temperatures[11]; applying high magnetic fields[56,57] or by adsorption on ferromagnetic substrates[4,5,45,47]. Adsorption of magnetic molecules with square-planar symmetry (e.g. metallo-porphyrins and metallo-phthalocyanines) on ferromagnetic substrates leads to an induced magnetic moment due to exchange coupling between the ad-molecules and the substrates. In order to tailor spins of the magnetic molecules it is desirable to alter the molecule-substrate interaction, e.g. passivating the bare ferromagnetic substrates with oxygen[13,16], covering it with graphene nanosheet[17] or by using metallic non-magnetic spacer layer i.e. lead[18] or chromium[58]. Exchange coupling of ad-molecules can also be modified by coordination with the external chemical ligand (spin-trans effect)[45].

Magnetic molecules adsorbed on the oxygen reconstructed ferromagnetic substrates were reported to couple AFM with substrate magnetization due to the 180° indirect exchange coupling mediated by oxygen adsorbed at the surface[13,16]. Termination of the cobalt substrate with oxygen leads to a weakening of the molecule-substrate electronic interaction, which in turn promotes the molecule-molecule interaction and molecular self-assembly on such surfaces. Graphene nanosheet on ferromagnetic nickel substrate also induces an AFM alignment of ad-molecules' spins with much weaker strength of the exchange coupling[17]. Changing the molecule-substrate interface, one can control the sign and strength of the molecule-substrate exchange coupling.

In this chapter we present study on FeTPPCl and MnTPPCl species adsorbed at nitrogen and chlorine reconstructed ferromagnetic Co(100) substrates. Despite having distinctive chemical properties, N is expected to involve its outermost 2p electron(s) in the magnetic coupling between the molecules centre and the substrate, via superexchange mechanism – likewise for the C and O spacer layers –

which is fundamentally very exciting to verify. The molecule-substrate magnetic coupling through the Cl spacer layer would involve the outermost 3p/3d electron(s) of chlorine atoms which may lead to weakening the exchange coupling. Nitrogen and chlorine reconstructed Co(001) substrates have been prepared according to the recipe described in the Chapter 3. Here onwards, nitrogen and chlorine terminated Co(001) substrates shall be denoted as N/Co and Cl/Co, respectively.

5.1 Mn- and FeTPPCl at N/Co(001)–STM study

Topography of the N/Co substrates with and without the ad-molecules was studied by means of STM and LEED. STM images presented in Figure 5.1a were acquired on N/Co substrate without molecules showing a periodic atomic structure of nitrogen atoms. Nitrogen atoms, resolved as bright spots (blue dots in Fig. 5.1a), are arranged into a c(2x2)-like pattern with respect to the substrate. Dark spots in Figure 5.1a correspond to vacancy sites surrounded by 4 Co atoms. Distance between the nearest nitrogen atoms is approximately 0.36 nm, well in agreement with the DFT+U calculation as described further below. Figure 5.1b shows an STM image with the FeTPPCl molecules self-assembled on N/Co substrate. Shape of the molecules is readily recognized from the image and the molecular pattern can be reproduced (cf. scheme in Fig. 5.1b). FeTPPCl are resolved with dark square centre and bright sides (i.e. phenyl rings). The molecules assemble forming a square 2D lattice with neighbouring molecules spaced approximately 1.3 nm apart, similar to FeTPPCl molecules on an oxygen terminated Co(001) substrates[13]. Previously, a random assembly of the molecules on bare Co(001) substrates has been discussed in terms of pronounced electronic interaction between delocalized π-electrons of the porphyrin macrocycle and the out-of-plane orbitals of the cobalt atoms[13]. The periodic assembly of the molecules on N/Co substrate indicates reduced molecule-substrate interaction. The reduced molecule-substrate interaction promotes self-assembly via π-π stacking of respective orbitals of the porphyrin's phenyl rings[59,60].

LEED pattern acquired on bare N/Co(001) substrate (inset of Fig. 5.1d) resolves spots originating from fcc Co(001) substrate (red circles) and these coming from c(2x2)-like nitrogen reconstruction (blue circles). The c(2x2) reconstruction of the surface is created by replacement of every second atom with the hetero ad-atoms[12]. LEED pattern shown in the Figure 5.1d was acquired on the sample with ad-molecules resolving faint spots attributed to the periodic assembly of the molecules. Molecules adsorbed at surfaces experience a broken translational symmetry of the crystal, e.g. N/Co surface – vacuum interface[61]. The broken translational symmetry causes that achiral M-TPPCl molecules at N/Co assemble into two mirror domains enclosing an angle of ±13° with respect to <110> axis of substrate as shown by STM and LEED images (cf. Fig. 5.1b,d, respectively). Similarly, such domains were reported for MnTPPCl species self-assembled on O-Co substrate; however the angle enclosed by domains and <110> axis was ±11° degree[13]. In the case of N/Co substrate, larger angle is attributed to an increased distance between Co and N atoms. In comparison, distance between N and Co is around 1.8Å, whilst the O-Co

spacing of oxygen terminated Co(001) substrate was reported to be 1.75Å. In both cases, metal ion of metallo-porphyrins adsorbs preferably on top of oxygen[13,16] and nitrogen atoms (see DFT+U calculations further below), respectively. Larger distance, thus, laterally increases the distance between metal centres of the molecules leading to the larger angle between mirror domains. Furthermore, the mirror domains show an internal chiral hierarchy, where the molecules in "*+13*" domains molecules are recognized with right-handed rotation, whilst these within "*-13*" domains show left-handed chirality (cf. Fig. 5.1c).

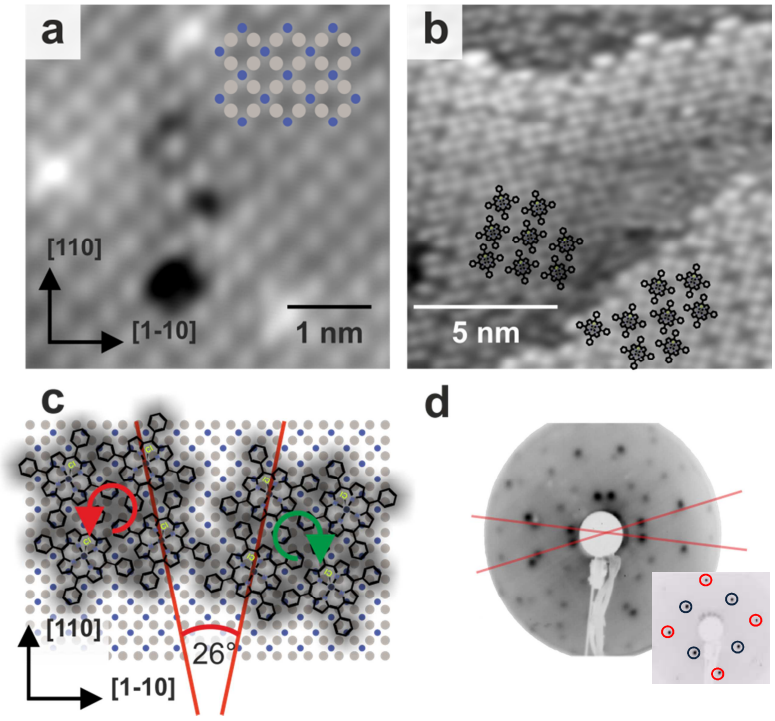

FIGURE **5.1** | Nitrogen adsorbed at Co(001) substrate forms c(2x2) reconstruction as resolved by STM (a) (U=−0.25V, I_t=−90 pA, T=300 K). Scheme resembles position of nitrogen (blue circles) and cobalt (grey circles) atoms at the surface. (b) STM image (U=−0.1 V, I_t=−10 pA, T=300 K) resolving self-assembled FeTPPCl molecules on N/Co with the sketch of the molecules presenting their spatial orientation in two mirror domains. (c) Scheme of the arrangement of molecules on N/Co surface into two mirror domains with right-handed (red arrow) and left-handed chirality (green arrow). Angle between two mirror domains is approximately 26° as resolved by STM (b) and LEED pattern (d) taken at E=24 eV on the N/Co sample with FeTPPCl molecules. Inset: LEED pattern acquired on N/Co substrate without molecules (E=62 eV). Red circles denote LEED spots originating from bare fcc Co(001) substrate and blue circles highlight spots corresponding to c(2x2)-like nitrogen reconstruction.

Both, Mn- and Fe-TPPCl molecules have central metal ion axially ligated with chlorine atoms. The chlorine ligand is likely to be detached from the molecules upon adsorption on bare metallic substrates (cf. MnTPPCl/Co[12] and CrTPPCl/Co in Chapter 4, FeOePCl/Ni[16], MnTPPCl/Cr/Co[58]) and re-adsorbs onto the substrate or desorb from the molecules into the vacuum. On the other hand Mn-TPPCl species

adsorbed on O/Co substrates have been shown to keep the chlorine atom in axial position facing the vacuum. Interestingly, FeOePCl species on O/Co have been shown to not carry chlorine ligand in the axial position. In our case the FeTPPCl molecules on N/Co are found to be ligated with chlorine as evidenced by XPS and STM measurement (Fig. 5.2a,b). XPS spectra acquired at Cl 2p shows that FeTPPCl molecules deposited on N/Co carry chlorine ligand (blue curve Fig. 5.2a). The molecules ligated with chlorine are resolved by STM showing a dark square centre (Fig. 5.1b and Fig. 5.2b). Annealing sample to T~420K leads to desorption of chlorine atoms as evidenced by red curve in Figure 5.2a. Loss of chlorine leads to a disorder in the self-assembled molecular domains with the molecules randomly distributed over the image area (cf. Fig. 5.2c). This suggests a stronger molecule-substrate interaction between FeTPP species and N/Co substrate compared to that of FeTPPCl and N/Co. Further evidence of chlorine loss is demonstrated by a change of the appearance of the molecular species, is further resolved on the molecules' appearance with the bright centres (Fig. 5.2c).

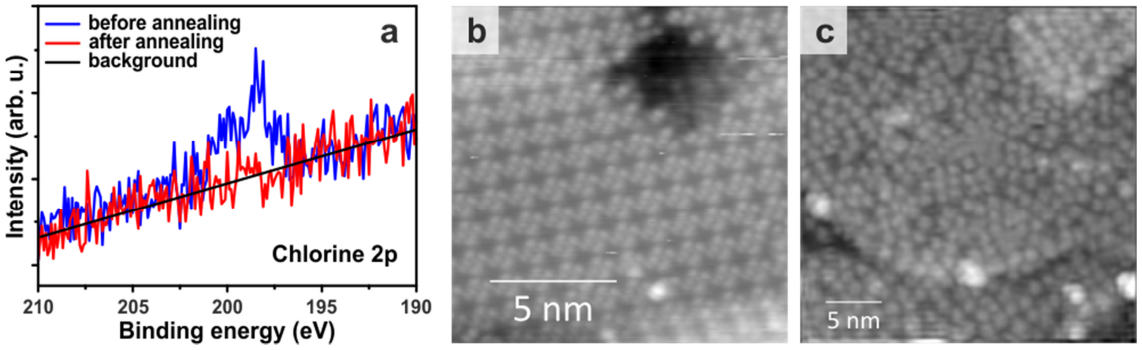

FIGURE **5.2** | Annealing of FeTPPCl/N/Co system results in chlorine loss as demonstrated by XPS data acquired at Cl 2p before (blue curve) and after annealing (red curve) (a). Desorption of chlorine from FeTPPCl molecules leads to a destruction of self-assembled layer (b) into a layer of randomly distributed FeTPP molecules(c).

5.2 Magnetic and electronic properties of Mn- and FeTPPCl at N/Co(001)

Magnetic measurements were performed on two systems; MnTPPCl/N/Co and FeTPPCl/N/Co. Both systems have not been heated above room temperature at any stage of the experiment assuring uniformity of the molecular layer. By means of the XAS/XMCD technique, magnetic and electronic properties of the MnTPPCl/N/Co and FeTPPCl/N/Co systems are resolved. Specifically XAS/XMCD spectra were taken at $L_{3,2}$ edge of Co, Mn and Fe ions and at the K edge of N. Experimental geometry is defined in the Figure 5.3a, showing the angle between ***k***-vector of incoming x-rays and the surface normal ***n*** being 70°. In this configuration XMCD is predominantly sensitive to the in-plane components of probed magnetic moments.

XAS spectra acquired at the Mn $L_{3,2}$ edges resolve three distinct peaks with the main one resolved at photon energy of about 642.0 eV and side ones at ~ 640 eV and ~ 643 eV. We assign these peaks to two different types of MnTPPCl molecules; with and without chlorine ligand as resolved by XMCD spectra measured for the same molecules adsorbed on O/Co[13]. XMCD spectra taken at Mn $L_{3,2}$ edges show two distinct peaks at ~640 and ~642 eV, matching energies of two of three peaks observed in our XAS spectra.

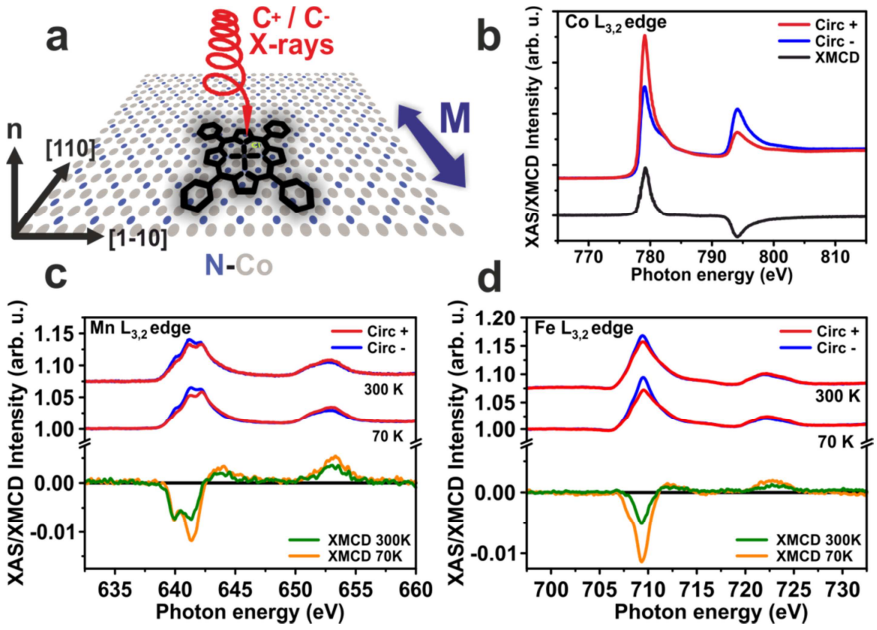

FIGURE **5.3 |** (a) Scheme of experimental geometry used in XAS/XMCD measurements on Mn- and FeTPPCl/N/Co systems. ***M*** denotes the orientation of substrate magnetization being switched by external magnetic field applied along [110] direction (easy axis of magnetization). The ***k***-vector of incoming circularly (C+, C-) polarized x-rays lies on the plane enclosed by surface normal ***n*** and [110] axis. (b) XMCD/XAS spectra taken at Co $L_{3,2}$ edges resolve magnetically saturated N/Co substrate (spectra were taken at T=300K). (c), (d) Mn and Fe $L_{3,2}$ edges XAS/XMCD spectra acquired at 300 and 70 K. The opposite sign of XMCD signal at Mn and Fe L_3 edge compare to that of Co suggests an antiferromagnetic molecule-substrate coupling.

The sign of XMCD signal acquired at Mn $L_{3,2}$ edge is of opposite sign to that measured at Co $L_{3,2}$ edge of N/Co substrate (Figure 5.2a,c), suggesting an AFM alignment between magnetic moments of MnTPPCl species and that of N/Co substrate. XMCD signal acquired for MnTPPCl molecules at room temperature (Fig. 5.2a green curve) resolves two peaks of same intensity. Upon cooling to 70 K (Fig. 5.2a orange curve) the intensity of XMCD signal is enhanced for peak at ~ 642 eV (by factor of 1.6) whereas intensity of peak at ~ 640 eV did not change. Note, that XMCD signal of N-Co substrate measured at Co $L_{3,2}$ edges is increased by 2% at 70K. Change in the amplitude of XMCD signal is directly connected with the strength of the exchange coupling that can be probed by temperature or magnetic field dependent measurements[16]. Therefore we assume that Mn(II)TPP species (XMCD maxima at

~640eV) are exchanged coupled with N/Co stronger than the Mn(III)TPPCl (peak at ~642 eV) molecules, i.e. surface spin-trans effect[45].

In order to probe the specific electronic magneto-chemical interaction between ad-molecules and N/Co substrate, we used FeTPPCl that have half-integer spin state (S=3/2) in bulk as well as on surface in comparison to S=2 MnTPPCl molecules[16]. XAS spectra acquired on the FeTPPCl/N/Co system at Fe $L_{3,2}$ edge (Fig. 5.2b) resolve spectral features at ~ 709 eV, signalizing Fe ion in the 3+ oxidation state[16]. XMCD signal acquired for Fe ions, shows, similarly to that of MnTPPCl molecules, the opposite sign with respect to the substrate magnetization (green curve in Fig 5.2b), demonstrating the AFM coupling of the Fe magnetic moments to the magnetization of N/Co substrate. Amplitude of observed Fe XMCD signal is increased, by factor ~ 2 for spectra acquired at 70K suggesting weaker exchange coupling.

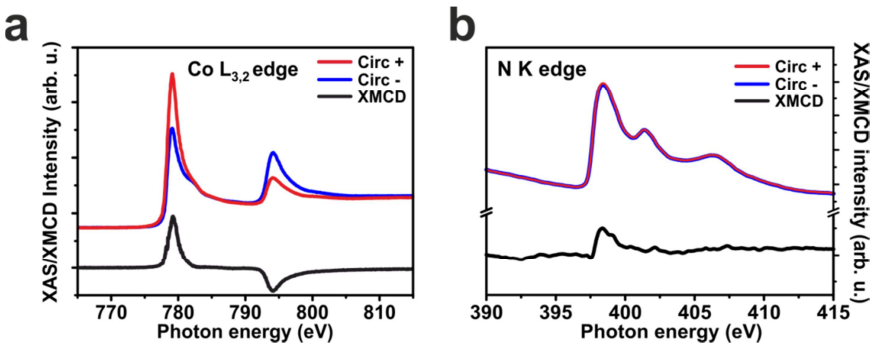

FIGURE **5.4 |** XAS and XMCD spectra of FeTPPCl/N/Co system acquired at (a) Co $L_{3,2}$ edge and (b) N K edge. Magnetic moments induced on nitrogen atoms couple ferromagnetically with the cobalt atoms. Spectra were recorded at T=70K in the grazing incidence geometry.

Atoms and molecules adsorbed at magnetic substrates are observed to possess an induced magnetic moment due to the exchange interaction. Oxygen atoms adsorbed on ferromagnetic cobalt thin films[62] possess a small induced magnetic moment ferromagnetically coupled to the substrate magnetization. Nitrogen atoms adsorbed on cobalt FM thin film are also expected to carry induced magnetic moment. In our XAS/XMCD study of MnTPPCl/N/Co and FeTPPCl/N/Co systems we performed measurements at K edge (1s -> 2p orbitals) of nitrogen atoms (Figure 5.4b). Due to the lack of spin-orbit coupling at s orbitals, the XMCD effect cannot occur at K edge. However the exchange coupling between nitrogen and cobalt atoms (in our case) leads to a spin polarization of the 2p orbital which give rise to XMCD effect at K edge[26]. XAS spectra acquired at K edge of nitrogen resolves three distinct peaks at energies ~ 398 eV, ~ 402eV and 406 eV, corresponding to a π-type and two σ-type antibonding orbitals, respectively[26]. Interestingly, the XMCD signal (Figure 5.4b) is resolved at energies corresponding to π-type antibonding orbitals. Magnetic moment induced on nitrogen atoms aligns along the same direction as the magnetization of surrounding cobalt atoms from the substrate, hinting a ferromagnetic exchange coupling.

5.3 DFT+U study -FePCl on N/Co(001)

Microscopic model of the magnetic interaction between FeTPPCl and N/Co substrate is discussed in conjunction with the results of DFT+U calculations with Van der Waals dispersion interactions included. In the *ab initio* calculations the FeTPPCl molecules have been replaced by truncated Iron-porphine (FeP) model[55]. As we proved experimentally, the adsorption of FeTPPCl on N-Co substrate does not lead to a loss of axial chlorine atom, which remains bonded on the vacuum side of the molecules.

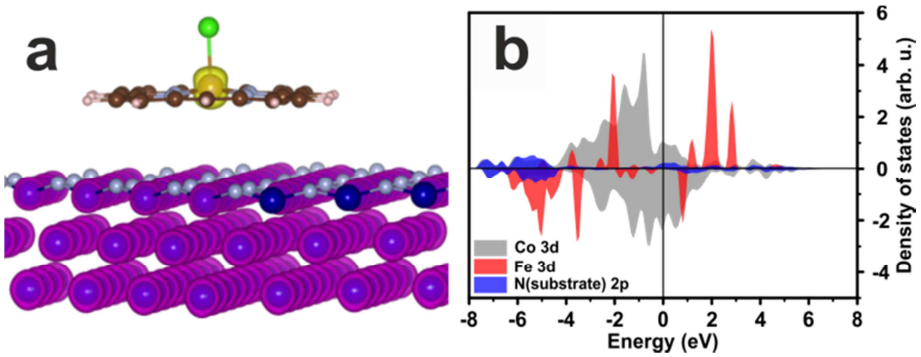

FIGURE **5.5 |** DFT+U calculations on FePCl/N/Co system demonstrates an AFM coupling between Fe ions of FePCl species and N/Co substrate. (a) Yellow colour of contour plot around Fe ion depicts opposite polarization of electrons with respect to the substrate magnetization (shown violet). Fe ion is pulled out of the porphine plane towards chlorine atom. (b) Plot of DOS for 3d orbitals of Co (grey), 3d orbitals of Fe(red) and 2p orbitals of bridging N(blue) resolving a small induced magnetic moment on bridging nitrogens, ferromagnetically coupled to Cobalt atoms. Fe atoms possess an induced magnetic moment being antiferromagnetically coupled with the underlying N/Co substrate.

However, we have studied both Fe porphine species with and without chlorine ligation. The DFT+U calculations evidence that the magnetic exchange coupling in the FeP/N/Co as well as in the FePCl/N/Co system is antiferromagnetic. DFT+U calculation further resolves the central metal ion (Fe) positioned preferably on top of the N atoms of the N-Co substrate suggesting that magnetic properties of the Mn/Fe ions will be governed by their interaction with the N atoms. An optimized Fe-N (substrate) distance for FeP/N/Co is 2.12Å and for FePCl/N/Co distance is larger, 3.49Å. These distances are consistent with the observed self-assembly for FeTPPCl molecules (i.e. physisorption) and random distribution of FeTPP molecules (i.e. chemisorption). Iron atom bonded to axial chlorine is drawn out of the porphyrin plane toward the chlorine atom (by 0.29Å) whereas for species without the Cl ligand the iron atom is pulled out of the porphyrin plane towards substrate's nitrogen atom (-0.30Å). The calculated spin-density and spin and orbital resolved density of states (DOS) is plotted in Figure 5.5. The spin-polarization on the bridging N-atom for the FeP/N/Co system indicates the 180° super-exchange mechanism. The strength of the exchange coupling for FePCl/N/Co is -7.00 meV as calculated by Noodleman's broken-symmetry approach[55]. The calculations further revealed that adsorption of

the atomic N on Co reduces the magnetic moments of Co atoms on cobalt surface from ~2 μ_B to ~1 μ_B. The spin-density plotted in Figure 5.5b clearly indicates a ferromagnetic exchange interaction of adsorbed nitrogen atoms to the substrate magnetization.

5.4 Mn- and FeTPPCl molecules on Cl/Co(001)

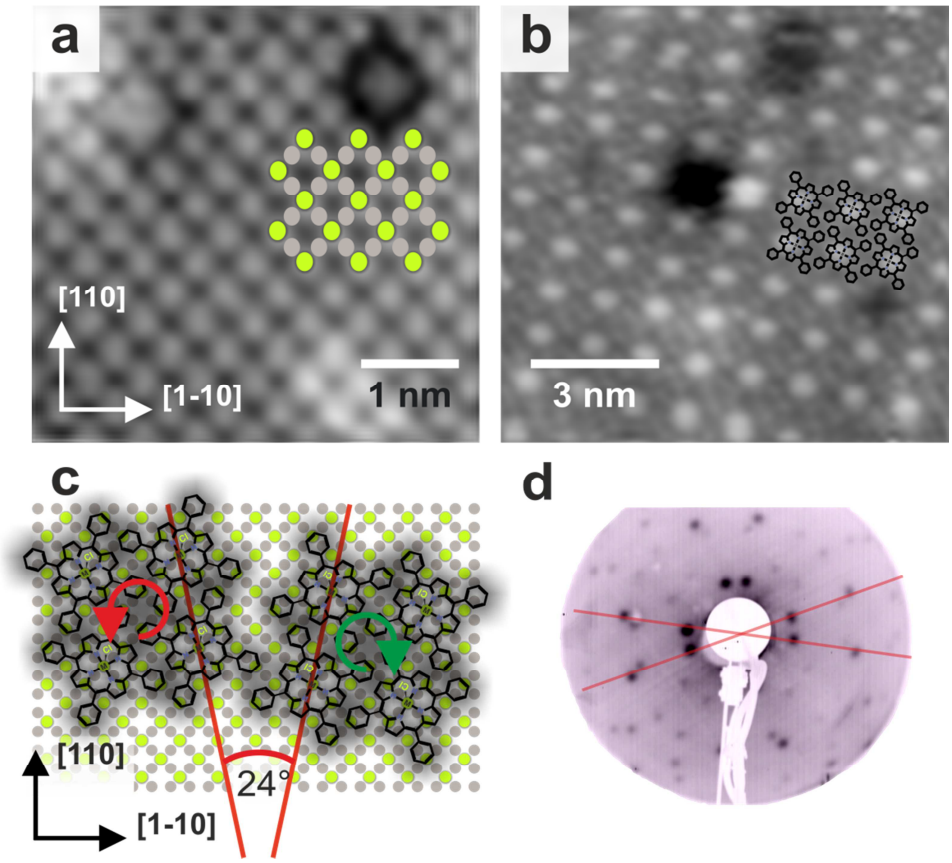

FIGURE **5.6** | STM images acquired on chlorine terminated cobalt substrate (a) without and (b) with adsorbed FeTPPCl molecules. Inset in the image (a) shows the position of Cl (yellow) and Co(grey) atoms in the Cl/Co(001) substrate. FeTPPCl molecules self-assemble on the Cl-Co surface into mirror domains with the molecules possessing left (green arrow) and right (red arrow) chirality inside these domains (c). Domains enclose angle of 12 degrees with respect to crystallographic axis. (d) LEED pattern acquired on the chlorine reconstructed substrate with adsorbed FeTPPCl molecules. STM image (a) acquired at U=−480 mV, I_t=−10 pA, T=300 K (a) and image (b) at U=−740mV, I_t=−10 pA, T=300 K.

The original proposition of A. Scheybal et al.[4], discusses possibility that the axial chlorine ligand from MnTPPCl adsorbs in between molecular metal centre and underlying magnetic substrate. This would lead towards FM alignment of the molecular spin with respect to the substrate magnetization as discussed

theoretically[12]. Chlorine, similarly to nitrogen, forms a c(2x2) reconstruction at Co(001) surfaces (Fig. 5.6a). Chlorine terminated Co(001) surface shows formation of large terraces that are atomically flat with atomically sharp step edges. Metallo-porphyrins adsorbed on the Cl-Co self-assemble into monolayer forming mirror domains as resolved by LEED (Fig. 5.6d). Lattice vector of these domains encloses an angle 12 degree with respect to [110] axis of underlying Cl/Co substrate. The self-assembly as discussed previously is driven by molecule-molecule interaction[60] between side phenyl rings. Mirror domains shows internal chiral rotation similar to that of metallo-porphyrins adsorbed on N/Co(001) and O/Co(001) substrates. The two mirror domains enclose an angle 24°, that is larger than one observed for MnTPPCl on O/Co[13] (angle = 22°), but smaller than the angle resolved for domains on N/Co (angle = 26°, see above). Distance between neighbouring chlorine atoms extracted from STM images is ~ 0.355 nm and Co-Cl distance is 0.175 nm. The observed distance and the angle between molecular domains is well in line with the previous observations, where shorter Co-O distance (0.175 nm) leads to an angle 22 degree[13] and longer Co-N distance (0.18 nm) results in the angle 26° (see previous section). In Figure 5.6b, missing molecule (dark square in image centre) in the monolayer of FeTPCl molecules enables identification of the FeTPPCl molecules. Centre of the molecules is resolved with bright protrusion that is attributed to the presence of axial chlorine atoms. Molecules lacking axial chlorine atom are resolved as the species with the dark cross at the centre of the molecules (see Fig. 5.6b). Based on the STM images, we conclude that majority of FeTPPCl adsorbed on Cl/Co(001) substrate possess the axial chlorine ligand.

5.5 Mn- and FeTPPCl on Cl/Co(001) - XAS/XMCD study

XAS/XMCD measurements on the MnTPPCl/Cl/Co and FeTPPCl/Cl/Co systems are presented in the Figure 5.7. XAS/XMCD spectra acquired at Co $L_{3,2}$ edges (Fig. 5.7a) shows magnetically saturated cobalt thin film. Adsorption of chlorine on top of Co(001) film results in the induced magnetic moment at the chlorine orbitals as resolved by XAS/XMCD spectra taken at Cl $L_{3,2}$ edge (2p->4s/3d transition)(cf. Fig. 5.7b). The fact that XMCD signal is resolved at $L_{3,2}$ edges hints towards the 3d orbitals of chlorine being spin-polarized due to the exchange coupling with the cobalt atoms. Note that XA spectra taken at $L_{3,2}$ edge corresponds to 2p -> 3d(4s) transition and as an s orbital does not possess an orbital angular momentum, the induced magnetic moment resolved by XMCD at the $L_{3,2}$ edge is attributed to the 3d orbitals. In addition, the XAS/XMCD spectra measured at the Cl L_1 edge (2s -> 3p transition) (inset Fig. 5.7b) do not resolve any signature of the induced magnetic moment on valence Cl 3p orbitals.

At first we analyse XAS/XMCD spectra acquired on MnTPPCl/Cl/Co system. Shape of XA Mn $L_{3,2}$ edge spectra (Fig. 5.7c) resemble similarities with the XA spectra acquired on MnTPPCl/O/Co[13,54] and MnTPPCl/N/Co systems, thus confirming 3+

oxidation state of Mn ions due to the presence of chlorine in the axial position. The XMCD spectra at Mn $L_{3,2}$ edges reveal an AFM coupling between the magnetic moment of MnTPPCl molecules and the magnetization of Cl-Co substrates. The XMCD signal shows single maxima at ~641 eV, being in contrast to two XMCD maxima resolved in previous studies on MnTPPCl/O/Co and MnTPPCl/N/Co. XMCD maxima at this energy were observed previously and attributed to Mn(II) ions, i.e. without axial ligand. Interestingly, the spectral feature resolved at photon energy ~640 eV in Mn XMCD spectra was observed for MnTPP(Cl)/Co and for MnTPPCl/N/Co systems, however was absent for the MnTPPCl/O/Co system[13]. Lowering temperature of the system to 70K causes an increase of Mn XMCD signal by factor of 2 (Fig. 5.7c).

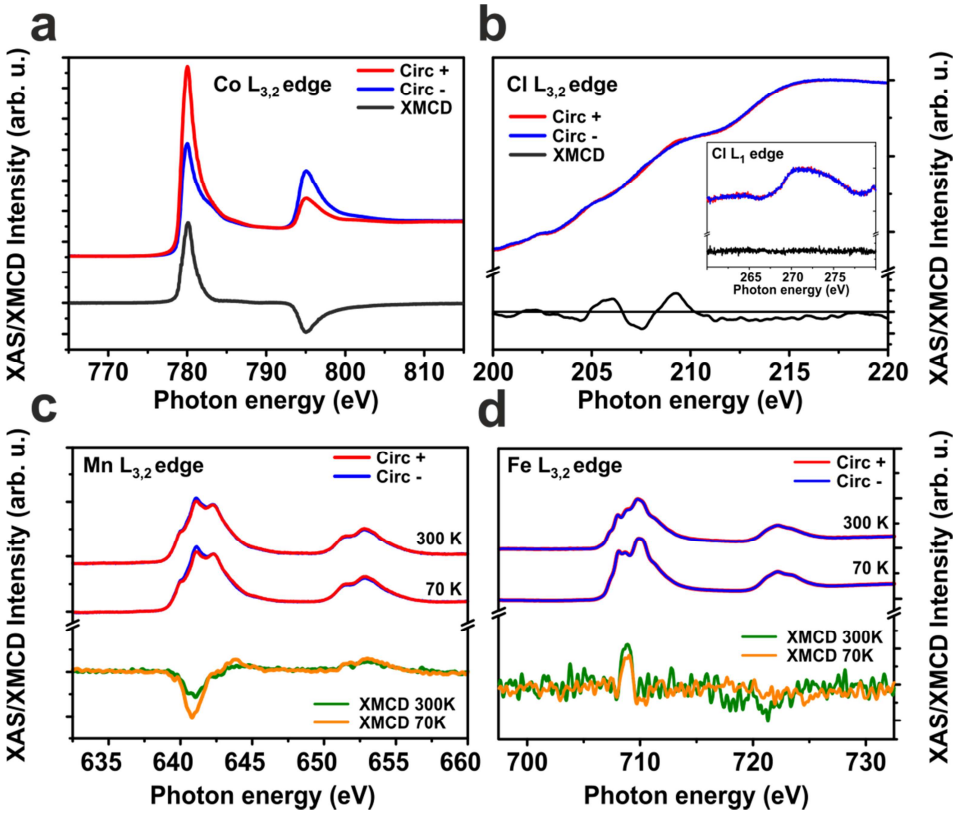

FIGURE **5.7** | XA/XMCD spectra of Mn- and FeTPPCl molecules adsorbed at Cl/Co(001) substrate. (a) XAS/XMCD spectra acquired at Co $L_{3,2}$ edges resolving magnetically saturated substrate. (b) XAS/XMCD spectra measured at $L_{3,2}$ edges of chlorine resolving an induced magnetic moment on 3d orbitals of chlorine. (c) Manganese atoms of MnTPPCl molecules possess an induced magnetic moment antiferromagnetically coupled to magnetization of Cl/Co(001) substrate. Adsorption of FeTPPCl species on Cl/Co(001) leads to a ferromagnetic coupling between magnetic moments of Fe atoms and that of the substrate.

FeTPPCl/Cl/Co system is even more interesting. The XMCD spectra measured at Fe $L_{3,2}$ edges shows a weak FM coupling between the magnetic moment of the Fe ions and Cl/Co substrate. The FM coupling is resolved by maxima/minima at

adsorption edges pointing the same direction in Co and Fe XMCD spectra (Fig. 5.7a and d, respectively). XMCD spectra of Fe ion acquired at 70K (Fig. 6d yellow curve) does not show significant change in the apparent height, however the small decrease in the peak maxima can be observed.

Additionally, the position of the XMCD maxima is found at ~709 eV, that would correspond to an induced magnetic moment on Fe(III) ions[63]. The XA spectra acquired at Fe $L_{3,2}$ edge differs significantly to those obtained on FeOePCl/O/Co[16] and FeTPPCl/N/Co (c.f. Fig 5.3d). While the XA spectra of later systems are characterized by narrow peak with small shoulders on both sides and the maxima at ~709 eV, the Fe $L_{3,2}$ XA spectra of FeTPPCl on Cl/Co(001) show a wide peak with the multiple maxima. Oxidation state of Fe ions in both FeOePCl/O/Co[16] and FeTPPCl/N/Co systems (see above) is found to be 3+. Chlorine as a strongly electronegative element does locally change the electrostatic potential at the surface and trivalent iron atom experiences stronger crystal field[54]. The shape of XA spectra of Fe ions in FeTPPCl/Cl/Co system is likely to be related with six-coordinated Fe ions[64] with two chlorine atoms in the axial position, i.e. one on the substrate side and one on the vacuum side. Therefore we assume that the majority of the Fe ions are six-coordinated in the 4+ oxidation and low spin (S=0) state. The XMCD signal observed at Fe $L_{3,2}$ edges can be attributed to an induced magnetic moment in the Fe(III)TPP species lacking chlorine ligand on the vacuum side, but strongly bonded to chlorine atoms at the substrate. These molecules were resolved by STM (Fig. 5.6b) as the species with dark centre cross.

5.6 Discussion

The magnetic and electronic interaction of the metallo-porphyrins (i.e. MnTPPCl and FeTPPCl) with the nitrogen and chlorine reconstructed cobalt surfaces have been investigated. The molecules adsorbed on N/Co and Cl/Co substrates do self-assembly and the assembly is driven by the molecule-molecule interaction via stacking of the π-π systems on the porphyrin's side phenyl groups. Achiral metallo-porphyrins with the C4 symmetry on the surface with the four-fold symmetry form two mirror domains that are rotated by 24° and 26° on chlorine and nitrogen reconstructed cobalt substrates, respectively. The formation of mirror domains with chiral arrangement is caused by the broken translational symmetry at the surfaces.

XAS/XMCD experiments performed at N K edge resolves the magnetic moment on nitrogen π-orbitals, i.e. out-of-plane p_z orbital of nitrogen. DFT+U calculations resolve central metal ion of FePCl species adsorbing on top of pre-adsorbed nitrogen atoms. Both, the MnTPPCl and FeTPPCl molecules adsorbed on N/Co couple their spins antiferromagnetically with respect to the substrate magnetization. The here observed AFM interaction is attributed to 180° indirect exchange coupling between metal centre and magnetic substrate mediated by the $2p_z$ orbitals of the nitrogen atoms adsorbed at the interface. Due to the exchange coupling of the nitrogen atoms with those of cobalt substrate, the nitrogen atoms at the interface possess small

magnetic moment that is ferromagnetically coupled to the substrate. The strength of the molecule-substrate magnetic exchange coupling is comparable in measure with the results reported for MnTPPCl and FeOeP molecules on the oxygen reconstructed Co(001) substrate[13,16]. Note that, porphyrin ligand of a M-TPPCl molecule contain four pyrrolic N atoms which are exchange coupled to the substrate[55,65]. Area of the surface covered by single M-TPPCl molecule contains approximately 5 times more nitrogen atoms as is the number of nitrogens in porphyrin ligand. Previous theoretical studies demonstrated that upon adsorption of metal-porphyrins on metallic substrates a sizable magnetic moment can be induced on nitrogen atoms of porphyrin macrocycle. The XMCD signal originating from porphyrin's nitrogens that are exchange coupled with magnetic substrate have been reported to be very weak and at the limit of detection by XMCD technique[66]. Therefore we conclude that XMCD signal resolved at the N-K edge of MnTPPCl/N/Co and FeTPPCl/N/Co systems is resolved on nitrogen atoms adsorbed at the cobalt substrate.

Molecules adsorbed on the Cl/Co experience a strong crystal field originating from the strongly electronegative chlorine atoms adsorbed at the surface. Therefore the electronic configuration of the 3d-metal centre in the porphyrin molecules is significantly different compare to metallo-porphyrins adsorbed on the nitrogen or oxygen reconstructed substrates. The crystal field influencing metal centre is especially apparent in the XA/XMCD spectra of FeTPPCl molecules. Magnetic moment of MnTPPCl species is shown to couple AFM with the Cl/Co substrate. The shape of the XMCD spectra of MnTPPCl differs from those observed on the nitrogen and oxygen reconstructed cobalt substrates with the single XMCD maxima at ~641 eV corresponding to Mn(III) ions. The most unexpected is the weak FM coupling of the FeTPPCl molecules adsorbed on Cl/Co. Coupling between metal ions and Cl atoms in the Mn(Fe)TPPCl/Cl/Co systems is shown to differ from the picture drawn for M-TPPCl/O/Co and M-TPPCl/N/Co systems. There, the exchange coupling is mediated by out-of-plane $2p_z$ orbitals of pre-adsorbed oxygen and nitrogen atoms, respectively. In case of Cl/Co we shown that chlorines' 3d orbitals are spin polarized due to the adsorption at the cobalt films. We demonstrate that magneto-chemical interaction between FeTPPCl species and Cl/Co substrates (i.e. Cl 3d – Metal 3d orbitals) is significantly different to those observed for the molecules on oxygen or nitrogen reconstructed substrates, where exchange coupling is mediated via $2p_z$ orbitals.

6

Study of Molecule-Substrate Interaction by X-PEEM

X-ray Photo-Emission Electron Microscopy, an imaging technique, reveals spatially resolved maps of the local x-ray absorption cross section. It thus provides a chemically sensitive tool for spectro-microscopy investigations revealing both electronic and magnetic properties within nanometer range; in combination with X-ray Magnetic Circular Dichroism and X-ray Absorption Spectroscopy. While being well established for studying magnetic nano-structures, down to the level of single nanoparticles[26,67,68], PEEM has not yet been used to investigate molecule–substrate spin-interfaces. Here, the X-ray PEEM (Fig. 6.1a) is exploited to study the chemical and magnetic interaction of adsorbed manganese(III) tetraphenylporphyrin chloride (Fig. 6.1b) with the native metallic and oxygen covered Co substrate as well as with Co substrates modified with a wedge shaped Cr spacer underneath the molecular layer.

6.1 X-PEEM Experiment

The magnetic domain pattern of the substrate is analysed by excitation of the Co thin films with circularly polarized x-rays in PEEM. The XMCD effect gives rise to a spatial intensity variation which scales with the projection of the local magnetic moment onto the X-ray propagation vector ***k***. Tuning the photon energy to the Co L_3 absorption edge (~778 eV) therefore reveals the individual magnetic domains of the Co(001) substrate (Fig. 6.1a, left inset). Magnetic domains of the substrate imaged white (black) [grey] correspond to a magnetization vector ***m*** aligned parallel (antiparallel) [perpendicular] to the incident photons. The element-specific sensitivity of PEEM to the magnetic moment induced in a single MnTPP(Cl) layer on Co(001) is demonstrated in Fig. 6.2a and Fig. 6.2b by tuning the photon energy to the Co and Mn L_3 edge, respectively. Note that upon adsorption onto the Co substrate the molecular species [Mn(III)TPPCl] is reactively modified to Mn(II)TPP by loss of the Cl ligand[12]. The magnetic domain pattern of the Co substrate is shown

*Parts of this chapter have been published in: J. Girovsky, et al. *Chem. Comm.*, **50**, 5190, (2014).

in Fig. 6.2a. By tuning the photon energy to the Mn L_3 edge (~ 640.4 eV) we obtain the magnetic contrast image of the molecular ad-layer (Fig. 6.2b). The latter (Mn) image reproduces the domain pattern of the Co film, thereby providing evidence for a ferromagnetic coupling of the molecules to the substrate.

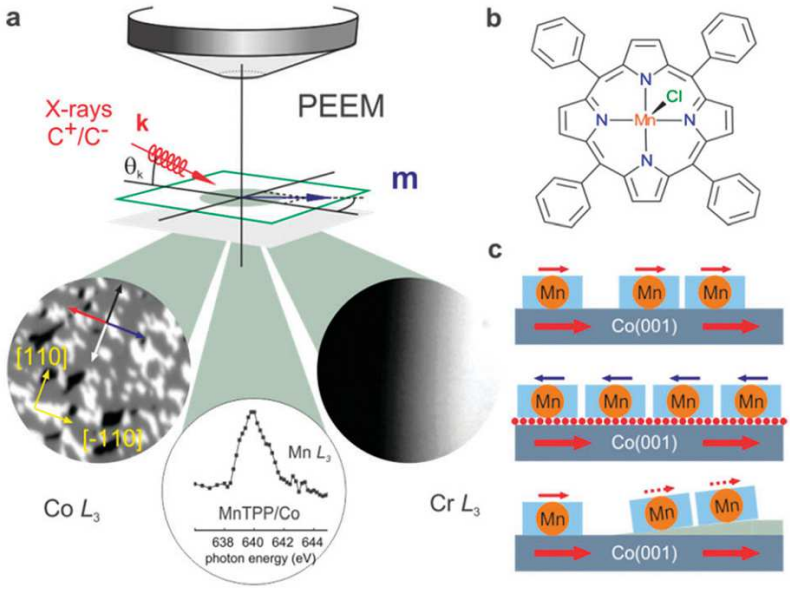

FIGURE **6.1 |** (a) Sketch of the experimental setup; Bottom left: magnetic contrast image of a bare Co film, bright (dark) areas denote a magnetization parallel (antiparallel) to the X-ray beam propagating along the ***k*** direction, grey areas reveal a magnetization perpendicular to ***k***; magnetic anisotropy directions i.e. <110> directions have been indicated by yellow arrows; Bottom centre: the Mn L_3 edge XA spectrum recorded on the MnTPP–Co system; Bottom right: X-ray absorption contrast (elemental contrast) of a Cr-wedge on Co. (b) Chemical structure of MnTPPCl. (c) Cartoon of MnTPPCl molecules and their magnetization on the different samples investigated; Co (top), oxygen-covered Co (centre) and a Cr-wedge layer on Co (bottom).

Such coupling has also been found in previous XMCD experiments[4,12]; DFT +U calculations on similar systems revealed that the magnetic interaction of the metal-centre's spin with that of the Co substrate can be due to an indirect exchange coupling mediated by the N-p_z electrons, which are spin polarized due to hybridization with Co substrate orbitals[12,45,55]. The magnetic contrast in our PEEM experiment is confirmed by the contrast reversal of the domain patterns when tuning the photon energy to the Mn L_2 edge (see Fig. 6.2e). The XMCD contrast in Fig. 6.2b amounts to about one to two percent of the total signal, and hence is similar to the spectroscopic findings reported in earlier work[4,12,45].

In comparison we investigate MnTPPCl layers on oxygen covered Co substrates where Mn ions couple antiferromagnetically to the Co substrate due to super-exchange via the O atoms, in analogy to bulk antiferromagnets[13,16]. XA spectroscopy (see Fig. 6.3b) and complementary X-ray photoelectron spectroscopy[13] additionally demonstrate that the chemical species is actually Mn(III)TPPCl (i.e. the Cl ligand

remains). The domain pattern of the Co substrate is shown in Fig. 6.2c and, indeed, when tuning the photon energy to the Mn L_3 edge (~641.0 eV), we find that the MnTPPCl molecules display an inverse magnetic contrast compared to that of the Co substrate (see Fig. 6.2d,f).

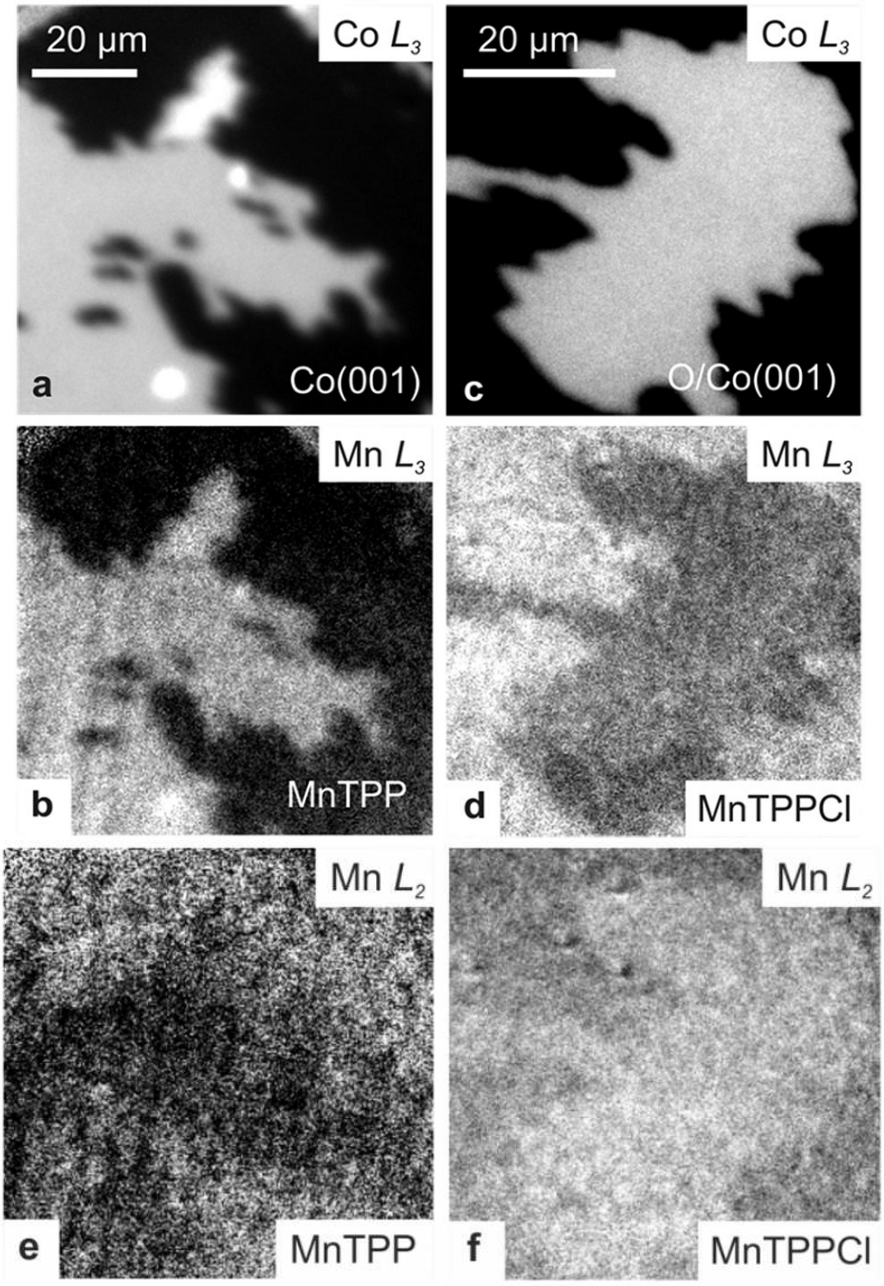

FIGURE **6.2** | Magnetic contrast images obtained at the Co L_3 edge (a,c) and at the Mn L_3 edge (b,d) and Mn L_2 edge (e,f) of the MnTPP(Cl) molecules on Co(001) and O/Co(001), respectively. Inverse magnetic contrast at Mn L_2 edge compares to those acquired at Mn L_3 edge confirming magnetic origin of the signal.

The magnetic exchange coupling of a monolayer of MnTPP to the Co substrate is studied in terms of the thickness of a Cr spacer layer in the form of a wedge (cf. Fig. 6.1c). Cr is known to promote a strong interlayer coupling in magnetic multilayers, such as Fe/Cr/Fe[29].The onset region of the Cr-wedge on the sample is detected when recording an intensity image with the photon energy set first to the Cr L_3 edge (~578.0 eV) and then to the pre-edge energy at 572.0 eV. Pixelwise division of both images reveals the Cr wedge in the field of view as shown in the right side of Fig. 6.4a (Cr rich regions appear bright). Fig. 6.4b and c show the magnetic contrast images of the Co substrate in the Cr wedge sample (MnTPP molecular layer on top).

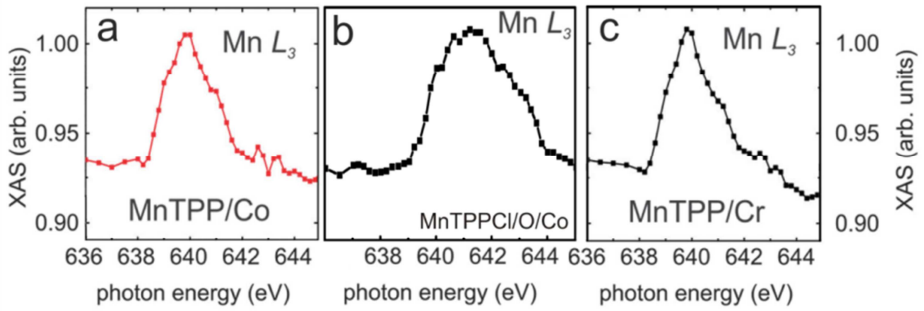

FIGURE **6.3** | XA spectra of MnTPP on Co(001)(a), MnTPPCl on O/Co(001) (b) MnTPP on Cr/Co (c).

Across the investigated coverage range of the Cr wedge no influence on the underlying magnetic domain pattern of the Co is found. However, the presence of Cr significantly alters the magnetic contrast detected from the MnTPP molecules across the wedge: the MnTPP molecules on the bare Co surface (left side of Fig. 6.4c) show magnetic contrast with FM coupling (cf. Fig. 6.2). With increasing Cr coverage the Mn contrast decreases (Fig. 6.4d, right hand side) and for even higher Cr thickness no magnetic contrast in the MnTPP molecules is found. XA spectra acquired at the Mn L_3 edge reveal the same spectral signature on Co or at any position of the PEEM image of the Cr wedge (Fig. 6.3c).

These spectra match with previously reported data on Mn(II)TPP on Co[13], thus, the oxidation state of the Mn ion is the same on Co and on Cr. The gradual loss of magnetic contrast in the molecules at the onset of the Cr wedge is unexpected when compared to the findings for tri-layered structures such as Co/Cr/Fe[69,70]. In such systems the ferromagnetic substrate gives rise to a thickness-dependent spin polarization in the Cr spacer layer, which induces a magnetization coupling to the top-layer film which is determined by the magnetization of the bottom substrate layer. In analogy to the top-layer in the inorganic system, the MnTPP molecules are expected to magnetically interact with the bottom substrate via the spin-polarized electrons of the Cr layer either directly via hybridization with the Mn d-electrons or indirectly via the N p_z electrons.

The gradual loss of a detectable effect suggests that this interaction mechanism via Cr is too weak to result in a stable coupling at room temperature. Notably, the

inter-layer coupling of paramagnetic MnTPP molecules through a Cr spacer differs from the corresponding case of only inorganic magnets in multilayers e.g. Fe/Cr/Fe in that the ad-molecules (which are paramagnetic in their bulk form) in the layer do not interact with each other, but only with the underlying substrate.

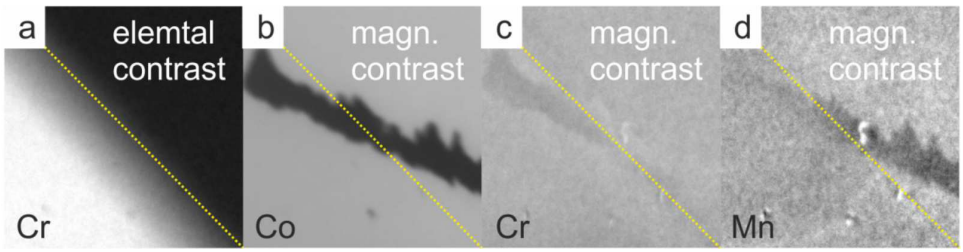

FIGURE **6.4** | Magneto-chemical contrast of MnTPP(Cl) on Cr-wedge on a Co(001) substrate (a) XA elemental contrast of the Cr-wedge. (b)-(d) Magnetic contrast image recorded at the same spot with the photon energy tuned to the Co L_3 edge in (b) to the Cr L_3 edge in (c) and to the Mn L_3 edge in (d) The yellow dashed lines denote the onset of the Cr-wedge with the Cr thickness increasing to the right.

Thus, the absence of inter-molecular interactions at elevated temperatures (>300 K) may be responsible for the absence of a stable coupling of the molecules to the Co substrate via the Cr wedge.

6.2 Discussion

We have demonstrated chemically-sensitive X-ray PEEM in combination with spin-sensitive XMCD to detect molecule–surface magneto-chemical interactions down to the single monolayer coverage. This spatially resolving spectro-microscopy technique is expected to be particularly advantageous when studying coupling phenomena on electronically complex such that antiferromagnetic materials, multiferroics or topological insulators as well as on patterned substrates. Furthermore, wedged samples enable a direct comparison of various interfaces in one measurement under identical conditions. Importantly, as a microscopy technique PEEM goes beyond the established photo-absorption spectroscopy in that it allows for the investigation of on-surface coordination chemistry and on-surface magneto-chemistry in real time and space.

7

Long-range Ferrimagnetic Order in 2D Kondo Lattice

Spin-bearing molecules on conducting substrates present a rich platform to study fundamental magnetic interactions in low-dimensional systems[71,72]. Especially, an observation of long-range magnetic order in low-dimensional systems is very intriguing, however, has been elusive, mainly due to the competition between the spin-reducing Kondo effect and magnetic exchange interactions[24,73,74,75]. In this chapter we study emergence of long-range ferrimagnetic order in a 2D supramolecular Kondo lattice consisting of paramagnetic hexadeca-fluorinated iron phthalocyanine (FeFPc) and manganese phthalocyanine (MnPc) co-assembled into a chessboard pattern on single-crystalline Au(111) substrates.

One of the intriguing challenges in magnetism is to create magnetic order in low-dimensional materials[24,71,72,73,74,75]. Interactions that could stabilise magnetic order between neighbouring spins, such as the Heisenberg-Dirac exchange coupling, cannot sustain long-range magnetic order in systems with dimension $d \leq 2$[76]. Moreover, for localised atomic or molecular spin moments surrounded by conduction electrons the Kondo screening occurs, when conduction electrons flip their spin to compensate the local magnetic moment[30]. This profound many-body state has been observed e.g., by Scanning Tunnelling Spectroscopy (STS) for many different magnetic atoms and molecules adsorbed on nonmagnetic metallic substrates[77,78]. To reach the goal of miniaturised spintronic and quantum computing devices[79,80] the Kondo effect is rather undesirable and strategies need to be developed to counteract it. One of the proposed possibilities is to engineer a strong hybridization between the adsorbed atom/molecule and a metallic substrate exhibiting strong spin-orbit coupling[81], which however, unfavourably for applications, alters the localised, single spin character of the adsorbent.

A fundamental question is whether there exists a mechanism that could provide an effective spin interaction to counterbalance the Kondo effect and induce magnetic order. An attractive candidate is the Ruderman-Kittel-Kasuya-Yosida (RKKY) interaction, which is mediated, too, by conduction electrons[82]. A magnetic ad-atom adsorbed on a metallic substrate acts as a scattering centre inducing Friedel-like

oscillations in the electron density of the surface and bulk states[83], whereby two distant spin centres can interact with a typical oscillatory behaviour, i.e., changing the coupling from ferromagnetic to antiferromagnetic depending on the distance[73]. Recently, a broadening of the zero-bias feature, detected by STS for FePc molecules physisorbed on a Au(111) substrate has been suggested to originate from magnetic exchange correlations between nearest neighbours due to Kondo and RKKY interactions[24], but the microscopic origin of the broadening could not be unambiguously identified and other mechanisms were also proposed[84,85,86].

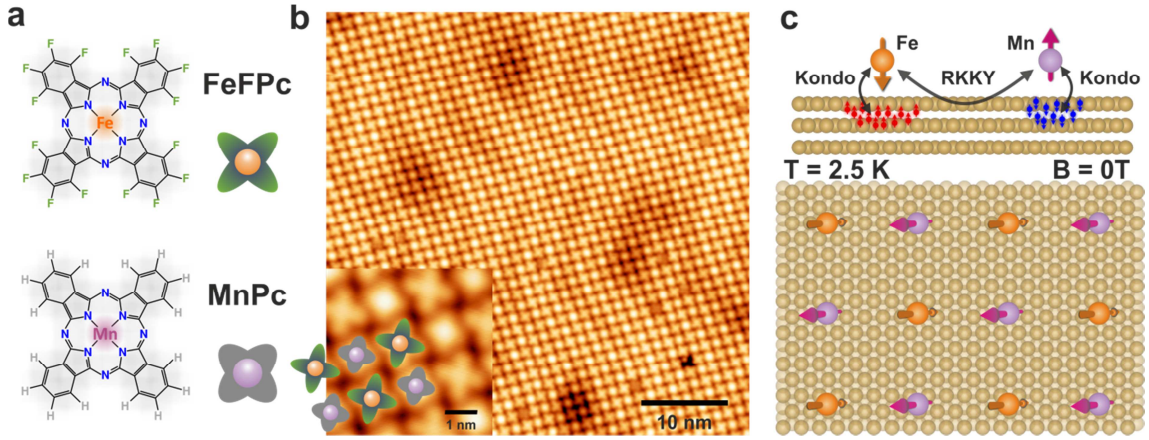

FIGURE **7.1 |** Competing magnetic interactions for spin bearing FeFPc and MnPc molecules adsorbed on Au(111). (a) Schemes of the hexadeca-fluorinated iron phthalocyanine [FeFPc, top] and the manganese phthalocyanine [MnPc, bottom] molecules. The former have all hydrogen atoms on the periphery of the molecule replaced with fluorine. The pictograms shown next to the molecular sketches are used to distinguish the molecules. (b) STM image [U = -2.2 V, I_t = -5pA, T=4.2K] acquired on an extended domain of FeFPc and MnPc molecules on a Au(111) substrate co-assembled in a checkerboard pattern. The inset shows a zoom of the STM image providing details of the checkerboard pattern. (c) Sketch of the two occurring magnetic interactions in the remanent state, the local many-body Kondo screening and the long-range Ruderman-Kittel-Kasuya-Yosida (RKKY) interaction of the magnetic molecular centres mediated by the conduction electrons of the Au(111) substrate.

7.1 MnPc+FeFPc array on Au(111)

Here we introduce a material that enables to explore the competition between the short-range Kondo effect and the long-range magnetic interactions. We have designed a supramolecular lattice consisting of two different metallo-phthalocyanines, hexadeca-fluorinated iron phthalocyanine [FeFPc – Fig. 7.1a (top)] and manganese phthalocyanine [MnPc – Fig. 1a (bottom)] by co-deposition on an inert, non-magnetic Au(111) substrate. The Au(111) substrate facilitates molecular self-assembly and hosts Shockley-type surface states that are ideal for promoting RKKY coupling between adsorbed spin moments[77]. The presence of the peripheral fluorine atoms in the FeFPc molecules and hydrogen atoms on the MnPc species directs the self-assembly into a chessboard arrangement as resolved by scanning

tunnelling microscopy (see Fig. 7.1b) through the C–H···F-C interactions[36,87]. Fluorine atoms at the periphery of FeFPc molecules are more pronounced when imaged by STM and the molecules are thus resolved bigger whilst MnPc molecules appear smaller (c.f. inset of Fig. 7.1b). Each molecule has four nearest neighbours of the opposite kind, whereas the next-nearest neighbours are of the same type. The periodic zig-zag-like pattern resolved by STM depicts a characteristic fingerprint of atomically clean Au(111) surfaces, the so-called herringbone reconstruction of the top-most layer. Figure 7.1c illustrates the fundamental magnetic interactions studied. The spin-bearing molecule acts as a magnetic centre, to which the spins of substrate electrons couple locally through the Kondo effect, while two spin centres can couple via the RKKY interaction mediated by the Au(111) substrate electronic states.

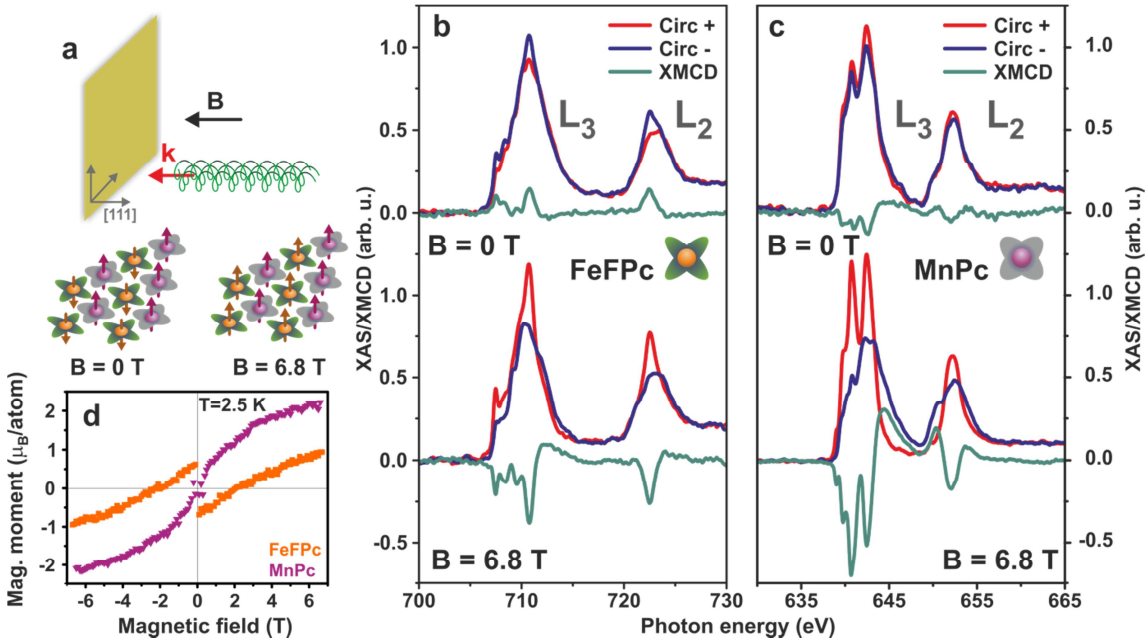

FIGURE **7.2** | Observation of long-range ferrimagnetic order in a 2D supramolecular layer. (a) Top: sketch of the experimental set-up, in which the X-ray Magnetic Circular Dichroism and X-ray Absorption Spectroscopy measurements are performed in normal incidence geometry, with the external magnetic field ***B*** and the ***k***-vector of the x-rays parallel to the surface normal, i.e. [111] direction. Bottom: illustration of the ferrimagnetically ordered spins at B=0 T and the ferromagnetically aligned spins at B=6.8 T. (b,c) XAS/XMCD spectra measured at the Fe $L_{3,2}$ and Mn $L_{3,2}$ edges at B=0 T (top) demonstrate remanent magnetic moments of FeFPc and MnPc molecules, which are aligned antiparallel. In the applied external magnetic field of B=6.8 T (bottom) both molecular spins align parallel to the applied field. (d) Hysteresis curves for individual molecules FeFPc (orange) and MnPc (violet). Magnetic moments of FeFPc molecules become aligned with the applied field for B ≥ 2 T. All measurements were performed at T= 2.5 K.

We have investigated the magnetic properties of the supramolecular array using element-selective X-ray absorption spectroscopy (XAS) and XMCD, which allows us to probe the magnetic moments of Mn and Fe individually. The measurement set-up

for experiments carried in out-of-plane and in-plane geometry are illustrated in Fig. 7.2 and Fig. 7.3, respectively.

In normal incidence geometry (Fig. 7.2a) the applied magnetic field ***B***, ***k***-vector of incoming x-rays and surface normal ([111]-direction) are parallel to each other, whilst for grazing geometry ***B*** and ***k*** are parallel enclosing an angle θ=70 degree with respect to the surface normal (Fig. 7.3a). Figure 7.2b,c shows the XAS/XMCD spectra acquired at normal incidence, at T=2.5K, and in magnetic fields of various strengths 0T and 6.8T, respectively. In absence of an external magnetic field, i.e. for B=0T, the XMCD spectra demonstrate remanent magnetic moments on both species with out-of-plane orientation (Fig. 7.2b,c-top), substantiating direct observation of long-range magnetic order in a 2D spin-bearing molecular layer. Interestingly, the magnetic moment on the Fe ion of FeFPc molecules is aligned *antiparallel* to that on the Mn ion of the MnPc molecules, as shown by the opposite signs of the XMCD signals. The antiparallel alignment of Fe and Mn magnetic moments hints at an antiferromagnetic coupling between Mn and Fe ions in the nearest neighbour positions. Applying a magnetic field of B=6.8T, both magnetic moments of MnPc and FeFPc are found to align parallel with the field (Fig. 7.2b,c–bottom).

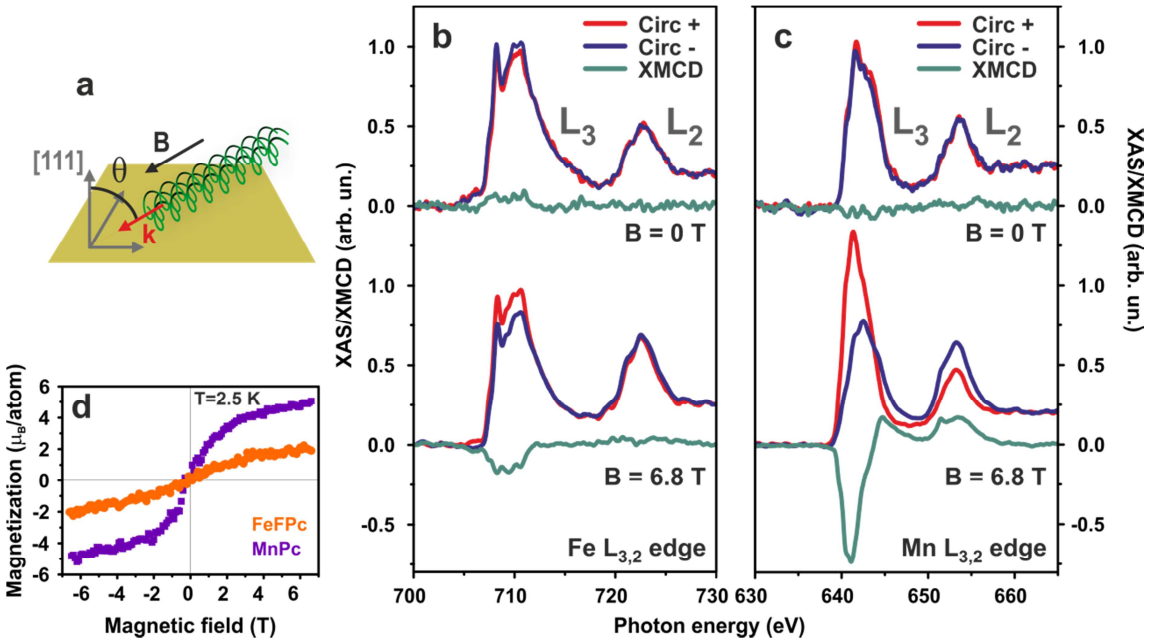

FIGURE **7.3** | XAS and XMCD spectra acquired on the supramolecular FeFPc-MnPc array self-assembled on Au(111) substrate in grazing incidence (θ = 70°) geometry at T=2.5K. (a) Sketch of the measurement setup. (b,c) Measured XAS and XMCD at the $L_{3,2}$ edges in zero field (top) and in an applied field of 6.8T for MnPc (b) and FeFPc (c) molecules. (d) Element-specific XMCD hysteresis loops measured on the Fe and Mn ions reveal no remanent magnetization.

The remanent magnetization of FeFPc molecules is readily recognized from the magnetization curve as a discontinuity at B=0T (Fig. 7.2d). The magnetization curve

of the MnPc molecules on the other hand, does not display an easily recognizable discontinuity at B=0T. The antiparallel alignment of magnetization between these two sublattices persists for magnetic fields smaller than ~2T. At B ~ 2T the corresponding Zeeman energy on FeFPc molecules and the long-range magnetic coupling energy become comparably large and the net magnetization of the Fe ions goes to zero (Fig. 7.2d). Figure 7.3 presents XAS/XMCD data acquired on the chessboard array in grazing incidence geometry. In this configuration the XAS/XMCD probes predominantly the in-plane components of the magnetic moments, with a part of the out-of-plane components contributing to the overall signal[26]. In zero applied external magnetic field the XMCD spectra acquired on MnPc molecules reveal no dichroic signal (Fig. 7.3c), suggesting that the remanent magnetic moments of the MnPc molecules are fully aligned along the out-of-plane direction. The XMCD spectrum acquired at the Fe $L_{3,2}$ edges of FeFPc molecules resolves a small remanent magnetization (Fig. 7.3b). Such a small contribution to the XMCD signal is attributed to the out-of-plane component. The hysteresis curves presented in Fig. 7.3d show no remanent magnetization on either of the molecules. Applying an external magnetic field of B=6.8T leads to alignment of both magnetic moments along the field.

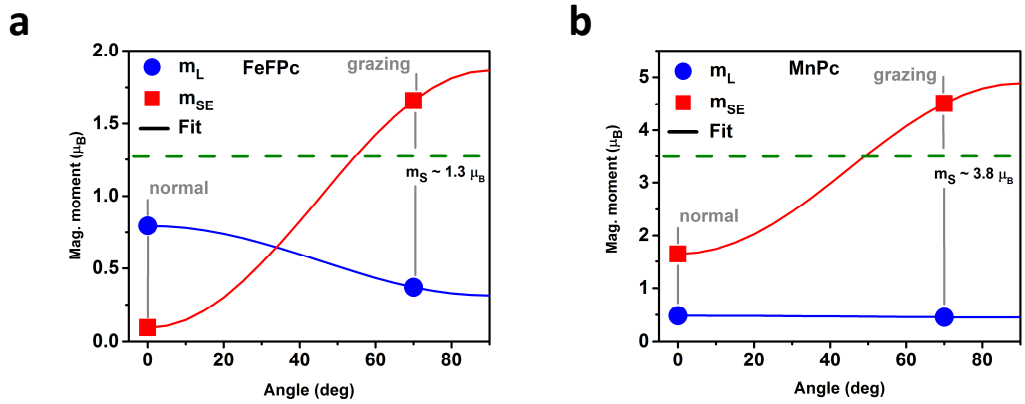

FIGURE **7.4** | Angular dependence of the magnetic moments measured in the field-aligned state. Angle dependence of the orbital and effective spin magnetic moment of FeFPc (a) and MnPc (b) molecules. Measured data points (symbols) are fitted to equations (7.1) and (7.2) for the orbital and spin effective moments, respectively, to obtain the isotropic spin moments. The dashed lines depict the extracted respective isotropic spin moments.

The XMCD signals of FeFPc and MnPc measured at normal and grazing incidence were analysed with the sum-rule method. In the magnetic field oriented state, we observe sizable induced spin magnetic moments, with larger in-plane than out-of-plane components. At normal incidence and at remanence, in contrast, the XMCD signals are dominated by the orbital magnetic moments (-0.39μ_B for FeFPc and 0.28μ_B for MnPc), as readily recognized also from the L_3 and L_2 XMCD peaks having the same sign[81] (Fig. 7.2b,c). The shape of the XMCD spectra is consistent with previous XMCD measurements on FePc films[56,88] and on MnPc thin films[89]. Previously, thick films of FePc molecules were reported to exhibit magnetic

anisotropy with the easy axis oriented *in-plane*[88]. Remarkably, here we have observed the first remanent magnetization in the *out-of-plane* direction. Such re-orientation of the predominant magnetisation direction could be related to a change of the molecular symmetry upon adsorption onto the Au(111) surface; specifically, here we find a symmetry change from D_{4h} to C_{4v} and C_{2v} for MnPc and FeFPc, respectively (see section on DFT+U calculations).

A change in the magnetic easy axis from in-plane to out-of-plane direction was deduced from STS data of FePc species adsorbed on oxygen-reconstructed Cu surfaces[15]. By using XMCD, only a reduction of magnetic moment anisotropy was observed for FePc on a graphene/Ir substrate[90]. Figure 7.4 reveals an angular dependence of the magnetic moments. In the field aligned state the size of the orbital moment of FeFPc decreases from a higher value observed in normal incidence to a smaller one measured in grazing incidence geometry. On the other hand, the angle dependence of the effective spin moment shows an opposite behaviour with a higher value in grazing incidence and smaller one in normal incidence. A somewhat similar behaviour is observed for MnPc, however with the change in the orbital moment being comparably smaller. Notably, the behaviour found here for FeFPc on Au(111) is different from that observed previously for thin films of FePc[73] and for the FePc/graphene/Ir system[90], where both effective spin moment and orbital moment increased with the incident angle resolving an easy-plane anisotropy. Considering that the orbital moment is pivotal to the magnetic anisotropy our data reveal an out-of-plane easy axis for FeFPc and MnPc in the supramolecular layer. Data points in Fig. 7.4 were fitted to following formulas:

$$m_L(\alpha) = m_L^{OP} cos^2(\alpha) + m_L^{IP}\, sin^2(\alpha) \tag{7.1}$$

$$m_{SE}(\alpha) = \; m_S + 7m_T^{IP}\left(2cos^2(\alpha) - sin^2(\alpha)\right) \tag{7.2}$$

, where $m_L^{OP}$and m_L^{IP} are the out-of-plane and in-plane components of the orbital magnetic moment, respectively. Symbol α denotes angle between the ***k***-vector of x-rays and the surface normal. The term m_T^{IP} stands for the in-plane component of the dipolar m_T term and $2m_T^{IP} + \; m_T^{OP} = 0$. Using these formulas we can extract the spin magnetic moment of the MnPc and FeFPc molecules as $\sim$ 3.8 μ_B and $\sim$ -1.3 μ_B, suggesting a spin S $\sim$ 3/2 – 2 for MnPc and S $\sim$ 1 for FeFPc. The reduced value of the FeFPc spin moment (as compared to the S=1 of a free FeFPc molecule) is consistent with the under-screened Kondo effect reported previously for FePc on Au[24].

Next, we investigated the Kondo interaction of both molecules adsorbed on nonmagnetic Au(111) substrate. The many-body renormalization of the energy levels leads to a sharp Kondo signature which is observed at the Fermi level for S=1/2 spins[78]. In our case both molecular species comprise magnetic centres, however, of higher spins. To investigate the onset of the Kondo effect we performed STS measurements with the tip positioned at the centre of the molecules.

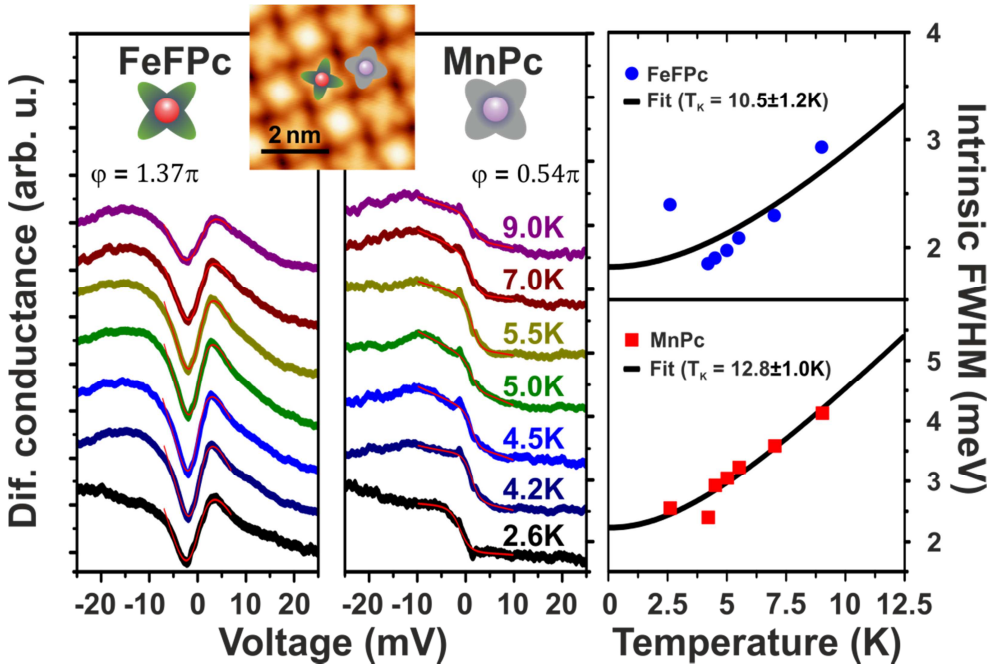

FIGURE **7.5 |** Temperature dependent differential conductance dI/dV spectra measured at the centre of FeFPc (left) and MnPc molecules (middle)**.** Both shows Kondo features around zero bias with dip-like feature for FeFPc and a step-like shape for MnPc. Fitting to Frota function (red lines) extracts Kondo temperature for both molecules(right).

Figure 7.5 shows differential conductance spectra (*dI/dV*) for both FeFPc and MnPc molecules around the Fermi energy, i.e., around zero bias, in the temperature range of 2.6 – 9.0K. The spectra of both molecules exhibit zero bias anomalies, i.e., a dip-like feature in the spectra of FeFPc molecules and a step-like shape for the MnPc species, well in line with data reported previously[24,91]. Measurements of differential conductance spectra in the temperature range 2.6 K to 9.0 K result in a smearing and gradual suppression of these features towards higher temperatures confirming their Kondo character. The strength of the Kondo coupling is often expressed in terms of the Kondo temperature that is extracted from the temperature-dependent spectra fitted to a modified Frota function[92]. In our case, the Kondo temperature of MnPc and FeFPc molecules is T_K=12.8±1.0K and T_K=10.5±1.2K, respectively. These values are somewhat lower/higher compared to those reported for single MnPc (T_K=36K) and FePc molecules (T_K=2.6K) on Au(111)

A Kondo resonance splitting of an individual MnPc molecule adsorbed on a thin Pb layer on top of a Fe layer has been previously observed with STS and was attributed to an RKKY-type interaction between the molecule and the magnetic iron layer underneath the lead[18]. A broadening and splitting of the Kondo resonance has been also observed for FePc molecules on a Au(111) surface which was tentatively proposed, too, to originate from the RKKY interaction[24]. The unambiguous identification of the involved interactions, however, was compromised by magnetic anisotropies and spin quantum numbers larger than S=1/2[93] which complicate the assignment of the Kondo peak splitting to two split S_z=±1/2 sublevels. Moreover, the

joint appearance of orbital and spin degeneracies leads to other, orbital Kondo effects[84] also affecting the interpretation of the Kondo peak splitting. Broadening of the Kondo peak of FePc on Au has been discussed in terms of Fe valence fluctuations[85] and, for Fe porphyrins on Au(111), to an adsorption induced Fe spin switching[86]. For the here-investigated bi-molecular layer we do not observe a clear splitting of the Kondo resonance, even in presence of the observed long-range magnetic order.

7.2 DFT+U calculations

To elucidate the origin of the observed long-range magnetic order we performed electronic structure calculations using the density-functional theory with on-site Coulomb *U* correlations (DFT+*U*) added to capture the strong d-electron interactions at the Fe and Mn centres. In the open 3d-shell of the central metal ion of the metallo-phthalocyanine there are strong on-site d-d Coulomb correlations, which are captured by the supplemented Hubbard *U* and exchange constant *J*. In the present calculations *U* and *J* were taken to be 4 eV and 1 eV, respectively. The supramolecular chessboard pattern is described by a periodic simulation-cell containing 2x2 molecules, while the Au(111) substrate is modelled with three atomic Au layers. The atomic positions have been optimized by complete self-consistent relaxation of all forces in the 588-atom simulation cell. We find an optimized Fe-Mn distance of 14.35Å, in agreement with the 13.9±0.3Å measured with STM. Upon adsorption of FeFPc and MnPc on Au(111) we find that the molecular geometry slightly changes. In the gas phase, the FeFPc and MnPc molecules have *D4h* symmetry, but adsorbed on the Au(111) surface MnPc adopts *C4v* and FeFPc *C2v*. In case of FeFPc two of its benzene rings moved slightly towards the substrate, while in case of MnPc the phthalocyanine plane came closer to the substrate yet with the Mn atom positioned 0.17Å above the macrocyclic ring.

Importantly, the calculations predict a ground state with *antiparallel coupling* between the spin moments on nearest-neighbour FeFPc and MnPc molecules, and a ferromagnetic coupling of each of the species to their next-nearest neighbour. The *ab initio* computed spin-density, shown in top-view in Fig. 7.6a, attests the antiparallel coupling between the FeFPc and MnPc spin moments. The computed 3d spin-only moments of -2.1μ_B and 3.7μ_B, for FeFPc and MnPc, respectively, are in close agreement with those determined by XMCD (of 1.3μ_B and 3.8μ_B, in the field-aligned configuration). The spin-resolved partial 3d-densities of states (DOS) of the central Fe and Mn ions, calculated with the DFT+U approach are shown in Fig. 7.7. These partial densities give the following orbital populations of the 3d metal ions: $(d_{xy})^2\ (d_{xz}, d_{yz})^{2.6} (d_{z^2})^1 (d_{x^2-y^2})^{0.7}$ (i.e., $(b_{2g})^2\ (e_g)^{2.6} (a_{1g})^1 (b_{1g})^{0.7}$) for FeFPc, and $(d_{xy})^1\ (d_{xz}, d_{yz})^2 (d_{z^2})^1 (d_{x^2-y^2})^{0.8}$ for MnPc, where the population of the $d_{x^2-y^2}$ orbital is responsible for a reduction of the total spin S.

To determine the cause of the ferrimagnetic coupling we have performed additional calculations in which the Au substrate was removed. The computed 3d

moments without the Au substrate were very similar, 2.0 μ_B and 3.6 μ_B, respectively. These values correspond to S = 1 for FeFPc and S ≈ 3/2 – 2 for MnPc. In this case, no notable magnetic interaction between the neighbouring molecules was obtained, establishing that the molecule-molecule spin coupling is not due to a weak exchange interaction mediated by the overlap of phthalocyanine ligands.

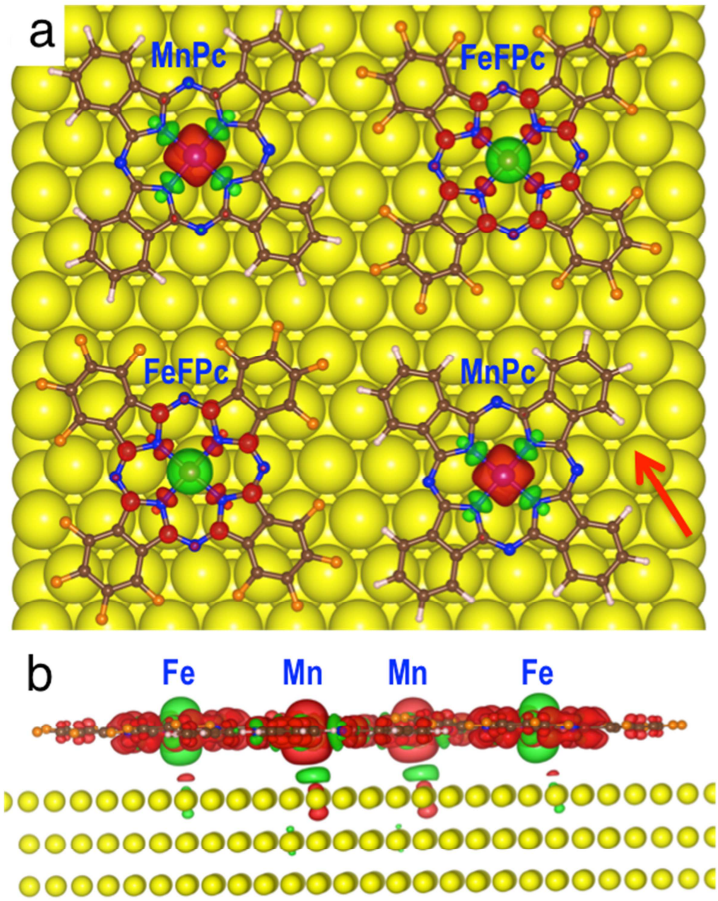

FIGURE **7.6 |** Density-functional theory-based calculations of the 2D supramolecular layer on the Au(111) substrate. (a) Top-view of the DFT+*U* computed spin densities. The red isosurfaces depict the positive spin-density on the Mn atoms of the MnPc molecules and the green isosurfaces the negative spin-density on the Fe atoms of the FeFPc molecules. Note the opposite spin-densities on the ligand atoms surrounding the metal centres. (b) Side-view of the spin-density plot at an enlarged isodensity value ($5x10^{-3}$ eÅ^{-3}), which shows the interaction of the spin-magnetization on the metallo-phthalocyanines with the Au substrate atoms. At this isodensity value, the dominant spin polarization is clearly visible. The direction of the side-view is given by the arrow in panel (a). Colour code: yellow atoms depict the Au(111) substrate atoms, brown the carbon atoms, blue the nitrogen atoms, white the hydrogen atoms and orange the fluorine atoms.

Rather, the conductive Au(111) substrate is pivotal for mediating the oscillatory magnetic interaction between FeFPc and MnPc, which implies that the RKKY interaction is responsible for stabilising the long-range magnetic order. Figure 7.6b shows a side-view of the calculated magnetisation density. We find that the electron density underneath the metal-ion centres exhibits a small spin-polarisation, with a spin-polarised lobe that is opposite to the dominant spin-polarisation on the adjacent molecular centre. This evidences an antiferromagnetic coupling between mobile substrate electrons, predominantly the surface electrons, and the molecular spin, reminiscent of local Kondo coupling.

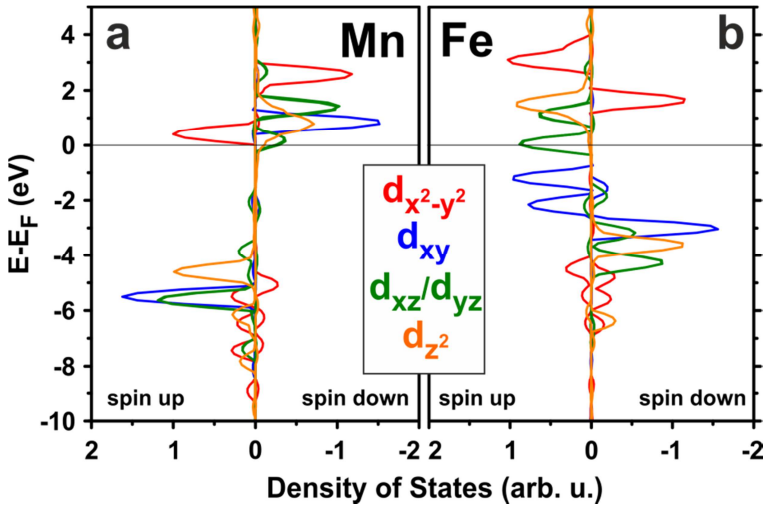

FIGURE **7.7** | Partial Density of States for the 3d orbitals of (a) Mn and (b) Fe within FeFPc and MnPc molecules assembled on Au(111), computed with the DFT+U method.

7.3 Discussion

Our element-specific XMCD measurements demonstrate the direct evidence for long-range ferrimagnetic order in a binary 2D molecular lattice. This unexpected long range order of anisotropic moments is observed below the Kondo temperature of ~12K, and is assigned to the RKKY interaction, mediated by the surface-state electrons of the Au(111) substrate in our experimental and theoretical analysis. Customizing the strength of the fundamental interactions in 2D Kondo lattices by the modification of the molecular building blocks unlocks new possibilities to study low-dimensional quantum phase transitions in synthetic materials and opens up new avenues for building molecular spintronic devices.

Summary

The thesis compiles studies on magnetic exchange interaction between metallo-porphyrins and magnetic substrates and the exchange coupling between metallo-phthalocyanines adsorbed on non-magnetic substrates. Monolayers of paramagnetic molecules adsorbed on the surfaces were investigated by X-ray Absorption Spectroscopy, X-ray Magnetic Circular Dichroism, Scanning Tunnelling Microscopy and Spectroscopy and X-ray Photoelectron Spectroscopy. Additionally, molecule-substrate interface was investigated with the Photo-Emission Electron Microscope.

Paramagnetic Cr(III)TPPCl molecules adsorbed on the surface of thin ferromagnetic cobalt film were observed to couple *antiferromagnetically* with the magnetization of the substrate. The actual species which were resolved at the substrate had been identified as Cr(II)TPP molecules due to the loss of the axial chlorine ligand. Therefore Cr(II) ion possesses four electrons on the 3d-shell i.e. chromium exhibits less-than half filled 3d orbital. This leads to an observed antiparallel alignment of the molecular spins. The Goodenough-Kanamori-Anderson theory has been used to explain the origin of the magnetic interaction that is attributed to the indirect exchange coupling between the Cr ion and Co substrate mediated by the nitrogen atoms in the porphyrin macrocycle. Specifically, an empty $d_{x^2-y^2}$ orbital of Cr ion is filled with an electron from the nitrogen atoms, which are spin-polarized in opposite direction to the magnetisation of the substrate. These findings demonstrate that the magnetic coupling of molecules on magnetic surfaces could be controlled by redox reactions on the centre metal ion of the magnetic molecules. Specifically, donation (withdrawal) of an electron to (from) the metal centre and transformation of the initial $d^4(d^5)$ configuration to the final $d^5(d^4)$ configuration changes the sign of the exchange coupling. This type of transition has been successfully demonstrated for MnTPP molecules adsorbed on Co substrates by their ligation with nitric oxide acting as an electron acceptor. The electron population of the 3d-shell of the Mn ion changed from d^5 to d^4 configuration[45].

The magnetic exchange coupling between metallo-porphyrins and ferromagnetic substrates through a non-magnetic insulating spacer layers has been investigated for Mn- and Fe-TPPCl species deposited on the nitrogen and chlorine c(2x2) reconstructed cobalt substrates. Both molecules align their magnetic moments antiparallel with respect to the magnetization of N/Co. The antiferromagnetic molecule-substrate interaction is governed by the 180° indirect exchange coupling occurring between molecular and substrates spins mediated by the $2p_z$-orbitals of the nitrogen atoms adsorbed at the surface. This has been evidenced by the XMCD measurements at the $L_{3,2}$ edges of the centre metal ions and by the XMCD signal

resolved at the π* resonances measured at the nitrogen K edge. Termination of the cobalt substrate with nitrogen led to a reduction of the interaction between delocalized electrons of the porphyrin ring and the electronic states of the substrate. This on one hand stabilized the axial chlorine ligand at the metal centre as evidenced by the XA spectra resolving the 3+ oxidation state of Mn and Fe ions. On the other hand, the reduced molecule-substrate interaction facilitates the diffusion of ad-molecules and induces molecular self-assembly as resolved by STM and LEED. Two mirror domains rotated by 26° with respect to each other, have been observed due to the broken translational symmetry at the surface of the crystal and chiral assembly of the achiral molecules.

The investigation of the magnetic properties of chlorine c(2x2) reconstructed cobalt substrates as presented in this thesis are the first of its kind. Even more, the investigation of the magnetic properties of paramagnetic molecules adsorbed on such substrates had helped to answer one of the very first questions proposed by Andreas Scheybal et al. [4] on the role of chlorine atom in the exchange coupling. Similarly to nitrogen and oxygen reconstructed substrates, the chlorine atoms adsorbed at the surface of cobalt thin films reduce the molecule-substrate interaction and induces molecular self-assembly of Mn- and FeTPPCl. The two chiral mirror domains are rotated by 24° to each other. Both, the MnTPPCl and the FeTPPCl molecules adsorbed on Cl/Co, has been found in the 3+ and 4+ oxidation state, respectively, confirming presence of axial chlorine ligand. XMCD measurements of the centre metal ions had revealed a relatively weak antiferromagnetic exchange coupling of MnTPPCl to the Cl/Co. Surprisingly, the magnetic moments of FeTPPCl molecules were observed to couple ferromagnetically with significantly lower exchange coupling strength. The magnetic interaction in both cases was attributed to indirect exchange coupling between the metal centres and cobalt substrate, mediated by the 3d-orbitals of the chlorine atoms adsorbed at the interface. The XMCD spectra at Cl $L_{3,2}$ edges resolve a sizeable magnetic moment on the 3d-orbitals of pre-adsorbed chlorine.

The exchange coupling between paramagnetic MnTPPCl molecules and ferromagnetic cobalt substrate could be tuned by changing the medium involved in the magnetic interaction. The exchange coupling on nitrogen and chlorine reconstructed cobalt substrates has been observed to be mediated via localized electrons of adsorbed atoms. Such exchange coupling can be understood by the deterministic picture of the Goodenough-Kanamori-Anderson rules. The magnetic interaction could also be mediated be the delocalized electrons of the conducting material. A non-magnetic chromium spacer layer, in the wedge shape, which has been placed between the cobalt substrate and the magnetic molecules, reduces the strength of the exchange coupling with increasing thickness of the chromium. The conduction electrons in the chromium layer are spin-polarized at the interface with cobalt substrate. With increasing thickness the induced spin waves decay exponentially from the molecule-chromium interface and only a fraction of the electrons remains spin-polarized. Thermal excitations also disturb the magnetic ordering of the MnTPPCl molecules. Furthermore, chemically-sensitive X-ray PEEM

in combination with spin-sensitive XMCD was able to spatially resolve the magneto-organic interface that could be used to investigate also the non-uniform exchange coupling at novel spin-bearing organic materials.

The magnetic moments of paramagnetic MnPc and FeFPc molecules have been stabilized by adsorption on non-magnetic Au(111) substrate. The molecules self-assemble into a 2D checkerboard array with alternating Mn-Fe-Mn spin arrangement. The adsorbed molecules were not covalently bonded and the interaction was mediated by the surface electrons via RKKY-type exchange coupling between nearest neighbours. XMCD measurements performed in normal incidence at T∼2K and B=0T revealed remanent magnetic moments on both, MnPc and FeFPc molecules, and these magnetic moments were coupled *antiferromagnetically*. Magnetization curves measured for FeFPc molecules resolved that at B∼2T the Zeeman energy competes with the energy of the exchange. At stronger fields the magnetic moments of the Fe atoms align along the direction of the external magnetic field. The XMCD spectra further reveal that the magnetic moments of both molecules have significant contribution from the orbital angular momenta. Magnetic measurements performed in grazing incidence showed very small remanent magnetization on FeFPc molecules that is attributed to out-of-plane components. The out-of-plane alignment of magnetic moments hints towards Ising-like configuration. Magnetization curves measured at grazing incidence resolve magnetic moments as paramagnets. The magnetic centres on conducting substrates are often accompanied by the Kondo effect that screens the magnetic moment of the impurity. The STS measurements on both molecules resolved Kondo peak, a signature of the Kondo effect at zero bias voltage. Those two effects, Kondo and RKKY, are rather competing then collaborative, but in this case they are observed for the first time in co-existence leading to a long-range ferrimagnetic order in 2D supramolecular Kondo lattice.

Exchange coupling between spin-bearing molecules and various substrates has been studied aiming towards the possibilities to tailor magnetic properties of the molecules. Versatility of various systems can be used to stabilize the magnetic moments of the single magnetic ion molecules. The fundamental understanding of the exchange coupling across the organic-inorganic interface is starting point towards future *spintronic* devices. Very intriguing is a fact that depending on the occupancy of the 3d shell of transition metal ions the magnetic moments we can tune exchange coupling of the molecules from FM to AFM and vice versa. The need for high density storage devices could be satisfied by the construction of large periodic magnetic structures such as the 2D spin arrays. Magnetically ordered molecules in 2D arrangement with spins aligned in one direction can also be used in the quantum computers due to the weak quantum entanglement and highly coherent superposition of the spins. All of these observations are the fascinating examples of the richness of the physics at the nanoscale and demonstrate large opportunities for further research.

References

1. Heinrich, A. J. Single-Atom Spin-Flip Spectroscopy. *Science* **306,** 466–469 (2004).
2. Hirjibehedin, C. F. *et al.* Large Magnetic Anisotropy of a Single Atomic Spin Embedded in a Surface Molecular Network. *Science* **317,** 1199–1203 (2007).
3. Crommie, M. F., Lutz, C. P. & Eigler, D. M. Confinement of Electrons to Quantum Corrals on a Metal Surface. *Science* **262,** 218–220 (1993).
4. Scheybal, A. *et al.* Induced magnetic ordering in a molecular monolayer. *Chem. Phys. Lett.* **411,** 214–220 (2005).
5. Wende, H. *et al.* Substrate-induced magnetic ordering and switching of iron porphyrin molecules. *Nat. Mater.* **6,** 516–520 (2007).
6. Vincent, R., Klyatskaya, S., Ruben, M., Wernsdorfer, W. & Balestro, F. Electronic read-out of a single nuclear spin using a molecular spin transistor. *Nature* **488,** 357–360 (2012).
7. Mannini, M. *et al.* Magnetic memory of a single-molecule quantum magnet wired to a gold surface. *Nat. Mater.* **8,** 194–197 (2009).
8. Gatteschi, D. & Sessoli, R. *Molecular nanomagnets*. (Oxford University Press, 2006).
9. Blundell, S. J. & Pratt, F. L. Organic and molecular magnets. *J. Phys. Condens. Matter* **16,** R771–R828 (2004).
10. Cavallini, M., Facchini, M., Albonetti, C. & Biscarini, F. Single molecule magnets: from thin films to nano-patterns. *Phys. Chem. Chem. Phys.* **10,** 784 (2008).
11. Mannini, M. *et al.* Quantum tunnelling of the magnetization in a monolayer of oriented single-molecule magnets. *Nature* **468,** 417–421 (2010).
12. Chylarecka, D. *et al.* Indirect Magnetic Coupling of Manganese Porphyrin to a Ferromagnetic Cobalt Substrate. *J. Phys. Chem. C* **115,** 1295–1301 (2011).
13. Chylarecka, D. *et al.* Self-Assembly and Superexchange Coupling of Magnetic Molecules on Oxygen-Reconstructed Ferromagnetic Thin Film. *J. Phys. Chem. Lett.* **1,** 1408–1413 (2010).

14. Javaid, S. *et al.* Impact on Interface Spin Polarization of Molecular Bonding to Metallic Surfaces. *Phys. Rev. Lett.* **105,** 077201 (2010).
15. Tsukahara, N. *et al.* Adsorption-Induced Switching of Magnetic Anisotropy in a Single Iron(II) Phthalocyanine Molecule on an Oxidized Cu(110) Surface. *Phys. Rev. Lett.* **102,** 167203 (2009).
16. Bernien, M. *et al.* Tailoring the Nature of Magnetic Coupling of Fe-Porphyrin Molecules to Ferromagnetic Substrates. *Phys. Rev. Lett.* **102,** 047202 (2009).
17. Hermanns, C. F. *et al.* Magnetic Coupling of Porphyrin Molecules Through Graphene. *Adv. Mater.* **25,** 3473–3477 (2013).
18. Fu, Y.-S., Xue, Q.-K. & Wiesendanger, R. Spin-Resolved Splitting of Kondo Resonances in the Presence of RKKY-Type Coupling. *Phys. Rev. Lett.* **108,** 087203 (2012).
19. Huheey, J. E. *Inorganic chemistry: principles of structure and reactivity*. (HarperCollins College Publishers, 1993).
20. Wäckerlin, C. *et al.* Controlling spins in adsorbed molecules by a chemical switch. *Nat. Commun.* **1,** 1–7 (2010).
21. Hermanns, C. F., Bernien, M., Krüger, A., Miguel, J. & Kuch, W. Switching the electronic properties of Co-octaethylporphyrin molecules on oxygen-covered Ni films by NO adsorption. *J. Phys. Condens. Matter* **24,** 394008 (2012).
22. Wäckerlin, C. *et al.* On-surface coordination chemistry of planar molecular spin systems: novel magnetochemical effects induced by axial ligands. *Chem. Sci.* **3,** 3154 (2012).
23. Brouder, C. *et al.* Theory of X-ray natural circular dichroism. *J. Synchrotron Radiat.* **6,** 261–263 (1999).
24. Gambardella, P. *et al.* Supramolecular control of the magnetic anisotropy in two-dimensional high-spin Fe arrays at a metal interface. *Nat. Mater.* **8,** 189–193 (2009).
25. Tsukahara, N. *et al.* Evolution of Kondo Resonance from a Single Impurity Molecule to the Two-Dimensional Lattice. *Phys. Rev. Lett.* **106,** 187201 (2011).
26. Oppeneer, P. M., Panchmatia, P. M., Sanyal, B., Eriksson, O. & Ali, M. E. Nature of the magnetic interaction between Fe-porphyrin molecules and ferromagnetic surfaces. *Prog. Surf. Sci.* **84,** 18–29 (2009).
27. Stöhr, J. *Magnetism: from fundamentals to nanoscale dynamics*. (Springer, 2006).

28. Blundell, S. *Magnetism in condensed matter*. (Oxford University Press, 2001).
29. Goodenough, J. B. *Magnetism and the chemical bond*. (Wiley, New York-London, 1963).
30. Binasch, G., Grünberg, P., Saurenbach, F. & Zinn, W. Enhanced magnetoresistance in layered magnetic structures with antiferromagnetic interlayer exchange. *Phys. Rev. B* **39,** 4828–4830 (1989).
31. Hewson, A. C. *The Kondo Problem to Heavy Fermions*. (Cambridge University Press, 1993).
32. Dzyaloshinsky, I. E. Thermodynamic theory of weak ferromagnetism in antiferromagnetic substances. *Sov. Phys. JETP* **5,** 1259–1262 (1957).
33. Bode, M. *et al.* Chiral magnetic order at surfaces driven by inversion asymmetry. *Nature* **447,** 190–193 (2007).
34. Benes, E. Improved quartz crystal microbalance technique. *J. Appl. Phys.* **56,** 608 (1984).
35. Heinrich, B. *et al.* Magnetic anisotropies and exchange coupling in ultrathin fcc Co(001) structures. *Phys. Rev. B* **44,** 9348–9361 (1991).
36. Ruggiero, C. D., Choi, T. & Gupta, J. A. Tunneling spectroscopy of ultrathin insulating films: CuN on Cu(100). *Appl. Phys. Lett.* **91,** 253106 (2007).
37. Wäckerlin, C. *et al.* Two-Dimensional Supramolecular Electron Spin Arrays. *Adv. Mater.* **25,** 2404–2408 (2013).
38. Ikeno, H., de Groot, F. M. F., Stavitski, E. & Tanaka, I. Multiplet calculations of $L_{2,3}$ X-ray absorption near-edge structures for 3d transition-metal compounds. *J. Phys. Condens. Matter* **21,** 104208 (2009).
39. Schütz, G. *et al.* Absorption of circularly polarized X rays in iron. *Phys. Rev. Lett.* **58,** 737–740 (1987).
40. Carra, P., Thole, B., Altarelli, M. & Wang, X. X-ray circular dichroism and local magnetic fields. *Phys. Rev. Lett.* **70,** 694–697 (1993).
41. Thole, B., Carra, P., Sette, F. & van der Laan, G. X-ray circular dichroism as a probe of orbital magnetization. *Phys. Rev. Lett.* **68,** 1943–1946 (1992).
42. Scherz, A., Wende, H. & Baberschke, K. Fine structure of X-ray magnetic circular dichroism for early 3 d transition metals. *Appl. Phys. Mater. Sci. Process.* **78,** 843–846 (2004).

43. Nolting, F. *et al.* Direct observation of the alignment of ferromagnetic spins by antiferromagnetic spins. *Nature* **405,** 767–769 (2000).
44. Viefhaus, H. Low-energy electron diffraction. *Mater. Corros. Korros.* **38,** 404 (1987).
45. Wiesendanger, R. Spin mapping at the nanoscale and atomic scale. *Rev. Mod. Phys.* **81,** 1495–1550 (2009).
46. Brede, J. *et al.* Spin- and Energy-Dependent Tunneling through a Single Molecule with Intramolecular Spatial Resolution. *Phys. Rev. Lett.* **105,** 047204 (2010).
47. Lodi Rizzini, A. *et al.* Coupling Single Molecule Magnets to Ferromagnetic Substrates. *Phys. Rev. Lett.* **107,** 177205 (2011).
48. Auwärter, W. *et al.* Site-specific electronic and geometric interface structure of Co-tetraphenyl-porphyrin layers on Ag(111). *Phys. Rev. B* **81,** 245403 (2010).
49. Theil, C., van Elp, J. & Folkmann, F. Ligand field parameters obtained from and chemical shifts observed at the Cr $L_{2,3}$ edges. *Phys. Rev. B* **59,** 7931–7936 (1999).
50. Kuck, S. *et al.* Disposition of the axial ligand in the physical vapor deposition of organometallic complexes. *J. Vac. Sci. Technol. Vac. Surf. Films* **28,** 795 (2010).
51. Panchmatia, P. M., Sanyal, B. & Oppeneer, P. M. GGA+U modeling of structural, electronic, and magnetic properties of iron porphyrin-type molecules. *Chem. Phys.* **343,** 47–60 (2008).
52. Perdew, J. P., Burke, K. & Ernzerhof, M. Generalized Gradient Approximation Made Simple. *Phys. Rev. Lett.* **77,** 3865–3868 (1996).
53. Grimme, S. Semiempirical GGA-type density functional constructed with a long-range dispersion correction. *J. Comput. Chem.* **27,** 1787–1799 (2006).
54. Hocking, R. K. *et al.* Fe L-Edge XAS Studies of $K_4[Fe(CN)_6]$ and $K_3[Fe(CN)_6]$: A Direct Probe of Back-Bonding. *J. Am. Chem. Soc.* **128,** 10442–10451 (2006).
55. Ali, M. E., Sanyal, B. & Oppeneer, P. M. Tuning the Magnetic Interaction between Manganese Porphyrins and Ferromagnetic Co Substrate through Dedicated Control of the Adsorption. *J. Phys. Chem. C* **113,** 14381–14383 (2009).
56. Stepanow, S. *et al.* Mixed-valence behavior and strong correlation effects of metal phthalocyanines adsorbed on metals. *Phys. Rev. B* **83,** 220401(R) (2011).
57. Brune, H. & Gambardella, P. Magnetism of individual atoms adsorbed on surfaces. *Surf. Sci.* **603,** 1812–1830 (2009).

58. Girovsky, J. *et al.* Investigating magneto-chemical interactions at molecule–substrate interfaces by X-ray photo-emission electron microscopy. *Chem. Commun.* **50**, 5190-5192 (2014).
59. Jung, T. A., Schlittler, R. R. & Gimzewski, J. K. Conformational identification of individual adsorbed molecules with the STM. *Nature* **386,** 696–698 (1997).
60. Barth, J. V. Molecular Architectonic on Metal Surfaces. *Annu. Rev. Phys. Chem.* **58,** 375–407 (2007).
61. Raval, R. Chiral expression from molecular assemblies at metal surfaces: insights from surface science techniques. *Chem. Soc. Rev.* **38,** 707 (2009).
62. Scherz, A. Spin-dependent X-ray Absorption Spectroscopy of 3d Transition Metals: Systematics and Applications. PhD thesis (2003).
63. Bernien, M. *et al.* Fe-porphyrin monolayers on ferromagnetic substrates: Electronic structure and magnetic coupling strength. *Phys. Rev. B* **76,** 214406 (2007).
64. Hocking, R. K. *et al.* Fe L-Edge X-ray Absorption Spectroscopy of Low-Spin Heme Relative to Non-heme Fe Complexes: Delocalization of Fe d-Electrons into the Porphyrin Ligand. *J. Am. Chem. Soc.* **129,** 113–125 (2007).
65. Girovsky, J. *et al.* Antiferromagnetic coupling of Cr-porphyrin to a bare Co substrate. *Phys. Rev. B* **90,** 220404(R) (2014).
66. Djeghloul, F. *et al.* Direct observation of a highly spin-polarized organic spinterface at room temperature. *Sci. Rep.* **3,** 1272 (2013).
67. Fraile Rodríguez, A., Nolting, F., Bansmann, J., Kleibert, A. & Heyderman, L. J. X-ray imaging and spectroscopy of individual cobalt nanoparticles using photoemission electron microscopy. *J. Magn. Magn. Mater.* **316,** 426–428 (2007).
68. Fraile Rodríguez, A. *et al.* Size-Dependent Spin Structures in Iron Nanoparticles. *Phys. Rev. Lett.* **104,** 127201 (2010).
69. Unguris, J., Celotta, R. & Pierce, D. Observation of two different oscillation periods in the exchange coupling of Fe/Cr/Fe(100). *Phys. Rev. Lett.* **67,** 140–143 (1991).
70. Kuch, W. *et al.* Element-Selective Magnetic Imaging in Exchange-Coupled Systems by Magnetic Photoemission Microscopy. *Surf. Rev. Lett.* **5,** 1241–1248 (1998).
71. Zhao, A. Controlling the Kondo Effect of an Adsorbed Magnetic Ion Through Its Chemical Bonding. *Science* **309,** 1542–1544 (2005).

72. Franke, K. J., Schulze, G. & Pascual, J. I. Competition of Superconducting Phenomena and Kondo Screening at the Nanoscale. *Science* **332,** 940–944 (2011).
73. Wahl, P. *et al.* Exchange Interaction between Single Magnetic Adatoms. *Phys. Rev. Lett.* **98,** 056601 (2007).
74. Prüser, H. *et al.* Long-range Kondo signature of a single magnetic impurity. *Nat. Phys.* **7,** 203–206 (2011).
75. Spinelli, A. *et al.* Exploring the phase diagram of the two-impurity Kondo problem. *Nat. Commun.* **6,** 10046 (2015).
76. Mermin, N. D. & Wagner, H. Absence of Ferromagnetism or Antiferromagnetism in One- or Two-Dimensional Isotropic Heisenberg Models. *Phys. Rev. Lett.* **17,** 1133–1136 (1966).
77. Madhavan, V. Tunneling into a Single Magnetic Atom: Spectroscopic Evidence of the Kondo Resonance. *Science* **280,** 567–569 (1998).
78. Ternes, M., Heinrich, A. J. & Schneider, W.-D. Spectroscopic manifestations of the Kondo effect on single adatoms. *J. Phys. Condens. Matter* **21,** 53001 (2009).
79. Bogani, L. & Wernsdorfer, W. Molecular spintronics using single-molecule magnets. *Nat. Mater.* **7,** 179–186 (2008).
80. Hanson, R., Kouwenhoven, L. P., Petta, J. R., Tarucha, S. & Vandersypen, L. M. K. Spins in few-electron quantum dots. *Rev. Mod. Phys.* **79,** 1217–1265 (2007).
81. Gambardella, P. Giant Magnetic Anisotropy of Single Cobalt Atoms and Nanoparticles. *Science* **300,** 1130–1133 (2003).
82. Van Vleck, J. Note on the Interactions between the Spins of Magnetic Ions or Nuclei in Metals. *Rev. Mod. Phys.* **34,** 681–686 (1962).
83. Hasegawa, Y. & Avouris, P. Direct observation of standing wave formation at surface steps using scanning tunneling spectroscopy. *Phys. Rev. Lett.* **71,** 1071–1074 (1993).
84. Minamitani, E. *et al.* Symmetry-Driven Novel Kondo Effect in a Molecule. *Phys. Rev. Lett.* **109,** 086602 (2012).
85. Fernández, J., Aligia, A. A. & Lobos, A. M. Valence fluctuations in a lattice of magnetic molecules: Application to iron(II) phtalocyanine molecules on Au(111). *EPL Europhys. Lett.* **109,** 37011 (2015).

86. Wang, W. *et al.* Intramolecularly resolved Kondo resonance of high-spin Fe(II) - porphyrin adsorbed on Au(111). *Phys. Rev. B* **91,** 045440 (2015).
87. Hipps, K. W., Scudiero, L., Barlow, D. E. & Cooke, M. P. A Self-Organized 2-Dimensional Bifunctional Structure Formed by Supramolecular Design. *J. Am. Chem. Soc.* **124,** 2126–2127 (2002).
88. Bartolomé, J. *et al.* Highly unquenched orbital moment in textured Fe-phthalocyanine thin films. *Phys. Rev. B* **81,** 195405 (2010).
89. Kataoka, T. *et al.* Electronic configuration of Mn ions in the - molecular ferromagnet -Mn phthalocyanine studied by soft X-ray magnetic circular dichroism. *Solid State Commun.* **152,** 806–809 (2012).
90. Lisi, S. *et al.* Graphene-Induced Magnetic Anisotropy of a Two-Dimensional Iron Phthalocyanine Network. *J. Phys. Chem. Lett.* **6,** 1690–1695 (2015).
91. Liu, L. *et al.* Revealing the Atomic Site-Dependent g Factor within a Single Magnetic Molecule via the Extended Kondo Effect. *Phys. Rev. Lett.* **114,** 126601 (2015).
92. Frota, H. Shape of the Kondo resonance. *Phys. Rev. B* **45,** 1096–1099 (1992).
93. Otte, A. F. *et al.* The role of magnetic anisotropy in the Kondo effect. *Nat. Phys.* **4,** 847–850 (2008).

Acknowledgements

Within these lines I would like to thank people who have helped me during the whole course of my doctoral studies.

In the first, I want to thank my supervisor Thomas Jung for the opportunity to work in his group, for his contribution to my scientific carrier and for the overall support during the time spent in the group.

I am also grateful to Nirmalya Ballav for his enthusiasm, supervision and support during many beamtimes. He was always 3 and half hour ahead of all of us.

I would like to thank Armin Kleibert for the support on many beamtimes, for his time spent to teach me how to handle precious beamline equipment.

Many thanks goes to my recent and former colleagues who have been helping me with the experiments, by preparing and transferring the samples, with the data analysis and for keeping good team spirit in the most critical times. I sincerely thank Jan Nowakowski, Milos Baljozovic, Dorota Siewert, Christian Wäckerlin, Aneliia Wäckerlin, Tatjana Hählen, Harald Rossmann, Sylwia Nowakowska, Thomas Nijs, Li Jingyi and Elise Aeby. The thank also goes to many students that helped to run the experiments and to the beamline staff: Frithjof Nolting, Armin Kleibert, Carlos Vaz, Cinthia Piamontenze, Jan Drieser, Juri Honegger and Pascal Schifferle for their support during the beamtimes.

I shall not forget Rolf Schelldorfer, our remarkable technician who can handle any technical problem and who from I learned a lot about the technical things during our office discussions. Without him, the equipment would not run and the experiments could not be performed.

I gratefully acknowledge Peter Oppeneer and Kartick Tarafder who performed the DFT+U calculations. To Peter Oppeneer goes thank for the scientific discussions that consumed a lot of the storage place at the email servers.

Last, but not the least thank you is for my friends: Dusan, Stephanie, Bennie, Michele, William, Cyprian, Goran, Sebastian, Rajmund, Jiri, Monika, Slavka, Sabi and Kubi.

The biggest thank you is reserved for my wife Zuzana and my family who supported me during the whole time, in the work and at home.

Publication List

1. **J. GIROVSKY**, J. LI, J. NOWAKOWSKI, M. BALJOZOVIC, C. WÄCKERLIN, D. SIEWERT, A. WÄCKERLIN, T. HÄHLEN, A. KLEIBERT, P. M. OPPENEER, T. A. JUNG, & N. BALLAV, ***Magneto-chemical Interaction of Spin-Bearing Porphyrins with Ferromagnetic Surface via Nitrogen and Chlorine Spacer Layers***. (submitted).

2. **J. GIROVSKY**, J. NOWAKOWSKI, EHESAN M. ALI, M. BALJOZOVIC, H. ROSSMANN, T. NIJS, E. AEBY, S. NOWAKOWSKA, D. SIEWERT , G. SRIVASTAVA, C. WÄCKERLIN, J. DREISER, S. DECURTINS, SHI-XIA LIU, P. M. OPPENEER, T. A. JUNG & N. BALLAV, ***Long-range ferrimagnetic order in supramolecular 2D Kondo lattice.*** (submitted).

3. **J. GIROVSKY**, K. TARAFDER, C. WÄCKERLIN, J. NOWAKOWSKI, D. SIEWERT, T. HÄHLEN, A. WÄCKERLIN, A. KLEIBERT, N. BALLAV, T. A. JUNG, & P. M. OPPENEER. ***Antiferromagnetic coupling of Cr-porphyrin to a bare Co substrate.*** *Phys. Rev. B* **90**, 220404(R) (2014).

4. A. SHCHYRBA, C. WÄCKERLIN, J. NOWAKOWSKI, S. NOWAKOWSKA, J. BJÖRK, S. FATAYER, **J. GIROVSKY**, T. NIJS, S. C. MARTENS, A. KLEIBERT, M. STÖHR, N. BALLAV, T. A. JUNG & L. H. GADE. ***Controlling the Dimensionality of On-Surface Coordination Polymers via Endo- or Exoligation.*** *J. Am. Chem. Soc.,* **136**, 26, 9355–9363 (2014).

5. **J. GIROVSKY**, M. BUZZI, C. WÄCKERLIN, D. SIEWERT, J. NOWAKOWSKI, P. M. OPPENEER, F. NOLTING, T. A. JUNG, A. KLEIBERT & N. BALLAV. ***Investigating magneto-chemical interactions at molecule-substrate interfaces by X-ray photo-emission electron microscopy***. *Chem. Commun.*, **50**, 5190-5192, (2014).

6. C. WÄCKERLIN, P. MALDONADO, L. ARNOLD, A. SHCHYRBA, **J. GIROVSKY**, J. NOWAKOWSKI, MD. E. ALI, T. HÄHLEN, M. BALJOZOVIC, D. SIEWERT, A. KLEIBERT, K. MÜLLEN, P. M. OPPENEER, T. A. JUNG & N. BALLAV. ***Magnetic exchange coupling***

of a synthetic Co(II)-complex to a ferromagnetic Ni substrate. *Chem. Commun.*, **49**, 10736-10738, (2013).

7. C. WÄCKERLIN, K. TARAFDER, **J. GIROVSKY**, J. NOWAKOWSKI, T. HÄHLEN, A. SHCHYRBA, D. SIEWERT, A. KLEIBERT, F. NOLTING, P. M. OPPENEER, T. A. JUNG AND N. BALLAV. ***Ammonia Coordination Introducing a Magnetic Moment in an On-Surface Low-Spin Porphyrin***. *Angew. Chem. Int. Ed.,* **52**, 4568-4571 (2013).

8. C. WÄCKERLIN, J. NOWAKOWSKI, SHI-XIA LIU, M. JAGGI, D. SIEWEERT, **J. GIROVSKY**, A. SHCHYRBA, T. HÄHLEN, A. KLEIBERT, P. M. OPPENEER, F. NOLTING, S. DECURTINS, T. A. JUNG and N. BALLAV. ***Two-Dimensional Supramolecular Electron Spin Arrays***. *Adv. Mater.*, **25**, 17, 2404-2408 (2013).

9. J. NOWAKOWSKI, C. WÄCKERLIN, **J. GIROVSKY**, D. SIEWERT, T. A. JUNG and N. BALLAV. ***Porphyrin metalation providing an example of a redox reaction facilitated by a surface reconstruction***. *Chem. Commun.*, **49**, 2347-2349, (2013).

10. P. SZABO, **J. GIROVSKY**, Z. PRIBULOVA, J. KACMARCIK, T. MORI and P. SAMUELY. ***Point-contact spectroscopy of the phononic mechanism of superconductivity in YB_6***. *Supercond. Sci. Technol.* **26,** 045019, (2013).

11. C. WÄCKERLIN, K. TARAFDER, D. SIEWERT, **J. GIROVSKY**, T. HÄHLEN, C. IACOVITA, A. KLEIBERT, F. NOLTING, T. A. JUNG, P. M. OPPENEER and N. BALLAV. ***On-surface coordination chemistry of planar molecular spin systems: novel magnetochemical effects induced by axial ligands***. *Chem. Sci.*, **3**, 3154–3160 (2012).